THESIS FOR THE DEGREE OF DOCTOR OF PHILOSOPHY IN THE NATURAL SCIENCES

Plant aquaporin regulation:

Structural and functional studies using diffraction and scattering techniques

MICHAEL JÄRVÅ

GÖTEBORGS UNIVERSITET

University of Gothenburg
Department of Chemistry and Molecular Biology
Göteborg, Sweden, 2015

Thesis for the Degree of Doctor of Philosophy in the Natural Sciences

Plant aquaporin regulation:

Structural and functional studies using diffraction and scattering techniques

Michael Järvå

Cover: Front view of the tetrameric spinach aquaporin SoPIP2;1 in complex with Hg^{2+} and Cd^{2+}

ISBN 978-91-628-9374-3
Available online at http://hdl.handle.net/2077/38173

Department of Chemistry and Molecular Biology
Biochemistry and Biophysics
University of Gothenburg
SE-413 90 Göteborg, Sweden

Printed by Ale Tryckteam AB
Göteborg, Sweden, 2015

to science

Sweep the garden,
any size

Abstract

Water is the basis for life as we know it. It is only logical then that all organisms have evolved specialized proteins, aquaporins, which regulate water flow across their membranes. Plants, which are immobile, depend more on their environment and also use water flows to move, to breathe, and to grow. This is reflected by the much more diverse set of aquaporins plants facilitate. These work in cohort to tightly control the water flow throughout the plant.

The aim of this thesis has been to deepen the understanding of a spinach leaf aquaporin, SoPIP2;1 and to develop new tools for structural studies of membrane proteins. We have studied how the SoPIP2;1 function is modulated by pH, calcium and mercury using X-ray crystallography and water transport assays in proteoliposomes. We elucidated the pH gating mechanism, discovered an additional binding site for calcium, found an unusual activating effect of mercury and hypothesized a novel mechanism by which this occurs.

We have also used X-ray scattering techniques for structural studies of SoPIP2;1 in solution, thereby circumventing the need for crystallization. Using WAXS we studied the calcium-induced structural changes of SoPIP2;1 in detergent micelles. However, solvation in detergent micelles is a problem in many ways, both for the protein and for many research tools. To deal with this we explored the nanodisc system, which is a soluble discoidal bilayer in which membrane proteins can be reconstituted – thus creating a homogenous population of soluble membrane proteins without the need for detergent. We then used this tool to extract useful structural data from SoPIP2;1 using SAXS/SANS.

Abbreviations:

AQP	Aquaporin	ER	Endoplasmic reticulum
PIP	Plasma membrane intrinsic protein	Cholate	3,7α,12α-Trihydroxy-5ß-cholan-24-oic acid
NIP	Nodulin-26-like intrinsic protein	β-OG	n-Octyl-β-D-glucopyranoside
TIP	Tonoplast intrinsic protein	DDM	n-Dodecyl-β-D-maltopyranoside
SIP	Small basic intrinsic protein	DM	n-Decyl-β-D-maltopyranoside
XIP	uncategorized X intrinsic protein	GFP	Green fluorescent protein
GIP	GlpF-like intrinsic protein	IMAC	Immobilized metal affinity chromatography
HIP	Hybrid intrinsic protein	SEC	Size exclusion chromatography
SAS	Small-angle scattering	CMC	Critical micelle concentration
SAXS	Small-angle X-ray scattering	NMR	Nuclear magnetic resonance
SANS	Small-angle neutron scattering	MSP	Membrane scaffold protein
WAXS	Wide-angle X-ray scattering	NPA	Asn-Pro-Ala
POPC	1-palmitoyl-2-oleoyl-sn-glycero-3-phosphocholine	MD	Molecular dynamics
SUV	Small unilamellar vesicle	HPLC	High performance liquid chromatography
MLV	Multi lamerllar vesicle	Å	Ångström (0.1 nm)
DNA	Deoxyribonucleic acid	Da	Dalton
ATP	Adenosine Tri-Phosphate	UV	Ultraviolett
ADP	Adenosine Di-Phosphate	IR	Infrared
SNARE	Soluble NSF Attachment Protein Receptors	GPCR	G-protein coupled receptors

Organisms:

Escherichia coli
Saccharomyces cerevisiae
Pichia pastoris
Plasmodium falciparum
Xenopus laevis
Arabidopsis thaliana
Glycine max L
Mesembryanthemum crystallinum
Medicago truncatula
Nicotiana tabacum
Oryza sativa L. cv Nipponbare
Populus trichocarpa
Solanum lycopersicum
Spinacia oleracea
Vitis vinifera L
Zea mays

List of Publications

Paper I — Frick, A., **Järvå, M.,** & Törnroth-Horsefield, S. (2013). Structural basis for pH gating of plant aquaporins. FEBS Letters, 587(7), 989–93. doi:10.1016/j.febslet.2013.02.038

Paper II — Frick, A*., **Järvå, M.***, Ekvall, M., Uzdavinys, P., Nyblom, M., & Törnroth-Horsefield, S. (2013). Mercury increases water permeability of a plant aquaporin through a non-cysteine-related mechanism. The Biochemical Journal, 454(3), 491–9. doi:10.1042/BJ20130377

Paper III — Sjöhamn J*, **Järvå M***, Andersson M, Sharma A, Neutze R, Törnroth-Horsefield S. (2015). Calcium induced protein conformational changes regulate the water transport activity of plant plasma membrane aquaporins. *Manuscript*

Paper IV — **Järvå M**, Kynde S, Törnroth-Horsefield S, Arleth L. (2015). SAXS and SANS investigation of SoPIP2;1 Aquaporin-tetramers in POPC-nanodiscs. Bench-mark of the nanodisc approach to extract structural information about membrane proteins. *Submitted to Acta Crystallographica D 2014-03-20*

* These authors contributed equally.

Contribution report

There are several authors on the papers presented here and my contribution to each of them is listed below. The focus of my thesis is on areas where I have made major contributions.

Paper I — I took part in writing of the manuscript, the making of the figures and the interpretation of the results.

Paper II — I cloned, expressed and purified the protein for the functional assays. I performed all the functional assays, analyzed the results & drew the conclusions from them. I made the figures and took large part in writing the paper.

Paper III — I expressed and purified the protein and took major part in designing and performing the experiment. I did all the functional assays, the analysis of them and took large part in writing the paper and making the figures.

Paper IV — I expressed and purified the membrane protein and the scaffold protein. I optimized the reconstitution and prepared the samples for the experiments. I took large part in writing the article and making the figures.

Contents

1. The scope of this thesis

When I laid the foundation for the story of this thesis I found myself somewhere in-between structural and physical biochemistry. Here I have tried to employ the tools from both worlds to grasp the mechanisms behind these tiny workers, our proteins. The lipid perspective is always important when explaining membrane protein behavior and structure. Although the scope of this thesis is not lipids in themselves, the importance of their role in membrane protein chemistry and how we can use them as tools to gain knowledge has always been present.

I have studied a spinach leaf water channel (SoPIP2;1) using scattering and diffraction with a dual goal; On the one hand, the more we look at this protein the more it teaches us about the complexity of nature, and on the other hand, this well studied protein has been an excellent candidate for further development of techniques in membrane protein research.

In **Paper I** we wanted to study the pH dependency of the gating mechanism in SoPIP2;1 With X-ray crystallography we determined the structure of a protein tetramer where we could visualize exactly how acidification can switch off protein function in times of stress.

In **Paper II** we wanted to investigate the structural mechanics behind SoPIP2;1's mercury sensitivity by determining the structure in complex with mercury, and by measuring its water transporting properties on different mutants.

In **Paper III** we turned our focus on the calcium dependency of SoPIP2;1. With wide-angle X-ray scattering (WAXS) we could observe the structural changes of the protein upon UV-triggered calcium release.

In **Paper IV** we wanted to utilize the recently popular nanodisc system to study membrane proteins using small-angle X-ray scattering (SAXS) in combination with small-angle neutron scattering (SANS). The nanodiscs provided a new, simple way of studying membrane proteins in a more native milieu, and we evaluated the current limits of this technique.

2. Proteins and lipids

2.1 Proteins are workers in the cell

Imagine a medieval city. Each inhabitant of this city has a purpose, a job, with a very specific task that he or she performs. No city would function properly without these tasks being performed correctly, and by a specific amount of workers. Each city is surrounded by walls patrolled by guards to protect itself from outside forces. To control influx and efflux of both people and goods the guards of the wall has to maintain gates. The government resides in the castle in the center of the city, surrounded by an inner city wall. This government is in charge of changing work force distribution in response to the demands of the city. In times of war or natural disaster, the government rallies its army and the city gates are closed, and during calmer times more incentives are given for expansion.

A cell is much like a medieval city where its inhabitants are proteins. Each protein has a very specific task it is evolutionary distilled to perform, and each task has a very specific amount of proteins assigned to it, decided by the governing transcription machinery residing in the nucleus of eukaryotic cells. The walls of the cell, the cell membrane, protects the cell from the outside world and the guards of this wall are the membrane proteins that control biomolecule influx and efflux as well as relaying important signaling molecules to the inner cell compartments.

If we want to understand the cell, we have to study its inhabitants, the proteins, what they work with, and how they do their job. In the human genome the number of different protein encoding genes is estimated to over 19,000[1] – not taking into account variations due to posttranscriptional and posttranslational modifications. It is important to fully understand each and every one of them so that we can better understand diseases, develop better medicine and, as always, hope for serendipitous discoveries that can change the world.

We readily use smaller organisms such as mice, flies, plants, yeast, and bacteria as model organisms for humans, because everything in nature originates from a common ancestor. Plant research is also very important because of the ever growing need to feed our societies. In the next decennia substantial improvements in agriculture is needed to accommodate the increase in population and living standards that we see today.

2.2 A brief history of protein research

The story of protein research began in the early 18th century when Antoine Fourcroy and others started to characterize wheat gluten and found it to be similar to extracts from other plants as well as milk, although they weren't called proteins at the time[2]. The word "protein" was coined much later, in 1838, by the Dutch chemist Gerardus Johannes Mulder after having it suggested to him in a letter from the Swedish chemist Jöns Jacob Berzelius[3]. By this time the constituents of proteins were starting to be identified but it took until 1935 to identify threonine as the last of the 20 essential amino acids[4]. During that decennium the enzyme urease was proven to be a protein[5], and hemoglobin was identified as the color component of blood and it became the first crystallized protein[6]. By the 20th century an image had started to emerge suggesting that proteins were something more than just bulk matter.

With the advent of X-ray crystallography in the early 20th century, protein scientists wondered if it would ever be possible to determine the structure of something as large as a protein. Since protein crystallization had already been developed as a purification method the idea did not seem too far-fetched. Being able to determine the three dimensional structure of a protein would open up huge possibilities in the field. To be able to see these otherwise intangible molecules would help scientists to understand protein function at a much faster pace than previously. In 1958 Sir John C. Kendrew managed to solve the structure of sperm whale myoglobin[7] – a feat that awarded him the Nobel prize in chemistry in 1962.

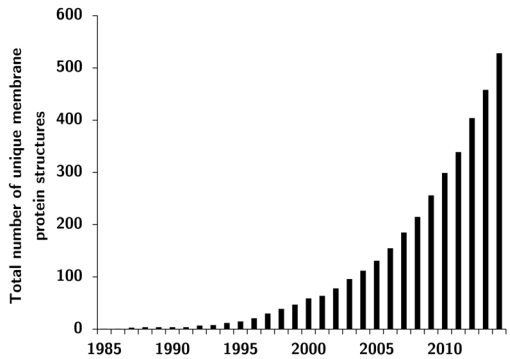

Figure 2.1 The total number of unique membrane protein structures deposited in the PDB database each year from 1985 to 2014. Data taken from http://blanco.biomol.uci.edu/mpstruc/ 2015-02-20

There is a metaphor that is not entirely accurate, but serves to visualize the principle of X-ray crystallography. Imagine a crystal chandelier hanging from the roof of a dark, empty, room. Propose that you can't image it directly, but you can illuminate it using

a very strong and precise flashlight. If you observe all the tiny reflections across the walls in the room as you walk around the chandelier the location and intensity of these spots can then be used to calculate exactly what the chandelier looks like.

As of 2015, over 98,000 protein structures are publicly available in the protein data bank[8], out of which over 55,000 are unique structures. However, the number of unique membrane protein structures is only 520[9] – less than 1% of the total (Figure 2.1). In contrast, 27% of the human proteome is estimated to be alpha-helical transmembrane proteins[10].

The first membrane protein structure, of photosynthetic reaction center, was solved in 1984[11], more than 25 years after the first soluble protein structure. This lag in progress was, and still is, because of the huge increase in difficulty in producing, purifying and crystallizing membrane proteins as compared to soluble proteins. In contrast to this, almost all commercially available drugs target proteins in some way, with approximately 70% of those being membrane proteins[12]. The importance of developing better methods for studying membrane proteins is obvious.

2.3 Lipid bilayers

Lipid bilayers assemble spontaneously from free lipids due to the hydrophobic effect. This provides the basis for sustainable life as these walls provide protection from the outside world, as well as the ability to build up osmotic and ionic gradients used for signaling and energy generation.

It is very easy to generalize these lipid bilayers to be a homogenous, invariable, sea of lipids whose only function is to compartmentalize organelles and carry membrane proteins randomly distributed across the membrane. This was for decades the generally accepted fluid mosaic model[13]. However, the understanding of the complexity of the membranes has increased over the years as we have developed more advanced tools. The bilayer is not a homogenous and invariable entity, which I will try and illustrate in this introduction. Before I describe the interplay between membrane proteins and properties of the bilayer, I will take some time to get to know the bilayer itself.

The choice of lipids and concentration of them helps the organisms to mold their membranes in to exactly what they need. The lipid metabolites and pathway strategy (LIPID MAPS) structure database currently contains over 37,000 different lipids[14], but

could theoretically be expanded to over 100,000 species[15], illustrating how much effort life spends on varying these compounds to suit different needs.

Lipid classification

The lipids are usually divided into three main groups: phospholipids, glycolipids and sterols (Figure 2.2). The head groups are either anionic or zwitterionic. Phospholipids can either be phosphoglycerides, most often built on glycerol-3-phosphate, or sphingolipids. Sphingolipids are built on a long-chain amino alcohol called sphingosine. Glycolipids are sphingolipids with a sugar instead of phosphate. Sterols and linear isoprenoids are derivatives of isoprene (2-methyl-1,3-butadiene).

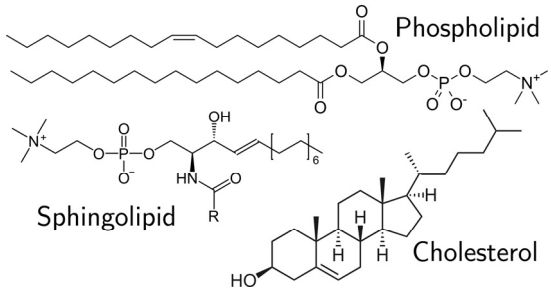

Figure 2.2 Examples of three common lipids. Phospholipids are usually made up by a phosphate group and a glycerol derivate. When a lipid is instead made up by an amino alcohol it's a sphingolipid. Cholesterol is the most common sterol.

Lipids in cells

The types of lipids and their concentration can be different depending on which side of the bilayer you're looking at. The observation of this asymmetry led to the discovery of the phospholipid transportation enzymes: flippases, floppases and scramblases[16–18]. Not only can lipid composition differ between inner and outer leaflet, they can polarize laterally into micro-domains called lipid rafts (Figure 2.3). When compared to the rest of the bilayer these rafts are enriched in sterols or sphingomyelin, giving them different properties such as increased thickness and decreased fluidity[19–22]. The discovery of lipid rafts helps us realize that the bilayer is a heterogeneous milieu where local microenvironments constantly are created and dissipated.

Prokaryotes have little to none of the sterols while it can vary up to 25% of dry membrane weight in eukaryotes[23]. The sterols interact with other lipids mainly through the hydrophobic effect, but prefers sphingomyelin because of hydrogen bonding with its amide head group[24,25]. Since sterols are bulkier and more rigid they fill out the space in between normal lipid tails, lowering their hydrocarbon chain flexibility and

increases bilayer packing density. This in turn lowers solute permeability and increases bilayer thickness and mechanical strenght[25]. An example of the cholesterol effect is that membranes with typical concentrations of cholesterol demonstrate a very low CO_2 permeability[26]. Depletion of cholesterol can increase this permeability by a factor of two[26].

Sphingolipids are a major component of plant plasma membranes[27]. Up to 40% of the plasma membrane can consist of sphingolipids and they tend to enrich the outer leaflet[28]. A notable example of adaptation is how plants handle phosphate shortage. During those times the phospholipids in the plant bilayers are replaced with galactolipids[29,30]. These non-phospholipids are similar to sphingolipids but lack the nitrogen. Most research on sterols in bilayers is done on cholesterol, but plants employ different kinds, such as stigmasterol and β-sitosterol. However, they exhibit similar, although not entirely equal, properties as cholesterol[31], thus studies done on cholesterol can mostly be transferrable to plant physiology.

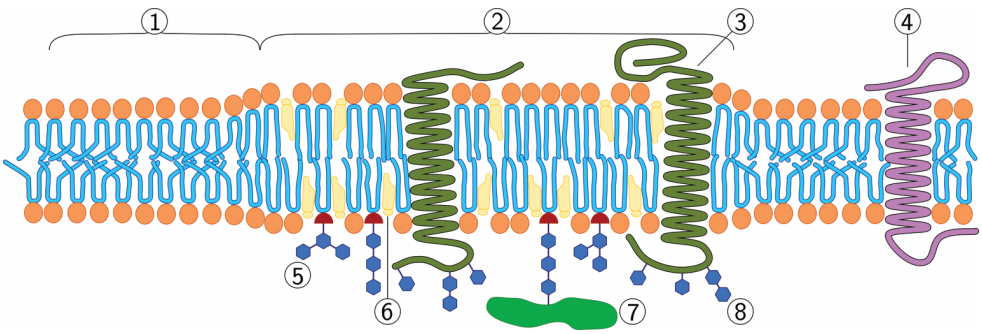

Figure 2.3 A simplified cross section view of a lipid bilayer. 1) Lipid bilayer 2) A cholesterol enriched raft portion 3) Transmembrane protein that preferentially moves into rafts 4) Transmembrane protein that preferentially moves into normal areas 5) Glycosylated lipid 6) Cholesterol 7) GPI-anchored protein 8) Glycosylated protein. Image based on original by Artur Jan Fijałkowski, distributed under a CC-BY 2.5 license.

2.4 Interplay between proteins and the lipid bilayer

The most important realization in this area of research is that bilayers do not only function to carry membrane proteins. Lipids have been shown to interact with, and help regulate, proteins. Some proteins are not stable without certain lipids, and some are not even functional. There's also a wide array of mechanosensitive proteins that are gated by external mechanical forces acting upon the lipid bilayer. In the following paragraphs I will exemplify this interplay between lipids and proteins.

Thickness and elasticity

There are many examples of proteins being altered by the bilayer thickness or elasticity: The maltose ABC transporter[32], the sugar transporter melibiose permease[33], diacylglycerol kinase[34], several ion channels[35], mitogen activated protein kinases[36], and the water transporters Aquaporin 0[37] and Aquaporin 4[38]. These findings all point towards an importance in matching the bilayer thickness with the hydrophobic regions of transmembrane proteins.

Protein-lipid direct interaction

Direct interaction with specific lipids is important for many protein functions. Acidic phospholipids has been show to affect activity of a variety of membrane proteins, including the translocon SecA[39–41], the neurotensin receptor 1[42], the nicotinic acetylcholine receptor[43], and a transmembrane bacterial chemoreceptor[44]. Similarly, cholesterol has been implicated in regulating membrane proteins such as the endothelial inward-rectifier potassium channel[45,46], and a calcium-activated potassium channel[47]. Cardiolipin is needed for functionality and stability in mitochondrial membrane proteins, such as: cytochrome c oxidase[48,49] and several carriers[50,51]. This dependency amongst the mitochondrial proteins is not very surprising as the mitochondrial membranes contain up to 20% cardiolipin[52].

Mechanosensitivity

Many ion-channels are mechanosensitive which makes it possible to respond to external stimuli such as sound, touch, gravity and pressure. The first mechanosensitive channel protein was found in 1983 by Falguni Guharay and Frederick Sachs in the skeletal muscle of chicken[53]. The now most characterized of these is the bacterial large-conductance mechanosensitive channel (MscL)[54]. Mechanical stimuli has been also been implicated to modulate function of at least four different water channels[37,55–57].

Lipid rafts

Lipid rafts has been seen to be enriched in glycosylphosphatidylinositol-anchored (GPI-anchored) proteins and certain transmembrane proteins[58–60] (Figure 2.3). Specifically it seems that rafts are used as a sorting mechanism in the Golgi apparatus to traffic proteins to the plasma membrane[61,62]. The enrichment of sterols in rafts increases the thickness of the bilayer. This can in turn make protein preferentially partition into these rafts as they want to minimize hydrophobic mismatch. The opposite could also be true; membrane proteins could induce rafts by recruiting sterols as a lipid shell.

3. Water transport across the cell membrane

All cell membranes are somewhat permeable to water due to diffusion through the lipid bilayers. This was also thought to be the main mode of water transport in cells for the longest time. The first entry of water pores in the literature comes from 1957 when Paganelli and Solomon measured the surprisingly high diffusion rate of water across human red blood cells[63]. To account for this they suggested that cylindrical water pores 3.5 Å in diameter were present in the membrane. An alternative hypothesis suggested kinks and defects in the lipid bilayer as a possible explanation for this diffusion deviation[64], but further evaluation calculated that such irregularities account for no more than 10% of the increased water flow[65].

In 1988, when Peter Agre's group was working on the rhesus blood group antigens they isolated an unknown 28 kDa protein that kept appearing on their gels[66]. They were intrigued, since as much as 20% of the initial purifications consisted of this contaminant.

Three years later, in 1991, they had managed to isolate the cDNA and found it to be related to proteins in a large variety of organisms: bacteria, plants, flies, and cows[67]. Since the protein seemed to exist in all kingdoms of life, and was present in both membranes of red blood cells in renal tubules, they speculated that this was the long sought for water channel. After a most likely intense year of research they published their proofs that this unknown 28kDa protein indeed was a water channel[68]. By injecting *Xenopus* oocytes with aquaporin cDNA and then measured swelling rates in response to osmotic shock they could see a dramatic increase in permeability compared to their controls. Their discovery gave Peter Agre the Nobel Prize in Chemistry in 2003.

3.1 The aquaporin family

Most membrane proteins can be divided in to three large classes: transporters, receptors and enzymes[10] (Table 3.1). Transporters transport atoms, ions, molecules and electrons across the membrane and responsible for maintaining homeostasis or creating biochemical gradients. Receptors are information mediators. They receive a signal in form of a binding ligand, and upon doing so they creates a cellular response.

The transport proteins are divided into three major families: 1) channels, which are either ion channels or aquaporins, 2) active transporters, which are either ABC-

transporters or ATPases, and 3) the solute carrier superfamily[10]. Transport occurs either downstream the gradient (passive transport), or upstream the gradient, using either an energy source such as ATP (primary active transport) or a coupled transport of a second solute travelling downstream (secondary active transport).

Aquaporins, which is the topic of this thesis, belong to the channel class of membrane transporters. They are passive transporters, always netting a water transport downstream an osmotic gradient. Even though the notion of a water channel may seem simple at first glance, it is an essential protein for all multicellular organisms and has a highly complex mechanism that ensures that ions and large molecules are excluded from the pore.

Table 3.1 Membrane proteins are divided into three major families which are then further divided into sub-classes. The genes are the amount estimated in the human genome. All data taken from Almén *et al.*[10].

Family	Class	Genes	Family	Class	Genes
Receptors	G-protein coupled and 7TM receptors	901	Transporters	Aquaporins & ion channels	250
	Receptor-type kinases	72		Solute carrier superfamily	2393
	Receptors of the immunoglobulin superfamily and related	149		Active transporters	81
	Scavenger receptors and related	63		Other transporters	51
	Other receptors	167		Auxiliary transport proteins	42
Enzymes	Oxidoreductases	123	Miscellaneous	Structure/Adhesion proteins	187
	Transferases	194		Ligand proteins	181
	Hydrolases	178		Protein of unknown function	57
	Lyases	17		Other	272
	Isomerases	5		Auxiliary transport proteins	42
	Ligases	6			
	Multuple EC proteins	6			

In mammals there are 13 aquaporin homologues (AQP0-12) expressed in a wide variety of tissues[69–71]. Human aquaporins concentrate urine in the kidneys[72,73], maintains lens transparency in eyes[74], maintains water homeostasis in the brain[75], keeps the skin moist[73], and is involved in tumor progression[76] just to mention a few examples. These twelve are divided into three subgroups based on homology and substrate specificity: aquaporins (AQP0,1,2,4,5,6,8), aquaglyceroporins (AQP3,7,9,10), and superaquaporins (AQP11,12)[77]. In addition to water the mammalian aquaporins have been shown to transport glycerol[78–82], urea[78,79,81,83], anions[84–86], CO_2[26,87,88], NH_3[87,89], hydrogen peroxide[90] and arsenite[91]. Aquaporins appear to serve a lot more functions than first believed.

3.2 Plant aquaporins

Have you ever wondered how plants move water from soil, through their roots and stem, to their leaves? The cohesion-tension theory has been the leading theory for over 100 years. In short, leaf evaporation lowers the water potential in the leaves, causing new water to move in from the stem. This in turn, creates a capillary effect throughout the plant, causing an inflow of fresh water from the soil through the roots[92]. Another important concept in plant physiology is turgor pressure. When the vacuole of a plant cell fills up the cell exert an outward pressure on the cell wall. This turgidity is what the plant relies on to maintain rigidity, as well as being used for cell expansion[93], opening and closing of the stomata[94] and being the driving force in opening and closing of petals[95].

The diversity of plant aquaporins

Plants demonstrate an even wider variety of aquaporins than mammals. There are 35, 36, 37, 33, 28 and 66 aquaporin homologues expressed in *Arabidopsis thaliana*[96], maize (*Zea mays*)[97], tomato (*Solanum lycopersicum*)[98], rice (*Oryza sativa* L. cv Nipponbare)[99], grapevine (*Vitis vinifera* L)[100], and soybean (*Glycine max* L)[101] respectively. Based on sequence homology, the plant aquaporins are divided into seven classes with the main five being: tonoplast intrinsic proteins (TIPs), plasma membrane intrinsic proteins (PIPs), NOD26-like intrinsic proteins (NIPs), small basic intrinsic proteins (SIPs)[102] and uncategorized X intrinsic proteins (XIPs)[103,104]. The remaining two classes have only been identified in some species of moss: GlpF-like intrinsic proteins (GIPs)[103,105], and hybrid intrinsic proteins (HIPs)[103,105].

PIPs are the most abundant aquaporin in the plasma membrane while the TIPs are the most abundant in the tonoplast (vacuolar) membrane[96,106]. NIPs localize to the plasma membrane[107,108] or the endoplasmic reticulum[109], but are most prevalent in the peribacteroid membrane of nitrogen-fixing symbiotic nodules of legume roots. SIPs localizes to the endoplasmic reticulum[110,111].

Aquaporins facilitate more than just water

As has been discovered the past ten years, the plants take up a variety of other solutes through the aquaporins in their roots. Plant aquaporins have been shown to transport urea[112,113], glycerol[112–115], formamide[89,115], acetamide[115], boric acid[108,113], silicic acid[107], lactic acid[116], methylammonium and NH_3[89], CO_2[117,118] and hydrogen peroxide[90].

The large number of plant aquaporin homologues and substrate specificities reflects the different life plants lead. Tight regulation of water flow is necessary to maintain water homeostasis in all organisms, but more so in plants. Plants are quite immobile and very dependent on the local environment for their survival, so they need to regulate their water intake and outflux in response to either sudden (e.g. flooding or drought) or gradual environmental changes (e.g. the night/day cycle). Apart from the transcriptional and translational regulation, which I will not go into detail here, there are two more direct modes employed: trafficking and gating, acting on the location and conformation of the actual protein.

3.2.1 Trafficking

Protein trafficking refers to how membrane proteins are regulated by transportation between different organelle membranes and vesicle membranes. The most studied aquaporin regulated by trafficking is AQP2, which is a vasopressin regulated water channel in the human kidney[119], but what is known about plant aquaporin trafficking?

Effects of osmotic stress

Osmotic and salt stress induces a relocalization of plasma membrane aquaporins in plant roots[120–123]. In the plant *Mesembryanthemum crystallinum*, McTIP1;2 is glycosylated and relocalized to the endosomal compartments during osmotic stress[121]. Under salt stress both AtPIPs and AtTIPs are heavily decreased in the plasma membrane, both by downregulation of expression and by relocalization into subcellular compartments[122]. This relocalization is mediated through hydrogen peroxide induced

dephosphorylation of the C-terminus[124]. Exactly why this regulation happens and what the effects are is still not entirely clear.

Heterotetramerization

When PIP1s are expressed alone in oocytes, they generally show little to no water transport where PIP2s, on the other hand, show a remarkable increase in water permeability[125]. It turns out that PIP1s does not localize to the plasma membrane correctly when expressed alone, and that they heterotetramerize with PIP2s *in vivo* to be correctly targeted to the plasma membrane. *In vivo* studies has confirmed that PIP1s are retained to the endoplasmic reticulum when expressed alone, but when co-expressed with PIP2s they are both correctly trafficked to the plasma membrane as a result of interactions between the two[126].

Several PIPs has a di-acidic motif in the N-terminal which can act as an endoplasmic reticulum (ER) export signal. When this motif was mutated in AtPIP2;1, ZmPIP2;4 and ZmPIP2;5, they were retained in the endoplasmic reticulum[127,128]. However, ZmPIP2;1 lacks this motif and is still exported, and inclusion of the motif in the N-terminal of ZmPIP1;2 was not sufficient for exportation[128]. There must be some additional, currently unknown, export or retention signal.

Membrane polarization

Although many aquaporins are homogenously distributed in the membrane, there are more and more instances where a polarization has been observed. The boron acid aquaporin AtNIP5;1 and the silicic acid aquaporin OsNIP2;1 are both preferentially trafficked to the outward facing plasma domains of root cells[129,130]. A single-molecule analysis of AtPIP2;1 in roots using variable-angle evanescent wave microscopy and fluorescence correlation spectroscopy showed a heterogeneous distribution in the plasma membrane and that membrane rafts and clathrin were involved in the subcellular cycling that followed salt stress[131]. Clathrin is a protein that plays a major role in creating the small vesicles used in cycling.

3.2.2 Gating

Regulation of mRNA transcription, protein translation, and protein trafficking, all work by regulating the physical presence of protein in the membranes. Protein gating works on the protein itself, and involves conformational changes often triggered by post-

translational modifications. Aquaporin gating is based on amino acid residues physically occluding the water conducting pore. These conformational changes are induced by either indirect or direct signals. Direct signals can be a change in pH where protonation of residues induces the gating, or binding of calcium. An example of indirect signal is phosphorylation where the kinases are the key proteins that respond to stimuli.

PIP and TIP gating

PIP aquaporins have a gating mechanism that can respond immediately to changes in pH, calcium concentration and phosphorylation[132]. Flooding of plant roots cause a rapid decrease in cytosolic pH due to anoxia[133], which leads to the closing of most PIP water channels in the plasma membrane[134–138]. The pH dependency of this gating is attributed to the protonation of a conserved histidine residue in an intracellular loop[132]. Calcium changes has a similar effect on PIP where an increase in cytosolic levels of Ca^{2+} almost completely inhibits the water transport[134,135,137]. Phosphorylation, one of the most common post-translational modifications, has been seen in a wide array of plant aquaporins including PIP2s where it increases their activity[139–143]. Upon drought the serine is dephosphorylated which lowers the water transport activity and closes the stomata[141]. Some TIP aquaporins has also been shown to be gated by pH, although the feature is not as common as with PIPs. VvTIP2;1[144] and AtTIP5;1[145] is inhibited by low pH attributed to a histidine in Loop D – similar to PIPs.

3.3 Structural features

To date, the crystallographic structure of eleven different aquaporins have been solved; five mammalian, AQP0[146], AQP1[147], AQP2[148], AQP4[149] and AQP5[150]; one yeast, Aqy1[56]; two from bacteria, AqpZ[151] and GlpF[152]; one from an archaea, AqpM[153]; one from the malarial parasite *Plasmodium falciparum*, PfAQP[154]; and one from the plant S*pinacia oleracea*, SoPIP2;1[132]. Together they have helped in shaping the current understanding of the aquaporin's structural features and the relationship to their function.

The functional unit of aquaporins is a homotetramer with each monomer independently transporting water in single file arrangement through the pore (Figure 3.1. All aquaporins consist of an α-helix bundle (1-6) with both their termini on the cytoplasmic side. There are five loops (A-E) where Loop B and D each fold into a half

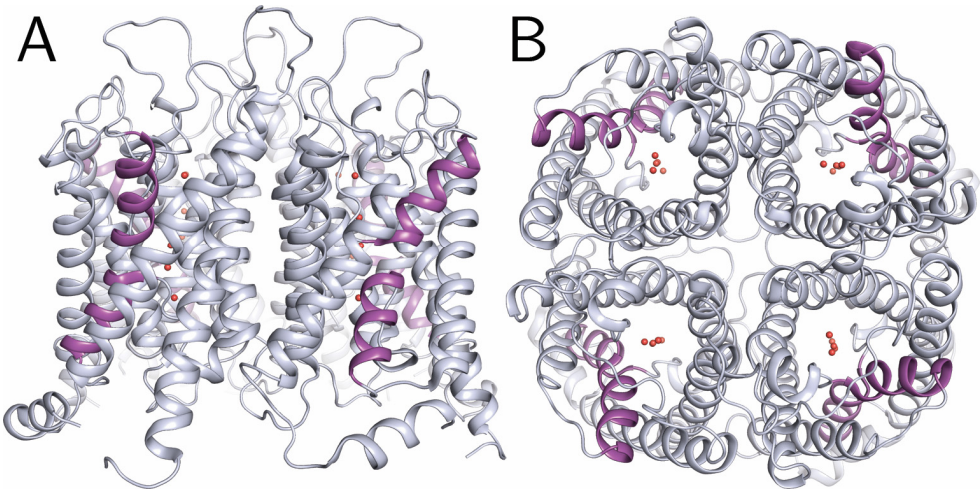

Figure 3.1 A) Front view of the AQP1 tetramer (PDB ID: 1J4N) with the half helices colored magenta. B) Top view of AQP1 tetramer showing the four fold symmetry and the single file transport of the water molecules in each pore.

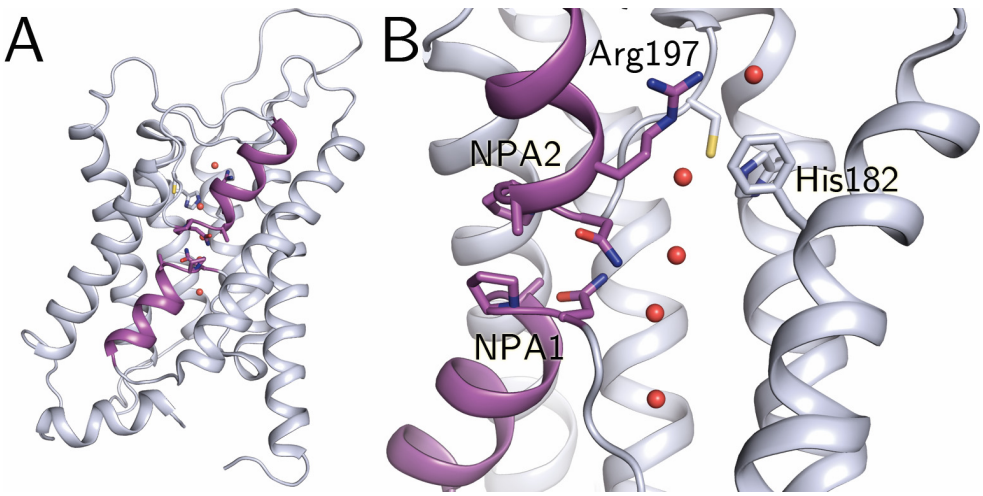

Figure 3.2 A) The AQP1 monomer with the half helices highlighted in magenta. B) Zoom in on the NPA-motif and selectivity filter with the highly conserved Arg197, and, to a lesser extent, His182.

helix that dips into the channel from each side, forming a seventh pseudo-transmembrane helix containing two copies of the highly conserved Asn-Pro-Ala (NPA) motif aligned in the central region of the pore (Figure 3.2).

Near the end of the extracellular side of the water pore four amino acid residues make up what is called the aromatic/arginine selectivity filter (SF). In AQP1 they consist of a His182 in helix 2, a Phe58 in helix 5, a Cys191 and an highly conserved Arg197 in Loop E[155] (Figure 3.2). The configuration of these four residues creates a narrow passage, 2.8Å in diameter, which sterically hinders all molecules larger than a water molecule from passing through. In the aquaglyceroporins this selectivity filter is altered to accommodate larger molecules[152,154].

3.3.1 Structural basis for aquaporin proton exclusion

The most remarkable feature of the aquaporin is its ability to exclude protons while maintaining near diffusion transport speed of water across the membrane[156]. Without this feature the organism would not be able to maintain a proton gradient across its membranes – dissipating the proton motive force needed for ATP-synthesis. The proton exclusion mechanism is not truly understood as of this writing, but many of its key aspects have been elucidated.

The Grotthuss mechanism

Before understanding how protons are excluded from the aquaporin water channel, the mechanism behind how protons are diffusing in water must be understood. Proton mobility in water is 5-8 times higher than that of other cations[157] which makes it apparent that there are other mechanisms in play, in addition to pure H_3O^+ diffusion.

In 1806 C.J.D. von Grotthuss proposed the first mechanism for proton diffusion in water where protons are rapidly transferred between water molecules via hydrogen bonds and transient hydronium ions[158]. Since then simulations[159–161] and experiments[162] has observed this complex phenomena to be true in essence, although the mechanistic details remains a topic of interest. Surely this proton conducting wire is what has to be broken in the aquaporin pore.

MD simulations[132,155,163,164] and X-ray crystallography[165] have shown that the oxygen in water aligns with the NPA-motif and that the water molecule undergoes a rotation through the pore, creating a bipolar orientation in the two halves of the channel. This would break the proton conducting wire needed for the Grotthuss mechanism.

Electrostatic barriers

A review from 2005 concludes that the proton exclusion mainly come from electrostatic effects from the NPA-motif and helix B and E macrodipoles[166]. This turned out to be contradicted by a later study where mutations in the NPA-motif and the selectivity filter were introduced[167]. When the asparagine in the NPA-motif was neutralized cation transport increased, but proton transport did not. When the selectivity filter's arginine and histidine were changed, to the much smaller alanine and valine, proton transport increased but cation transport did not. Proton exclusion turned out to be more reliant on the selectivity filter itself than on the NPA-motif, and the opposite was true for cations.

A collaboration between NPA and the selectivity filter

A follow up study looked further into the selectivity filter's role in more detail[168]. The selectivity filter works together with the NPA-motif in creating an electrostatic barrier, and to orient water molecules in such a way as to minimize hydrogen bonding for hydronium ions. They reasoned that, evolutionary, the NPA-motif arose first as a mean to mainly exclude cations, and that the selectivity filter came later to more effectively exclude protons through synergetic coupling to the NPA-motif.

In the subangstrom X-ray structure of a yeast aquaporin the high resolution allowed for some hydrogen bonds of the water molecules inside the pore to be visualized[165]. Each NPA-asparagine was seen to hydrogen bond to one water each, in contrast to the previously depicted situation where both asparagines hydrogen bonded to the same water molecule. This suggests that a central water molecule bonding to both asparagines could not be the main component preventing proton transport through the Grotthuss mechanism as often previously proposed. In the selectivity filter, however, four adjacent water molecules were modelled with partial occupancy. The electron density was too close to allow all four pockets to be occupied simultaneously. The findings led to the hypothesis that the two water molecules moves pairwise through

the selectivity filter while maintaining two hydrogen bonds each with the selectivity filter's His212 and Arg227. As the waters move through the selectivity filter, all four hydrogen bonding donor and acceptor interactions are filled, preventing proton transport via the Grotthuss mechanism.

This structure have contributed to the current consensus that the selectivity filter highly coordinates the water molecules in such a way that it disrupts the Grotthuss mechanism while the NPA-motif is responsible for the rotation of the water molecules through the pore. Furthermore, the NPA-motif together with the helix dipoles creates an electrostatic barrier that excludes cations from passing through. Aquaporins is an excellent example of how much evolutionary fine tuning can provide selectivity in channels, without compromising the transport speed.

3.3.2 The mercury effect

In 1970 Macey *et al*. was one of the first to discover the inhibitory effect of mercury on water transport across membranes[65,169]. With the addition of p-chloromercuribenzoate the osmotic water permeability of human red blood cells decreased 70%. Because this inhibitory effect is reversible with the addition of excess cysteine this further strengthened the hypothesis that water was transported by other means than just passive membrane diffusion. The mercury test has been readily used to test the activity of aquaporins, although nowadays the much less toxic mercury chloride is used.

Inhibition by mercury

Two inhibitory mechanisms have been shown for the aquaporins. In both cases the mercury ions bind to free cysteines in the protein. In the most common case, the responsible cysteine is located inside the water channel, making the binding mercury ion either sterically hinder any water transport[170,171] or, as shown by MD simulations, collapse the selectivity filter[172]. In the second case the mercury ion binds to cysteines further from the center, but is thought to induce a conformational change that constricts the pore[173,174].

Activation by mercury

Even though most aquaporins are either inhibited or unaffected by mercury there are a few rare exceptions. A notable example of the contrary is AQP6. When first studied it

was seen to be inhibited by mercury[175], but was later shown to instead be activated by mercury[86]. The water permeability was much lower than for AQP1, and the channel also transported anions. A follow up study confirmed the activation and located two cysteines that were responsible for the effect: Cys155 and Cys190 not located inside the water conducting pore itself[84]. When the two residues were mutated to alanine, the activation was abolished. A structural explanation for this activation still eludes us as no structure of AQP6 has been solved yet.

In **Paper II** we discovered that SoPIP2;1 was activated with the addition of sub-millimolar concentrations of mercury chloride. As further discussed in the results section this is a peculiar behavior since most aquaporins are either unaffected or inhibited by mercury. SoPIP2;1 doesn't share any cysteines with AQP6, or AQP1, so the mechanism by which this activation happens is most likely different from what is previously known.

3.3.3 Gating mechanisms

With high resolution structures comes the ability to investigate gating mechanisms in proteins. Here I will summarize what is known about aquaporin gating in Aqy1, AQP0 and AqpZ. The gating mechanism of SoPIP2;1 will be thoroughly evaluated in the results section.

Aqy1

The *P. pastoris* aquaporin Aqy1 is gated by its elongated N-terminus which was shown by its markedly increased activity in spheroplast assays when the N-terminus was deleted[56]. Each N-terminus in the tetramer intertwines with its neighboring monomer, creating a helical bundle. In turn, three conserved residues interacts to close the pore; an N-terminal tyrosine inserts into the water channel where it creates a hydrogen network between two water molecules and two glycines, tightening the pore diameter to 0.8 Å. Phosphorylation of a serine that sits in close proximity to the tyrosine, can in turn override this mechanism. MD simulations show that when the serine is phosphorylated the pore closing tyrosine is pushed out of the way[56].

Aqy1 was suggested to be mechanosensitive, opening its pore due to changes in membrane curvature or lateral pressure. In spheroplasts expressing an N-terminal truncated form of the aquaporin, the transport rate was increased 6-fold compared to wild type aqy1. However, when the same constructs were purified and reconstituted

into liposomes their activities were indistinguishable. This could possibly be explained by the fact that liposomes (100-500nm) have a membrane curvature that is a lot higher than in spheroplasts (1-5µm). Molecular dynamics simulations was used to apply lateral pressure, and to bend the membrane, and in both cases an opening of the channel was seen[56].

AQP0

AQP0 is a very interesting aquaporin because of its low water permeability[176] and its role in creating cell junctions[177]. In lens fiber cells they are so abundant that they form a quasi-crystalline state that maintains the lens transparancy[146]. In AQP0 a second constriction site is present at the cytoplasmic side of the pore where Tyr149, Phe75, and His66 narrows the diameter to 2 Å[178] or 1.5Å[146], widths that would allow zero water conductance. It is strange then that AQP0 shows water permeability in oocytes and proteoliposomes. The authors argue that the structure can fluctuate enough to widen the pore to >2.9Å, allowing for some passage of water but at a the cost of higher activation energy[146].

How is this protein gated then? AQP0 is modulated by calmodulin, a common signaling molecule that responds to changes in Ca^{2+} concentrations. When calmodulin then binds to the AQP0 tetramer it forces Tyr149 in the cytoplasmic restriction site to narrow the pore even further, thus completely abolishing its water transport capability[179].

A decrease in pH has been shown experimentally to increase the water transport rate of AQP0[180], but all structures determined at low and high pH has given contradictory results and has not revealed any mechanism for this gating[181].

AqpZ

In the bacterial AqpZ, Arg189 of the selectivity filter has been seen to flip between two conformations in both MD simulations and crystal structures[182]. In the first conformation the arginine points upwards towards the extracellular medium, making the channel open. In the second conformation the arginine points downwards into the channel, occluding the pore. It's suggested that protein-protein interactions in the protein crystal is responsible for the stabilization of two distinct conformations of arginine189, although the physiological relevance for this is still a mystery.

4. Methodology in membrane protein research

4.1 Artificial membrane protein carriers

The difference between soluble proteins and membrane proteins is apparent already in their naming. The natural environment for membrane proteins is a lipid bilayer. This creates one of the biggest challenges in membrane protein research: creating an environment in which the protein is stable, functional and accessible for probing. The intrinsic hydrophobicity of membrane proteins makes them prone to irreversible aggregation and improper folding in lab environments. In contrast, soluble proteins can often be stored long periods of time as lyophilized powder and readily refolds once liquid is added[183]. How can these important research targets be kept in an environment where they are easily manipulated and studied, while maintaining their integrity and stability?

4.1.1 Detergent micelles

Most of the methods involving protein research involve having the protein in solution. In order to solubilize membrane proteins the bilayer has to be removed without irreversibly damaging the protein. This is done using amphipathic molecules called detergents that most often consist of a single hydrophobic tail, and a polar or charged head group (Figure 4.1). They differ from lipids in that they are conical in shape and spontaneously form micelles above a certain critical micelle concentration (CMC) that is unique for each type of detergent. Longer chain detergents, that are more hydrophobic, typically have a lower CMC because their monomeric form is less soluble. (Table 4.1). Each detergent also has a specific aggregation number associated with it, which is the average number of detergent molecules per micelle (Table 4.1).

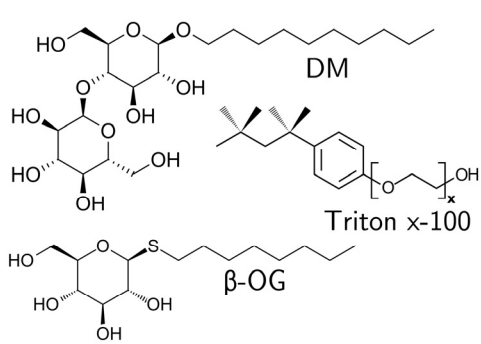

Figure 4.1 Examples of common detergents in membrane protein research. n-Dodecyl-β-D-maltoside (DM), n-octyl-β-D-glucoside (β-OG) and Triton x-100.

4.1.2 Liposomes

A way of mimicking the original lipid bilayer is to form artificial ones from purified lipid mixtures (Figure 4.2). These liposomes are optimally formed to be small unilamellar vesicles (SUVs) with diameters ranging from 100nm to 500nm. Reconstituting membrane proteins in to these liposomes is a common way to study transport over membranes. Not only does this provide a compartmentalized environment, it also creates a lipid environment more like the one *in vivo*. The lipid composition can be adjusted to suit the membrane protein but most often simple systems of 1-palmitoyl-2-oleoyl-sn-glycero-3-phosphocholine (POPC) or *E. coli* extracts are used.

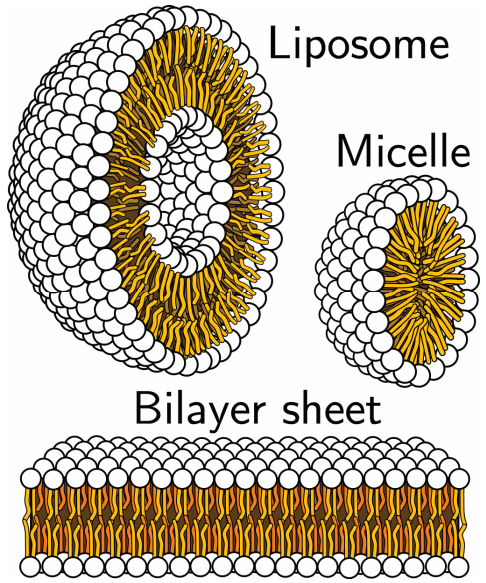

Figure 4.2 Three forms of membrane protein carriers. Liposomes have a lot smaller diameter than cells and have a lot higher curvature. Micelles can form if an amphipatic molecule has a conical shape.

4.1.3 Nanodiscs

Although liposomes provide a lipid environment, the method of reconstitution is quite crude. Furthermore, the vesicles are heterogeneous in size, form and in amount of protein reconstituted. The development of small discoidal bilayers called nanodiscs provides us with a new platform for working with membrane proteins (Figure 4.3). In this system two copies of a membrane scaffold protein (MSP, a derivative of human apolipoprotein A-1) wraps around a certain amount of lipids, creating a soluble bilayer[184]. The size of these nanodiscs can be precisely controlled by modifying the scaffold protein[185,186] making it possible to insert a single copy of a membrane protein complex in each disc. This property of the nanodiscs gives us the option of creating a homogenous population of soluble membrane proteins without the need of detergent, thereby eliminating many of the problems caused by detergent micelles and liposomes. Although the lack of compartmentalization makes it a less viable option for transport

assays, the system is well suited for studying binding of substrates, protein-protein interaction, protein dynamics, protein-lipid dependencies and more.

Many membrane proteins has already been reconstituted into nanodiscs including, but not limited to: ABC transporters[188], the translocon complex SecYEG[41], several G-protein coupled receptors (GPCRs)[189–191], Soluble NSF Attachment Protein Receptors (SNAREs)[192–194], bacterial outer membrane proteins[195] and several Cytochrome P450s[196,197]. In addition to this, the nanodiscs have already proven to be a viable technique for structural studies using SAS[190], NMR[198], EPR[193], Cryo-EM[41], and FRET[193].

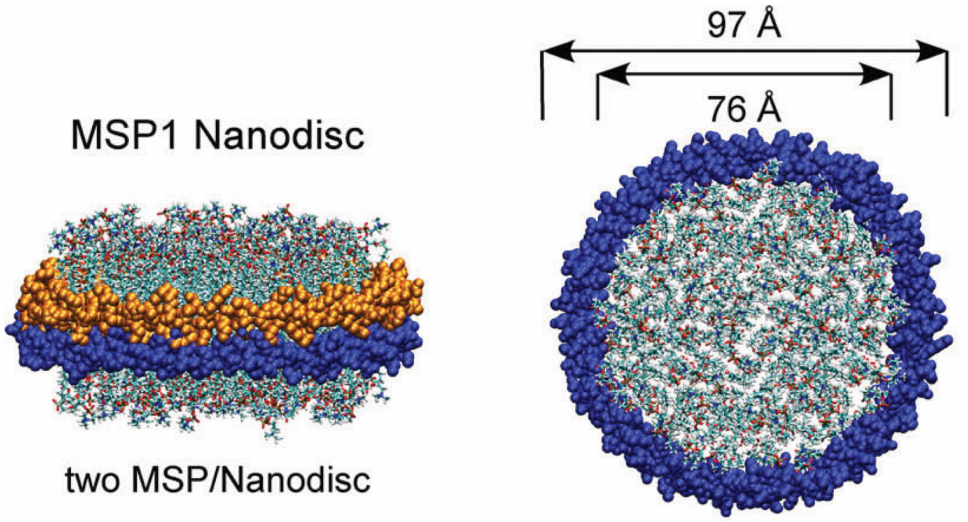

Figure 4.3 Side view, and top view of a nanodisc made from MSP1. The MSP wraps itself around a bilayer sheet, and because of the protein's fixed size, the diameter of the nanodisc is defined. Reprinted with permission from Stephen Sligar[187].

4.2 From gene to purified membrane protein

Target proteins have to be isolated and purified to suit the needs of the experiments and studies conducted. This can be a long a tedious journey – especially for membrane proteins. In theory the production and purification proceeds in a linear manner from cell cultures and membrane preparation to solubilization and chromatography purifications (Figure 4.4), but generally reality requires multiple iterative trial and error phases before a successful protocol can be established.

4.2.1 Cloning and overexpression for protein production

The choice between bacteria, yeast and insect cell hosts still has to be chosen from a protein to protein basis. The advantage of using a eukaryotic host for protein production is its ability to do post-translational modifications (e.g. glycosylation, disulfide bond formation, and proteolytic processing), its translocon mechanisms and differences in lipid composition[199]. S*accharomyces cerevisiae* has commonly been the major host for eukaryotic protein production, but in this work *Pichia pastoris* has been used, just as for many other eukaryotic membrane protein targets for structure determination[200].

P. pastoris is methylotropic, which is that it can grow on methanol as its sole carbon source. It was first isolated from chestnut trees in 1920 by the French scientist Guillermond[201], however, the first report of yeasts growing on methanol as the sole carbon source came in the late 1960s[202]. Since then, *P. pastoris* has been developed into a widely used tool for heterologous protein expression[203]. *P. pastoris* can be grown to much higher cell densities than S. *cerevisiae* and the ability to grow on methanol gives us the ability to exploit its incredibly strong aldehyde oxidase promoter for membrane protein overexpression[203]. In turn, the total yield can become higher than with other hosts (cells/liter and protein/cell).

The commercially available vectors for *P. pastoris* includes selectivity towards the antibiotic Zeocin™, which allows simple screening for jackpot clones of extraordinary protein production. When the vector containing the protein coding gene and Zeocin™ resistence is inserted into *P. pastoris*, some cells incorporate multiple copies into their genome. This in turn gives a much higher protein production. The equally higher Zeocin™ resistence can be used to screen for these jackpot clones using a high concentration of it. When

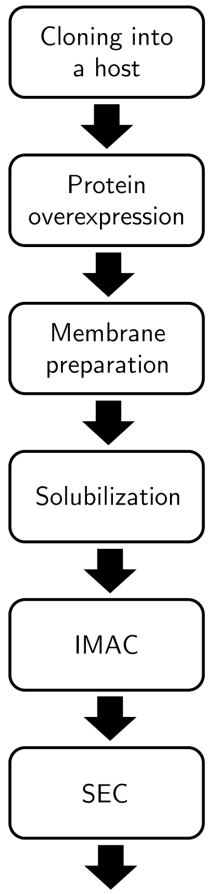

Figure 4.4 The path from cloning to pure protein is long and includes many iterative steps to find the best conditions and protocols for each new protein.

found, the production is scaled up using large volume shaker flasks or preferably fermentors. Harvested cells can be frozen and stored for long periods of time.

4.2.2 Protein purification

For membrane proteins the membranes of the cells have to be isolated in the first step of purification. The cells are lysed using one of the methods available for yeast (e.g. French press or X-Press[204]) and the membranes are spun down. Many protocols includes salt, urea or sodium hydroxide washing steps of the membranes to remove as much peripheral and integral proteins as possible. These can potentially contaminate the purification or interfere with binding to affinity chromatography columns. During the development of a purification protocol for one aquaporin (not in this thesis) I found that urea-washed membranes were sufficient to give pure protein, but a NaOH-wash was still required for the protein to bind to the affinity column.

Once the membranes are isolated, they are solubilized in detergent. Membrane solubilization is a critical step as it moves the protein from the inaccessible lipid environment to the water environment. The goal is to extract as much protein as possible from the membranes, but without harming the protein itself. Sometimes this step can be optimized, not only to get the most of the target protein, but to avoid too much solubilization of unwanted proteins. As always, there is a tradeoff between quality and quantity.

The choice of detergent can be a chapter by itself. In (Table 4.1) many common detergents used in membrane protein research is listed. Typically, membrane proteins are more stable in long chain detergents such as DDM and DM – something that is reflected by the large number of X-ray structures determined using these[200].

During protein purification, all of the target protein's properties have to be exploited to maintain stability and to gain purity during all stages of the process. Much of the development of new purification protocols is purely an iterative process where you make a qualified first guess about where to start and then sees what goes wrong and where.

Recombinant technologies have given us the ability to modify protein genes to suit our needs. Insertion of a poly-histidine tag in either the C- or N-terminus of the protein is very common as it enables the use of immobilized metal affinity chromatography (IMAC). Green fluorescent protein (GFP) is another fusion protein that helps during

all stages of expression and purification of membrane proteins because of its easy detection[205–207].

Most purification protocols ends with a size exclusion chromatography (SEC) step, unless a crude protein sample is satisfactory. With SEC, proteins are separated by their size, with smaller proteins being retained longer in the column. If the protein has a fluorescent tag, the HPLC can be equipped with a fluorescence detector to closely monitor the protein during all stages of purification. Apart from increasing the purity SEC also reveal how monodisperse the sample is. If a protein is prone to aggregation it is easily identified in this step, and the SEC can also be used to evaluate different buffer conditions and the effect they have on protein stability. Furthermore, a calibrated SEC column can be used to estimate protein weight and its oligomerization[208]. The importance of freshly SEC purified protein samples is highlighted in **Paper IV** where it was critical for the success of the experiments.

Table 4.1 A list of common detergents used in membrane protein solubilization, purification and crystallization.

Detergent	Short name	MW (Da)	Charge	Length (# carbons)	CMC (mM)	CMC (%)	N_A	Ref.
n-Dodecyl-β-D-maltopyranoside	DDM	511	N	12	0,17	0,0087%	78-149	[209]
n-Decyl-β-D-maltopyranoside	DM	483	N	10	1,8	0,087%	69-90	[209]
n-Nonyl-β-D-glucopyranoside	β-NG	306	N	9	6,5	0,20%	133	[209]
n-Octyl-β-D-glucopyranoside	β-OG	292	N	8	18-20	0,55%	27-100	[209]
Dodecyl-phosphocholine	FC-12	351	Z	12	1,5	0,05%	54-80	[209]
Decyl-phosphocholine	FC-10	323	Z	10	11	0,36%	24-53	[209]
Polyoxyethylene-(23)-lauryl-ether (C12 / 23)	Brij-35	1200	N	12	0,12	0,014%	N/A	[210]
Polyethylene-glycol P-1,1,3,3-tetramethyl-butylphenyl-ether	Triton X-100	647	N	14	0,23	0,015%	N/A	[210]
Lauryl Maltose Neopentyl Glycol	LMNG	1005,19	N	2x13	0,01	0,001%	N/A	[211]
Octyl Glucose Neopentyl Glycol	OGNG	568,69	N	2x8	1,02	0,0580%	N/A	[211]
n-Dodecyl-N,N-Dimethylamine-N-Oxide	LDAO	229,4	Z	12	1-2	0,03%	76	[212,213]
3-[(3-Cholamidopropyl)dimethylammonio]-1-propansulfonat	Chaps	615	Z	Steroid	2.4-8.6	0,34%	N/A	[210]
3,7α,12α-Trihydroxy-5ß-cholan-24-oic acid	Cholate	430,55	A	Steroid	14	0,60%	2.0-4.8	[214,215]

Charge is either Anionic, Zwitterionic or Neutral. CMC are measured in pure H_2O. N_A is the aggregation number of the micelle

4.3 Protein reconstitution

4.3.1 Proteoliposomes

Purified protein is solubilized in detergent micelles so in order to measure aquaporin activity they need to be transferred into liposomes. The reconstitution can be done in a two main ways, where both of the methods end with a detergent removal from the sample. Since the efficiency of the detergent removal is heavily dependent on the CMC of the detergent used, a detergent with a high CMC is preferred – such as β-OG or cholate (Table 4.1). This presents a problem when the target membrane protein is purified using low-CMC detergents (commonly DM or DDM). Detergent molecules still present after reconstitution introduces defects into the liposomes that make them more leaky or heterogeneous. If the purification detergent can't be changed to a detergent with a higher CMC because of instability issues there is a second possible adaptation. In these instances the reconstitution can still be done if the protein is concentrated enough so that the amount of low-CMC detergent added to the proteoliposomes mixture is as low as possible. However, extended dialysis or buffer exchange might still be needed.

The classical way to form proteoliposomes is to first form the liposomes and then insert the membrane protein (**Paper II**). Typically, lipids are dried to a thin film in a glass container and then rehydrated in a buffer. The lipids then form a mixture of free lipids and multi lamellar vesicles (MLVs) which are further treated by either sonication[216] or extrusion[217] to create small unilamellar vesicles (SUVs). A detergent is added drop wise up to a concentration where the liposomes become slightly destabilized, but without rupturing. After incubation with protein for some time, the detergent is removed by either dialysis or dilution, resulting in reconstitution of the membrane protein into the lipid bilayer.

A different method is to reconstitute the membrane proteins at the same the liposomes form (**Paper III**). First a mixture containing all elements is created: lipids, detergent, buffer, and protein. It is important that the detergent concentration is high enough to completely solubilize the lipids into micelles. The detergent can be removed by either dialysis, dilution or the use of polystyrene beads, called BioBeads[218], that preferentially adsorb detergent molecules through hydrophobic interactions. When the detergent concentration is diminished the lipids will spontaneously form protein-containing liposomes (proteoliposomes) of a very specific size, dependent on type of lipid and

buffer conditions. The method produces a larger amount of proteoliposomes which is crucial for a good signal-to-noise ratio in stopped-flow measurements.

4.3.2 Nanodiscs

The method for creating nanodiscs is very much like the proteoliposome reconstitution protocol but with the addition of membrane scaffold proteins and much more closely regulated parameters. The most important factors to consider for optimal yield are the lipid-to-protein ratios as well as temperature and choice of detergent (Table 4.2). Just as for proteoliposome formation, the choice of a detergent with a high critical micelle concentration is preferred as it is much easier to remove through the use of BioBeads or dialysis. It is also important that the lipids can be fully solubilized in the detergent. Typically cholate is used but not all membrane proteins are stable in this detergent. In those cases a different detergent can be used for purifying the membrane protein itself but still using cholate as the reconstitution detergent.

The best lipid-to-protein ratio is the one that has just the right amount of lipids to fit into the theoretical maximum yield of nanodiscs[219]. An excess of lipids can trigger formation of non-discoidal structures or exclusion of the target membrane protein from the nanodisc. Thus the preparation of lipid stock solution has to be meticulously prepared. A precise volume of lipid-chloroform solution is dried in a pre-weighted glass vessel under nitrogen gas for a couple of hours. The exact amount of lipids can then be measured by weight before solubilization in a cholate buffer.

Many experimental trial and errors have shown that the assembly process is optimal at temperatures slightly above the main phase transition of the lipids used[219]. The assembly temperature for nanodiscs made with POPC is 4°C as its transition temperature is -2°C[220].

Table 4.2 Recommended reconstitution temperatures depending on lipid type and the nanodisc properties depending on what membrane scaffold protein and lipids used. Data taken from[219].

	POPC	DMPC	DPPC	Diameter (Å)	Bilayer area (Å^2)
MSP1D1	61	77	82	98	4400
MSP1E1D1	79	102	106	106	5700
MSP1E2D1	103	122	134	119	7200
MSP1E3D1	125	148	167	129	8900
Temperature	4°C	25°C	37°C		

With the nanodiscs formed, the empty discs and the discs with reconstituted membrane protein has to be separated. An IMAC purification step binds only the discs with his-tagged membrane protein and allows empty discs to flow through. Since both empty and filled discs have basically the same size, SEC cannot separate them (Figure 4.5). A SEC step is included to remove aggregates and malformed discs. Since the lipid environment is much more native for the membrane protein than detergent micelles, formed discs are stable both with and without reconstituted protein and can be both frozen and refrigerated for days or even weeks – although a second SEC step is recommended prior to any experiments where ultra-high purity and homogeneity is required (**Paper IV**).

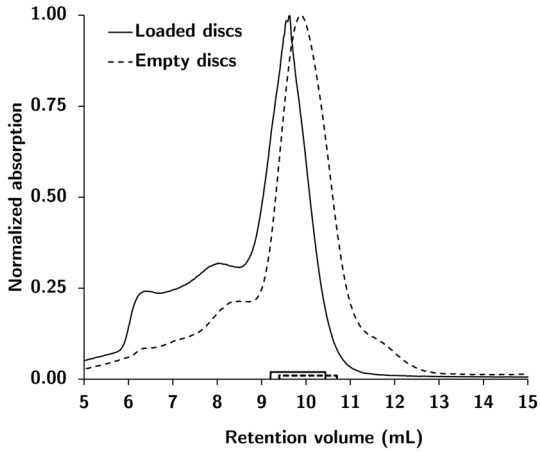

Figure 4.5 SEC profiles of empty vs filled MSP1E3D1 nanodiscs. The A_{280} is normalized to highlight their features. The difference in retention between empty and filled nanodiscs is not large enough to successfully separate them with this method alone.

4.4 Functional studies of water transport across membranes

4.4.1 Stopped-flow spectroscopy

Measuring sub-second kinetics first and foremost requires rapid mixing of the solutions. In stopped-flow spectroscopy samples are rapidly injected in to a cuvette via a mixer, followed by a sudden stop of the flow (Figure 4.6). The sample cell is illuminated with monochromatic light and scattering at 90°C is observed. Since everything is computer controlled dead times of just a few milliseconds can be achieved.

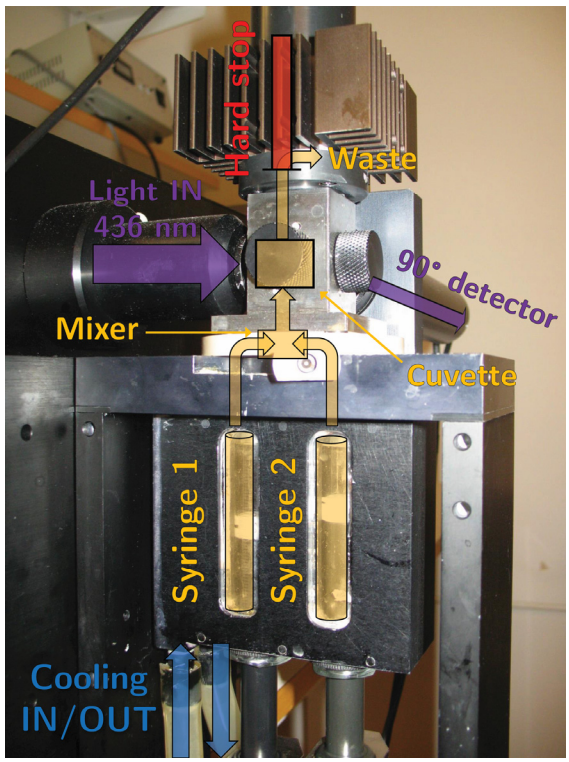

Figure 4.6 Stopped flow setup. Sample (syringe 1) and osmotic gradient (syringe 2) is simultaneously injected into a cuvette. The flow is forced to stop after a set amount of mixing time through the use of a hard stop. The 90° scattering is then collected for the duration of the measurement. Both syringes and cuvette are temperature controlled with a thermostatic water bath.

In kinetic measurements of water transport over lipid bilayers an osmotic gradient is the driving force. One syringe is loaded with a liposome solution and another syringe is loaded with a hyperosmotic buffer. Once the solutions are mixed the osmotic gradient creates an outward force, causing the vesicles to shrink rapidly. The change in diameter will cause the scattered light to increase in intensity (Figure 4.7). Worth noting is that for liposomes it is true that light scattering increases as vesicle volume decreases, but for larger vesicles the relationship can be far more complex[221]. This increase in intensity is tracked over time and averaged over several replicates to minimize noise. The end result is a curve that can be normalized and fitted with a one or two exponential equation on the form:

$$A_1 e^{-k_1(t-t_0)} + A_2 e^{-k_2(t-t_0)} + A_3 \qquad \text{(Equation 1)}$$

Where t_0 is the dead time of the stopped-flow system and k_n the fitted rate constants. When a single exponential curve is fitted ($A_2 = 0$) the rate constant represent the total passive diffusion through control liposomes or the collective water transportation capability of all the aquaporins in the proteoliposomes. When a two-exponential curve is more appropriate, the interpretation is that the rate constants represent the aquaporins and the passive diffusion respectively. This can occur when the passive diffusion is not negligible. However, the water transport through aquaporins still dominates the rate, which is reflected by the typically large differences between A_1 and A_2. Even though this is reasonable, little effort has been spent on studying the actual validity in how to interpret the two-exponential function.

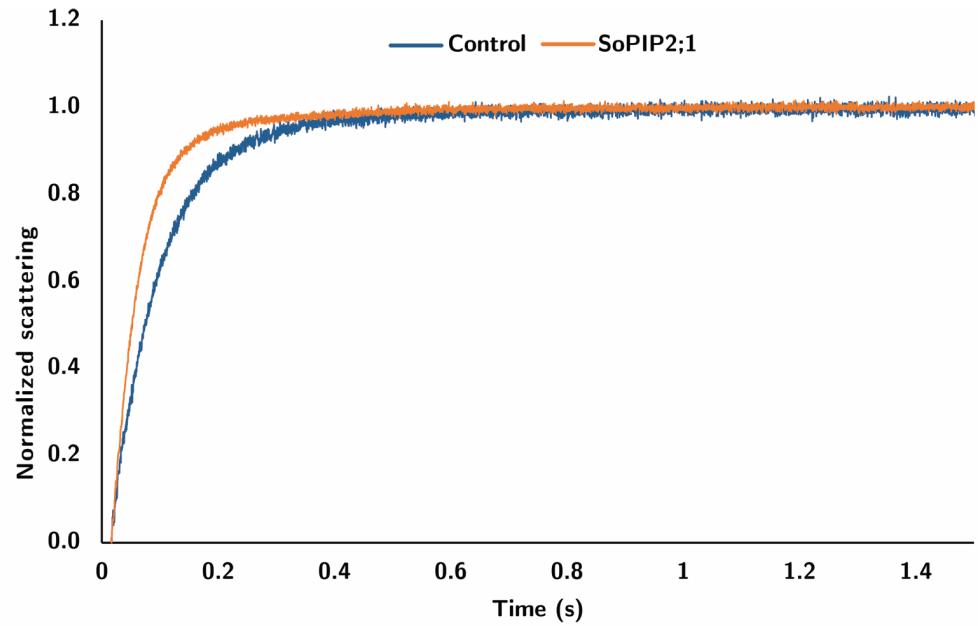

Figure 4.7 A typical stopped-flow graph, after averaging and normalization. Empty control liposomes (blue) are slower than proteoliposomes containing SoPIP2;1 (orange). When equilibrium is reached after 0.5 seconds the scattering stays constant.

4.4.2 Osmotic water permeability

The osmotic water permeability (P_f) is calculated according to the equation given by Van Heeswijk *et al*[222]:

$$P_f(\mu m \cdot s^{-1}) = \frac{k}{\left(\frac{S}{V_0}\right) \cdot V_W \cdot C_{out}} \qquad \text{(Equation 2)}$$

where k (s^{-1}) is the fitted rate constant, (S/V_0) (m^{-1}) is liposome external surface to internal volume ratio, V_W is the partial molar volume of water (18 cm^3/mol), and C_{out} is the external osmolality (mOsm/kg).

In theory, P_f would give us the ability to compare the effect of different aquaporins independent of vesicle size and osmotic gradient. In practice, it is at best a crude estimation that assumes perfectly spherical vesicles, a homogenous distribution of protein and a complete mixing of osmotic solution with vesicle solution. A decrease in the osmolyte concentration is strongly correlated with an increase in P_f[223]. This could stem from a concentration polarization near both sides of the vesicle wall (Figure 4.8). Even though it is a crude value it is very useful in comparing internal assays, and for roughly comparing permeability between different groups.

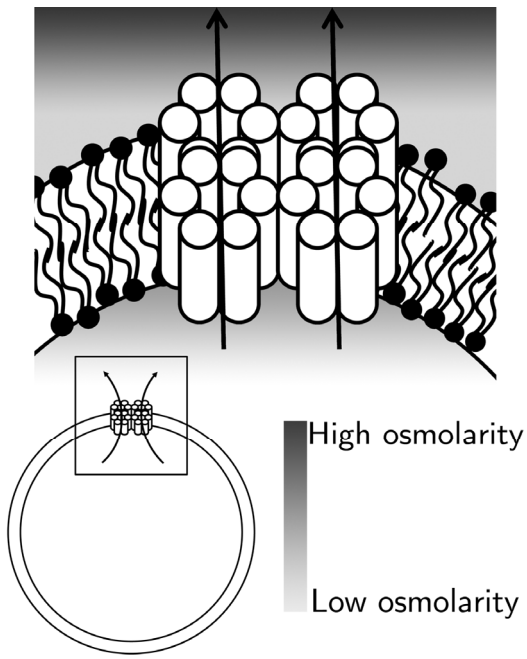

Figure 4.8 When water is transported out of a vesicle, the concentration of solute closest the lipid bilayer will change quicker than in the rest of the solution, resulting in slower kinetics.

4.5 X-ray crystallography

Using visible light in the range 400-700 nm it is impossible to visualize atomic spacing that typically are in the order of 1-2 Å since the physical resolution limit is λ/2. With X-rays, typically with a wavelength of 1 Å, atom spacing can be visualized. Unlike a microscope, where light is reflected off the specimen and focused through lenses onto a retina or camera, no X-ray lenses good enough exist[224]. Instead, the specimen image has to be collected in reciprocal space by diffraction and then simulation of the lens by applying Fourier transform recreates the image of the object. The incoming light is scattered by the electrons in the sample and, by using a protein crystal, constructive interference between each molecule enhance the pattern given. Sir William L. Bragg summarized the requirements for constructive interference in his famous law:

$$n\lambda = 2dsin(\theta) \qquad \text{(Equation 3)}$$

Where λ is the wavelength of the light, θ is the angle between the lattice plane and the incoming light, d is the distance between two planes and n is an integer. Constructive interference between two lattice planes happens if, and only if, the path difference between two scattered waves is a multiple of the wavelength. This constructive interference will give rise to a very specific diffraction pattern where each spot corresponds to a Bragg peak that is dependent on the crystal symmetry, while the intensities of these reflections contain information about the electrons in the molecules (Figure 4.9).

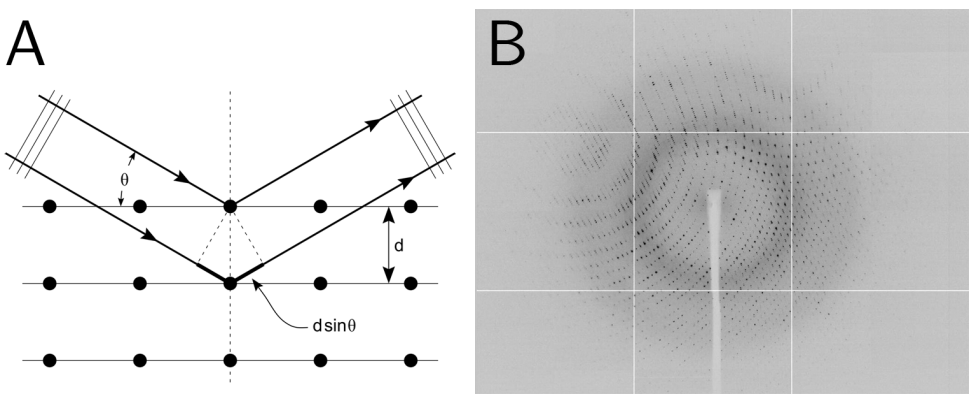

Figure 4.9 A) X-rays are scattered by electrons and gives rise to constructive interference when Bragg's law is satisfied. Figure by Hydrargyrum, distributed under CC-BL 3.0. B) The constructive interference from lysozyme crystal diffraction gives rise to complex patterns.

4.5.1 Crystallization

As perfect protein crystals as possible is needed for successful diffraction and much time is spent on optimizing crystallization conditions. In its essence the goal is to bring the protein solution from under saturation, into super saturation, and then trigger nucleation without precipitating the protein (Figure 4.10). Many strategies are available but one of the most common is the vapor diffusion technique where a small volume of protein solution is mixed with a precipitant solution and placed hanging from a glass lid over a reservoir solution (Figure 4.10). Over time this enclosed system will equilibrate and the water content of the hanging drop will decrease, thus increasing both protein and precipitant concentration and slowly move the solution into the nucleation stage. Once the crystal is fully grown and ready for transfer to an X-ray source the crystal is cryo cooled in liquid nitrogen to minimize radiation damage.

If a membrane protein migrate as a single peak on a SEC column that is a strong indication of its ability to crystallize[225]. A single peak is representative of a monodisperse protein-detergent complex. The detergent itself is also very important. Although many membrane proteins are best solubilized and purified in DDM and DM[200] those detergents produce large micelles (Table 4.2) that might interfere with crystal contacts formation.

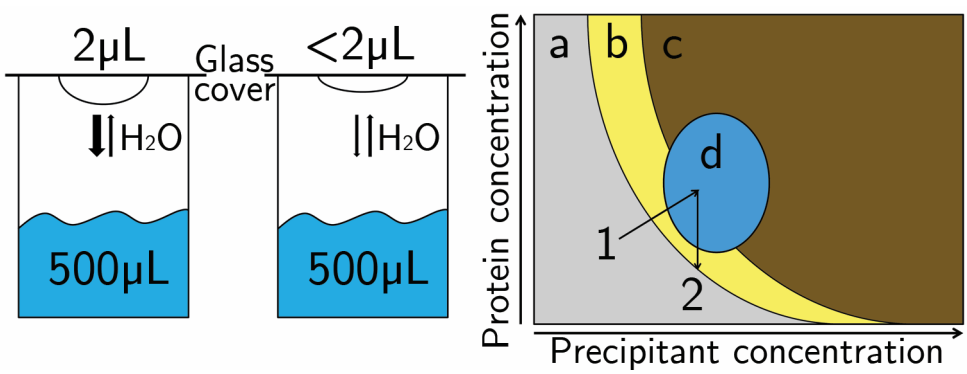

Figure 4.10 Left) The small amount of liquid in a hanging drop crystallization equilibrates with a large reservoir solution and upon shrinking the protein concentration increase to the point where nucleation and crystal growth starts. Right) In a hanging drop experiment the protein solution starts in zone a (under saturated), then slowly travels into zone b (super saturatation) where it either continues through to zone c (aggregation) or stumbles upon zone d (nucleation). The protein concentration gradually lowers and stops when it reaches zone a again.

In the same way lipids has been seen to be required for the function and stability of some proteins, lipids can be added in low concentration to the crystallization mixture to improve the quality of the crystals grown[226]. The use of lipids can be taken one step further by using the lipids in meso phases. During the last two decades Martin Caffrey's development of the lipidic cubic phase for crystallization has yielded much success[227]. As seen in (Figure 4.11) lipids take on various complex forms depending on water content and temperature. In the lipidic cubic phase the lipids form a single curved bilayer that separates two continuous, non-contacting, water channels. The crystals are then thought to grow in the interface between the cubic phase and a lamellar phase where the proteins gather laterally and stack upon each other[227].

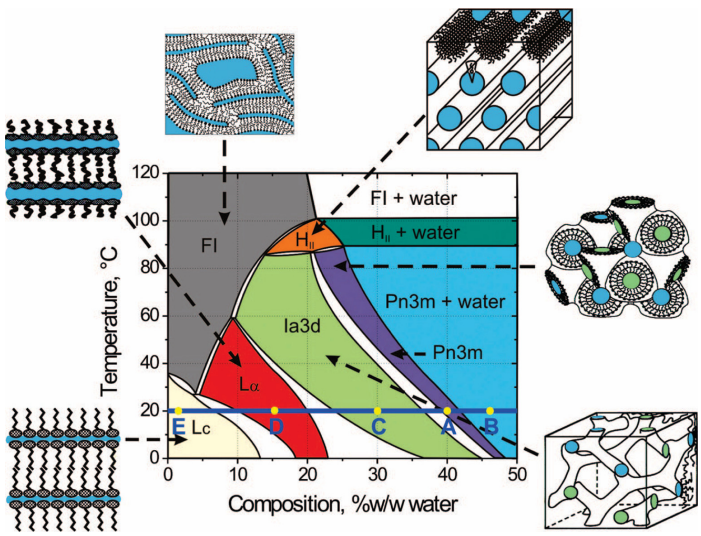

Figure 4.11 The phase diagram of monoolein illustrates the complex phases lipids go through. The cubic phases (A-C) can be used to crystallize membrane proteins. Reprinted with permission from Martin Caffrey[228].

4.5.2 Structure determination

When the Bragg peaks, or reflections, has been collected on a large amount of images there are a number of processing and refinement steps that has to be done before the protein structure can be determined (Figure 4.12). The goal of the experiment is to collect a dataset with as many reflections as accurately as possible to be able to

reconstruct the electron density of the molecule. Each reflection's index, intensity and phase have to be determined.

First, the reflections are indexed and their amplitudes are integrated. The resulting intensities are scaled and data sets are merged. In these first steps the unit cell parameters and space group are approximated. Many parameters such as the signal to noise ratio (I/σ), are taken into account when evaluating the quality of the data, and when deciding at what resolution shell to cut the data.

Second, the phases have to be found. This is the most notable obstacle to overcome in this process because the phase information is lost upon collection of the data and has to be retrieved elsewhere. The most common method is to use a previously determined structure of at least 30% sequence[229] identity and use its phases as a starting guess. If this option is not available the phases can be retrieved by experimental methods using heavy atom incorporation.

Third, the first electron density map and the first model generated is very crude so significant effort is spent on an iterative refining process where the phases are continuously improved upon. It is very important to remember that the process is very biased towards the model because of the dependency on the phases. If the phases are wrong, a model can still be made that looks right, but with proper evaluation during all stages of the process this will not happen.

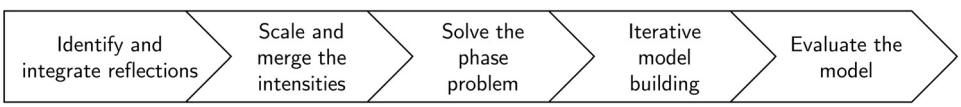

Figure 4.12 The theoretical structure determination process once diffraction is collected.

4.6 X-ray and neutron scattering

Although X-ray crystallography can give high resolution structures, these are only snapshots of stable conformations of the protein in crystallization conditions. In crystal structures, flexible regions are often unable to be modelled, and sometimes these regions are cut from the protein to produce better diffracting crystals. Solution scattering provide accurate structural information in the 10-50Å range and is method to study, for example, protein dynamics, protein-protein[230] or protein-ligand interactions, or to evaluate the validity of crystal structures[230].

In a typical X-ray scattering experiment a continuous flow of protein solution is passed through a thin quartz capillary where it is irradiated by X-rays (Figure 4.13). In neutron scattering the continuous sample flow is not needed because of the negligible radiation damage, but because of the much lower flux from neutron sources a larger amount of sample is needed.

Unlike crystals were the molecules are ordered in a lattice, the scattering from molecules in a solution is given by the average scattering of all the molecule's orientations. Instead of discrete points of constructive interference, solution scattering will create a continuous scattering pattern (Figure 4.13). The scattering is radially integrated and typically plotted as a function of the scattering angle (2θ) and the wavelength of the X-rays (λ) (Eq. 4).

$$q = \frac{4\pi}{\lambda}\sin(\theta) \qquad \text{(Equation 4)}$$

The scattering at low q describes the protein's overall shape while higher q's reveal more and more details. The resolution limit comes mostly from the lower information content in solution scattering because of the rotational averaging, but also from the significant amount of water scattering. Therefore the scattering from the buffer solution must be subtracted from the scattering from the protein solution.

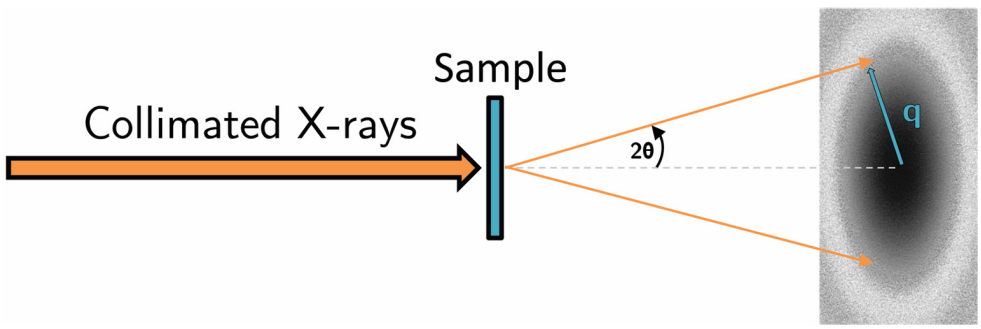

Figure 4.13 The basics of a SAS setup. X-rays hit the protein solution and gives rise to a continuous scattering pattern.

Data evaluation

If the protein solution is monodisperse, a Guinier plot (ln[I(0)] vs q^2) at low q's will be approximately linear[231], and its intercept and slope give information about the molecular mass and radius of gyration, R_g, of the protein[232,233]. This also serves as a

data quality check because if the Guinier plot is not linear, that indicates that the sample contains aggregates or protein-protein interactions.

The inverse Fourier transform of the scattering profile is used to give the pair distribution function, ρ(r), which is a histogram over the distances between all combinations of electron pairs in the molecule. The largest of these distances correspond to the maximum diameter of the molecule, D_{max}. For a homogenous sample the D_{max} should be well defined. The function at high r, beyond D_{max}, should not be negative (indicative of interparticle interference) or fluctuate (indicative of aggregation)[234].

Modelling

Pre-determined protein structures can be used to calculate theoretical scattering profiles and it has been shown that the scattering profile is unique for each protein studied so far[235]. The program CRYSOL is most often used to calculate scattering curves from high resolution X-ray structures[236]. The theoretical curve can be compared to experimental curves to validate the structure, where differences could suggest that the crystal structure is causing structural artifacts due to crystal packing.

Without a high resolution structure *ab initio* modelling is used, and for that purpose there are several algorithms[237,238]. This method shapes the protein by finite volume elements called dummy atoms, or beads, that are constrained by simple rules, such as being compact and interconnected. The placements of the beads are then placed to minimize the difference between the experimental curve and the model curve. The method suffers from having many models fitting the data so each model need to be rigorously evaluated to determine its correctness.

The problem with detergents

Even though SAS is a growing method for studying soluble proteins, it is struggling to accommodate the special needs membrane proteins have[239,240]. The detergents necessary to keep the membrane protein in solution poses two big problems in SAS[241]. 1) The a*b initio* modelling requires a uniform electron density, which is true for proteins in general. The detergent micelle around the membrane protein, however, has a very different electron density which the modelling tools can't accommodate. 2) The concentration of free detergent micelles in the protein solution is difficult determine – especially after protein concentration, which typically concentrates the detergent as

well. Proper buffer subtractions are essential to extract information from SAS, and unless the free micellar concentration is accurately subtracted the information will be useless.

The second of these issues can be overcome by the now common in-line HPLC setups available at SAXS beamlines[242], and by using a detergent with a very low CMC, such as DDM (Table 4.1). Feeding the eluate from SEC columns directly to the SAXS capillary provides as monodisperse sample as possible while ensuring a constant, and known, detergent concentration.

The first issue, however, is a bit more complex to get around. The detergent micelle can be modelled if there is crystallographic data available for the membrane protein, as proven by several papers on AQP0[241,243], but *ab inito* modelling of the membrane protein itself remains a problem to be solved.

Contrast variation with neutron scattering

Neutrons scatter off the nuclei of atoms instead of their electrons. The way this scattering occurs depends heavily, in a non-linear fashion, on both the atomic number and the isotope of the atom (Table 4.3)[244]. In particular, the scattering length for hydrogen is very different from deuterium which makes it possible to do contrast variations using deuterated water, D_2O.

Table 4.3 Scattering lengths for common elements (10^{-12}cm)[245].

H	D	C	N	O	P	S
-0.3742	0.6671	0.6651	0.940	0.5804	0.517	0.2847

5. Insights into SoPIP2;1 function

SoPIP2;1 constitutes 10% of the membrane proteins in the spinach leaf plasma membrane[139], where it maintains water homeostasis. Out of the eleven different aquaporins structures SoPIP2;1 is the only plant aquaporin available[132]. The ground breaking article provided a structure for both the open and the closed conformation of SoPIP2;1 and gave much insight into the mechanisms behind the gating of plant aquaporins. Since then follow up work together with this thesis has broadened the understanding even more and has revealed intricate and exquisite regulation mechanisms. A summary of all relevant residues and their roles are available in (Figure 5.1). It is known that aquaporin function and cell localization can rapidly change in response to changes in the environment. Phosphorylation, pH, and calcium ions all seem to modify the properties of many aquaporins in some way. What exactly is happening to the individual protein monomers in these situations?

SoPIP2;1, as well as other members of the PIP family has an elongated Loop D that can cap the channel in response to various changes in the environment. When closed the fully conserved Leu197 creates a hydrophobic barrier by inserting itself into the channel (Figure 5.2). Loop D itself is stabilized in this conformation by hydrogen and ionic bonds with Cd^{2+} (calcium *in vivo*), residues in the N-terminus and a neighboring monomer's C-terminus (Figure 5.2)[132]. The cadmium ion seemed to play a central role in this stabilizing network and its importance was reflected in that the best structure without cadmium as an additive crystallized in the open conformation, and only diffracting to 3.9Å.

Phosphorylation

Two phosphorylation sites have been demonstrated for SoPIP2;1 (Figure 5.1), and has been shown to increase its water transport rate upon phosphorylation[141]. The first site is at Ser115 in Loop B, and the second site is at Ser274 on the C-terminus. The first of these are conserved among all PIPs, with Ser274 being strictly conserved among PIP2s.

Phosphorylation of Ser115 is thought to cause a disruption in the hydrogen bonding network that stabilizes Loop D in its closed conformation[132]. As predicted, in the structure of a phosphorylation mimicking Ser115Glu mutant, the Cd^{2+} binding site was disrupted and the N-terminus was released[246]. However, the structure remained closed,

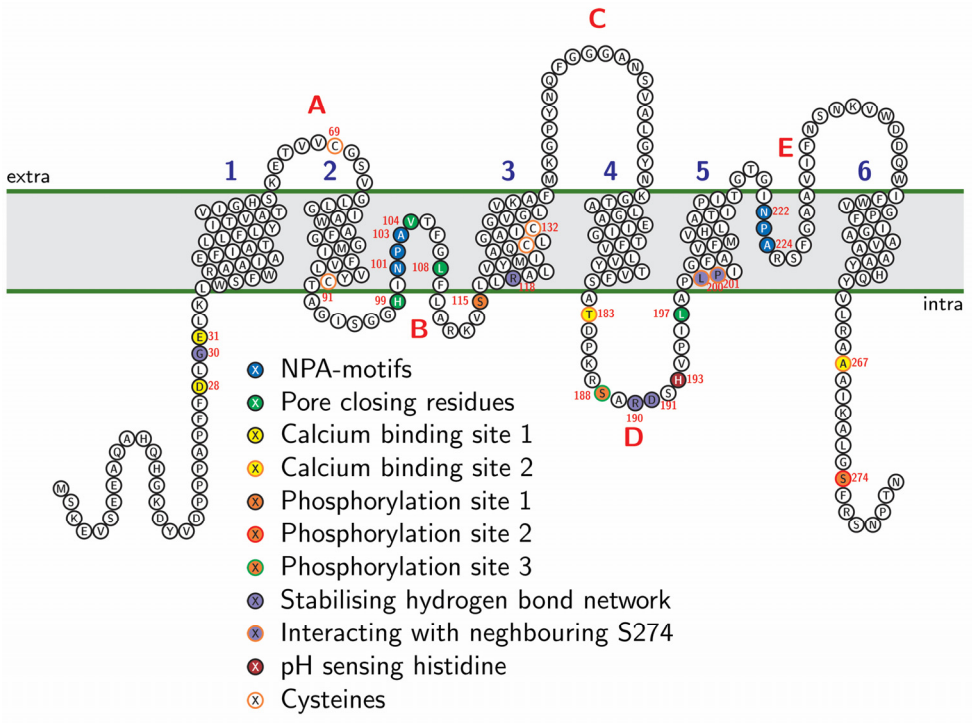

Figure 5.1 SoPIP2;1 topology illustrating the 6 trans-membrane helices (1-6), the Loops (A-E), and residues of interest. Generated using TexTopo[247].

which can be interpreted in different ways: 1) The phosphorylation of Ser115 is not enough to open the pore, 2) Glutamate is not a mimicking phosphorylation good enough, 3) The closed structure is stabilized by crystallization itself.

In MD-simulations the Ser115Glu mutant showed a significantly lower electrostatic potential compared to *in silica* phosphorylated wild type SoPIP2;1. Furthermore, functional assays did not show any increase in water transport compared to the wild type. Both points indicate that glutamate does not fully mimic Ser115 phosphorylation in this case.

At the C-terminal phosphorylation site the side chain of Ser274 interacts with the neighboring monomer's Pro199 and Leu200 in Loop D, stabilizing its closed conformation. In addition to this, the position of Ser274 would cause a steric clash with Leu197 in its open conformation (Figure 5.2). Phosphorylation of this serine

would break the interaction with Loop D and would in turn most likely destabilize the closed conformation[132]. Furthermore, in the phosphorylation mimicking Ser274Glu mutant this C-terminal is disordered beyond residue 267[246], just as in the open structure[132], which means that Ser274 would no longer clash with Leu197 if it were to adapt an open conformation.

In functional studies neither the Ser115Glu nor the Ser274Glu mutant presented an increase in water transport compared to the wild type[246]. A third phosphorylation site was proposed at Ser188 and the mutant Ser188Glu did indeed produce water transport assays with significantly higher water transport than the wild type. No structure is available for this mutant since it has been difficult to get high diffracting crystals. This is something that indicates that this mutant is indeed in a more open conformation since the extra flexibility of Loop D in the open position would make it harder to crystallize.

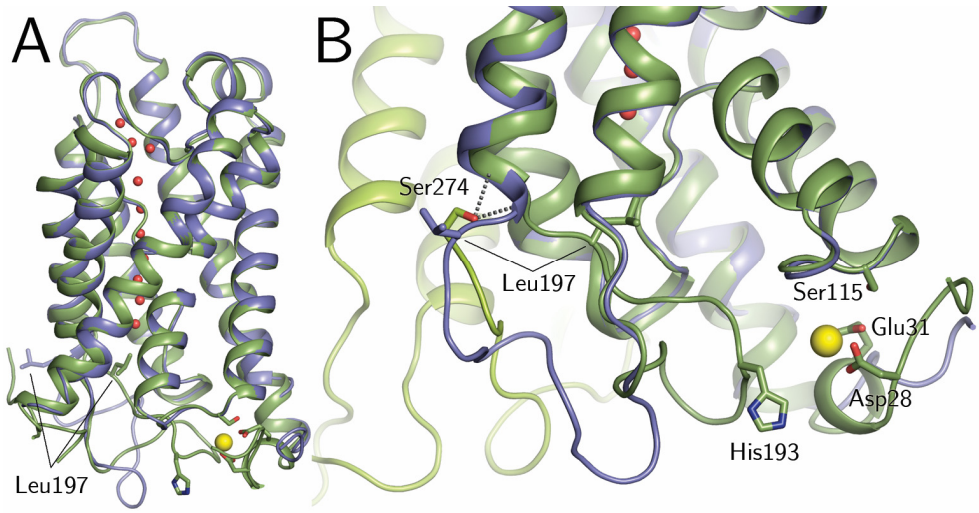

Figure 5.2 SoPIP2;1 closed (green; PDB ID: 1Z98) overlaid with open (blue; PDB ID: 2B5F). A) When closed, Leu197 constricts the pore. B) In the open conformation, the C-terminal becomes disordered, because Leu197 would otherwise cause a steric clash with Ser274. A cadmium ion (yellow), coordinated by Glu31 and Asp28, facilitates a hydrogen network between Loop D and the N-terminus, which stabilizes the closed conformation.

5.1 Ca^{2+} gating and binding sites in SoPIP2;1 (Paper II & III)

In the first structure of SoPIP2;1 a Cd^{2+} ion is modelled, which is thought to correspond to a Ca^{2+} binding site *in vivo*. The cadmium ion is coordinated by Asp28 and Glu31 (Figure 5.2). In turn Glu31 hydrogen bonds to the side chain of Arg118 that mediates the connection to the backbones of Arg190 and Asp191 on Loop D with the help of Gly30 and three water molecules[132]. Glu 31, Arg118, Arg190 and Asp191 are strictly conserved in PIPs. Asp28 is strictly conserved in PIP2s, but is conserved as glutamic acid in PIP1s.

A new cadmium site

A second binding site for calcium was hypothesized in a study on *Beta vulgaris* roots where Ca^{2+} was found to inhibit water uptake with a biphasic dose-response curve[134]. In **Paper II**, we discovered this second binding site, again occupied by Cd^{2+}. Here Thr183 from Loop D and Ala267 from the C-terminus octahedrically coordinate Cd^{2+} with four water molecules (Figure 5.3).

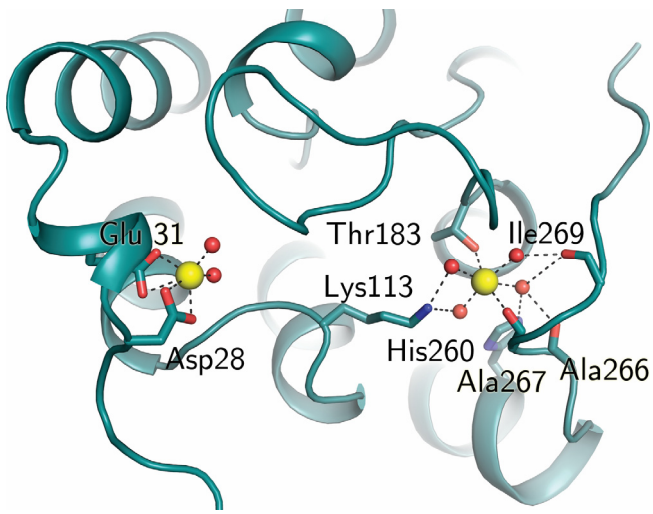

Figure 5.3 The second cadmium is octahedrically coordinated by Thr183, Ala267 and four water molecules. These water molecules are in turn bound to residues of the C-terminal, and Loop B.

What physiological implications could this C-terminus stabilization have? As already mentioned, in the open structure Loop D swings out the pore-closing Leu197 which causes a steric clash with Ser274 of the neighboring protomer. To avoid this steric clash the C-terminal is forced to become disordered. However, if the C-terminal is stabilized the activation energy for overcoming this steric clash increases, which would switch the equilibrium towards the closed conformation.

Functional assays

In **Paper III** we performed functional assays of SoPIP2;1 with and without Ca^{2+}. Initially no effect was seen upon incubation with Ca^{2+}, but when the protocol was adapted to ensure that Ca^{2+} was present on the inside of the vesicles, SoPIP2;1 was inhibited (Figure 5.4). This does confirms the calcium effect and it also implies that SoPIP2;1 preferentially inserts itself into the bilayer with its termini facing inwards, just as *in vivo*. In a similar assay describing Ca^{2+} mediated inhibition of AtPIP2;1, the authors' protocol also ensures the presence of calcium on both sides of the vesicles[137].

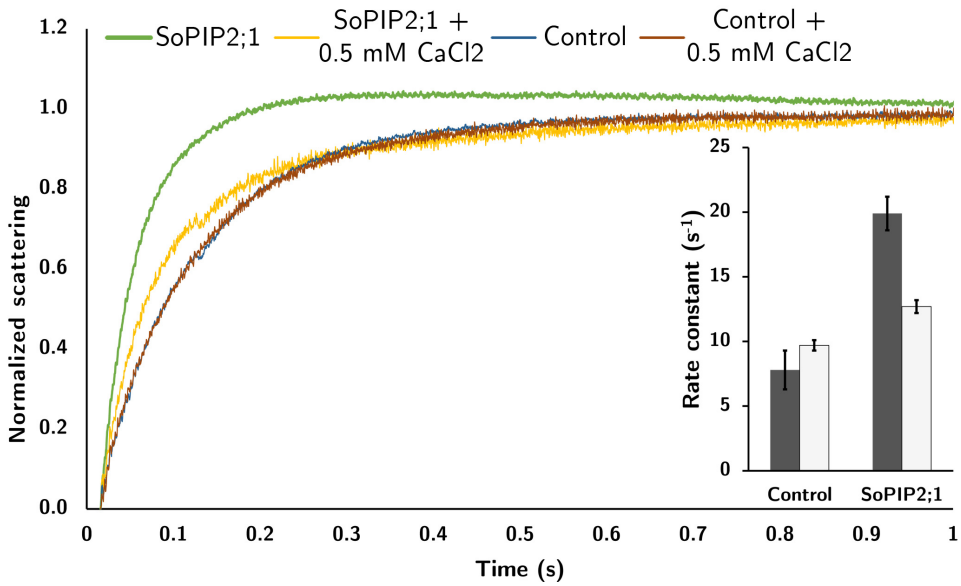

Figure 5.4 Proteoliposomes with SoPIP2;1 (green) show a high water conductivity, while proteoliposomes with Ca^{2+} are much closer to the control curves (blue and brown). Folded in on the right side are the fitted rate constants without (dark grey) and with 0.5 mM Ca^{2+} (light grey).

5.2 pH-gating of SoPIP2;1 (Paper I)

For most pH sensitive PIPs the regulation was seen to originate from the protonation of a conserved histidine in Loop D[136,138]. In the closed structure of SoPIP2;1, at pH 8.0, the pH sensitive His193 in Loop D was unprotonated so its structural mechanism could not be explained in detail. However, a hypothetical mechanism was suggested[132]; upon protonation the histidine side chain can rotate and create a salt bridge to Asp28 which could strengthen Loop D's anchor to the N-terminus. This could also make up for bindings lost due to phosphorylation.

In **Paper I** we wanted to see if we could visualize this histidine flip. To do so we crystallized SoPIP2;1 at pH 6.0 and determined its structure to 3.1Å. In one out of the four monomers His193 was flipped towards the N-terminus as proposed, presumably protonated. Since the pKa of the imidazole ring of histidine is ~6, the same as the crystallization condition, it is reasonable that not all of histidines should be protonated.

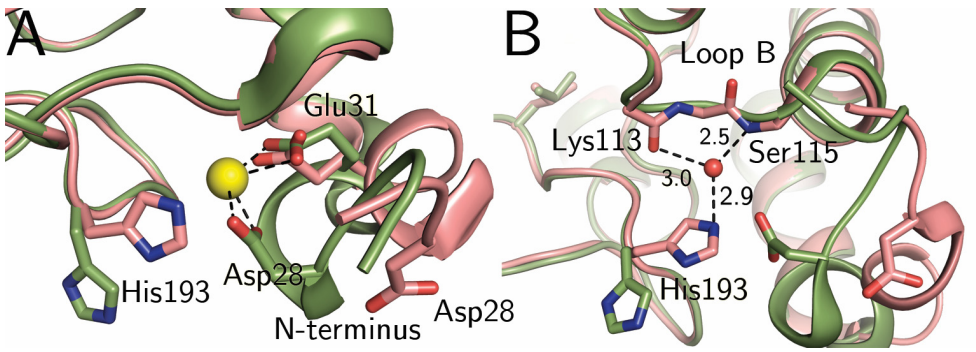

Figure 5.5 A) From the closed structure at pH 8 (green), His193 was proposed to interact with Cd^{2+} at the N-terminus by flipping its sidechain. This flip could be seen in the structure at pH 6.0 (pink) B) Without Cd^{2+}, the N-terminus has moved away and the flipped histidine sidechain interacts with the backbone of Loop B via a water molecule, anchoring Loop D in the closed position.

In this case, no cadmium ion was present in the crystallization conditions, which presented us with a different scenario for the histidine protonation than previously suggested. Without cadmium the N-terminal has moved away compared to the pH 8.0 structure, and the proposed His193 interaction partner, Asp28, is inaccessible (Figure 5.5). Instead the His193 is hydrogen bonding to a water molecule which in turn hydrogen bonds to the backbones of Lys113 and Ser115 in Loop B (Figure 5.5). The

interaction with the backbone of Ser115 makes the serine's possible phosphorylation less able to interfere with the Loop D anchoring due to low pH.

However, these findings do not necessarily contradict the previously proposed mechanism where cadmium is present. Mutational studies of both Asp28 and Glu31 has shown that they are to some extent involved in the pH sensitivity of PIP2[137], supporting a role for the Ca^{2+}-binding site in pH-gating.

The implications of our proposed mechanism involving interactions with Loop B are that SoPIP2;1 can stabilize the closed conformation by low pH, despite phosphorylation of Ser115 and low concentrations of calcium. Physiologically it permits the plant to respond appropriately to a wide variety of conditions, whether it be pH, calcium or phosphorylation or all at once.

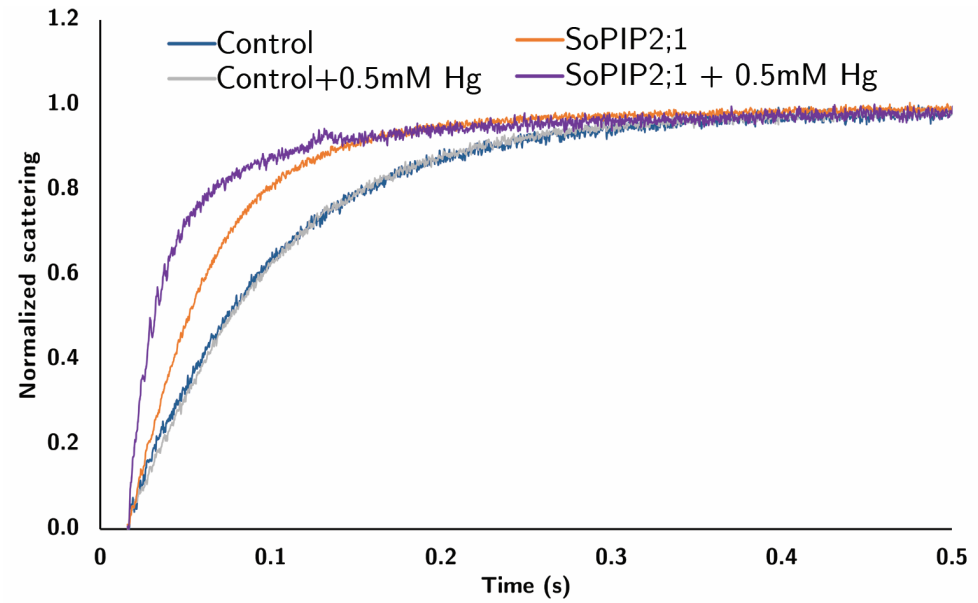

Figure 5.6 Control curves (blue) and controls with mercury (grey) show no difference in transport activity. Mercury treated SoPIP2;1 proteoliposomes (purple) show a significantly higher activity than untreated proteoliposomes (orange).

5.3 The mercury effect on SoPIP2;1 (Paper II)

In **Paper II** we wanted to investigate the effect of mercury and discovered that it significantly increases the water transport rate of SoPIP2;1, instead of exhibiting the more common inhibitory effect on AQPs (Figure 5.6). We wondered if this activation acted on the gating equilibrium or if it was a mechanism separated from this.

Establishing a fully open channel

The previously studied Ser188Glu mutant was proven to be significantly more active than the wild type because of the mimicked phosphorylation. If mercury could increase the transport rate of this mutant even further, that would indicate that the mechanism was separate from the gating. However, no significant activation of the Ser188Glu mutant could be seen in the activity assays (Figure 5.7). We concluded that mercury acts upon the gating equilibrium and that there is a state of maximum openness that SoPIP2;1 can achieve.

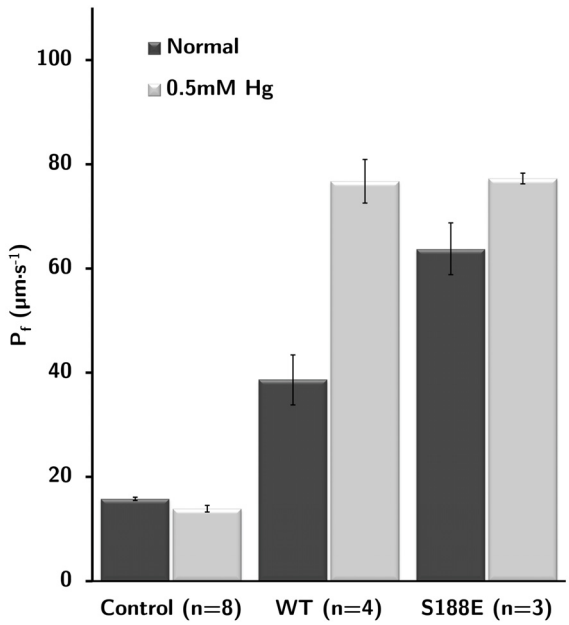

Figure 5.7 Functional assays of SoPIP2;1 shows that the effect of mercury on the S188E mutant is much lower compared to the WT and that there is a state of maximal openness of SoPIP2;1. Errors are reported as standard error of the mean.

Cysteine to serine mutation studies

Since cysteines were the only residues previously implicated in mercury sensitivity in aquaporins we focused our efforts on these. SoPIP2;1 has four cysteines (Figure 5.1): Cys69, Cys91, Cys127, and Cys132. Cys69 sits in the cytoplasmic Loop A but is involved in a cysteine bridge, Cys91 is on Helix 2 and is facing towards a neighboring

protomer, and Cys127 and Cys132 is on Helix 3 facing the lipid environment. Out of these four the contestant to being the culprit in the mercury activation was Cys91 because of its location between two protomers where it could influence Loop D in the adjacent protomer. The only solvent exposed cysteine is Cys69 which is unlikely to bind mercury because of the cysteine bridge. In contrast, the cysteines identified in AQP6 as being the mercury sensitive are closer to the solvent area with one being at the cytoplasmic end of helix 4 and the other in Loop E.

We determined the structure of SoPIP2;1 in complex with mercury to 2.15Å (Figure 5.8). Compared to the closed structure it was very similar to the closed structure without mercury. Out of the four cysteines in each monomer, Cys91, Cys127 and Cys132 bound mercury, while Cys69 was involved in a cysteine bridge as expected.

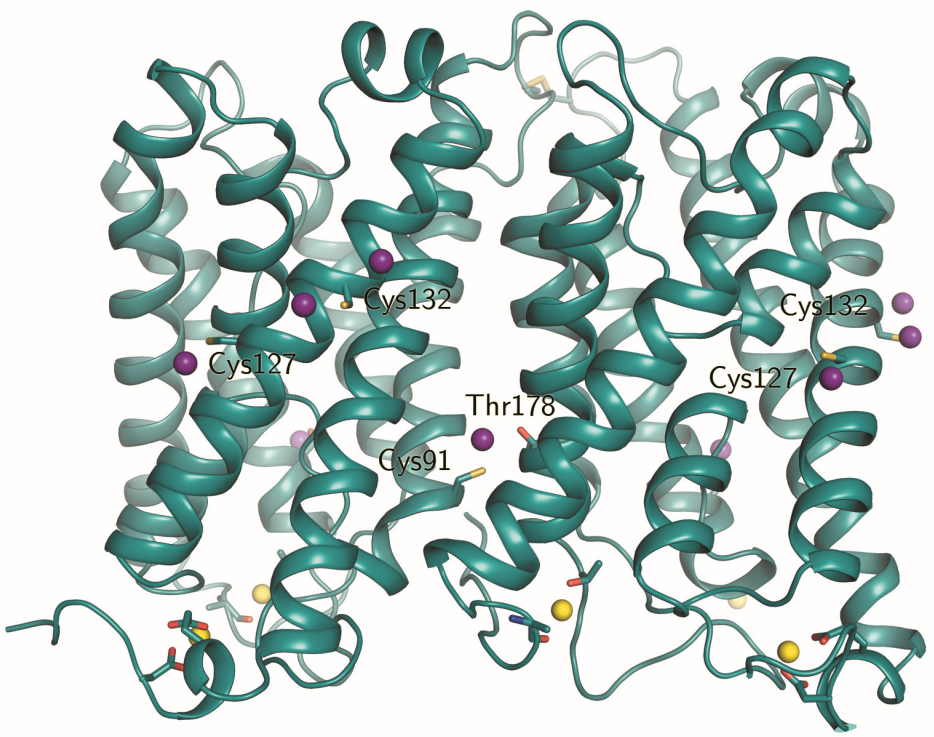

Figure 5.8 The structure of SoPIP2;1 in complex with mercury (mercury) reveals that all cysteines except Cys69 binds mercury. In particular Cys91 coordinates a mercury ion together with Thr178 of a neighboring protomer.

Since SoPIP2;1 is activated by mercury in proteoliposomes it was strange that the determined structure was closed. However, the open structure has been notoriously hard to crystallize, likely because of the flexibility Loop D has in the open conformation. In addition to this the Cd^{2+} ions required in the crystallization conditions stabilizes the closed conformation.

Next step was to make cysteine to serine mutants to deduce which cysteine was the important one for its mercury sensitivity. Six mutants were made: Cys69Ser, Cys91Ser, Cys127Ser, Cys132Ser, Cys127Ser:Cys132Ser, Cys91Ser:Cys127Ser:Cys132Ser. All cysteine to serine mutants were reconstituted into proteoliposomes and their activities were measured with and without treatment with 500 µM $HgCl_2$ (Figure 5.9). Out of the four single mutants Cys132Ser was the only one that was less activated than the wild type, however this was not statistically significant ($p>0.05$). In addition, the double mutant Cys127Ser:Cys132Ser and the triple mutant Cys91Ser:Cys127Ser:Cys132Ser was indistinguishable from the wild type. In conclusion, no cysteine could be implicated in the mercury activation.

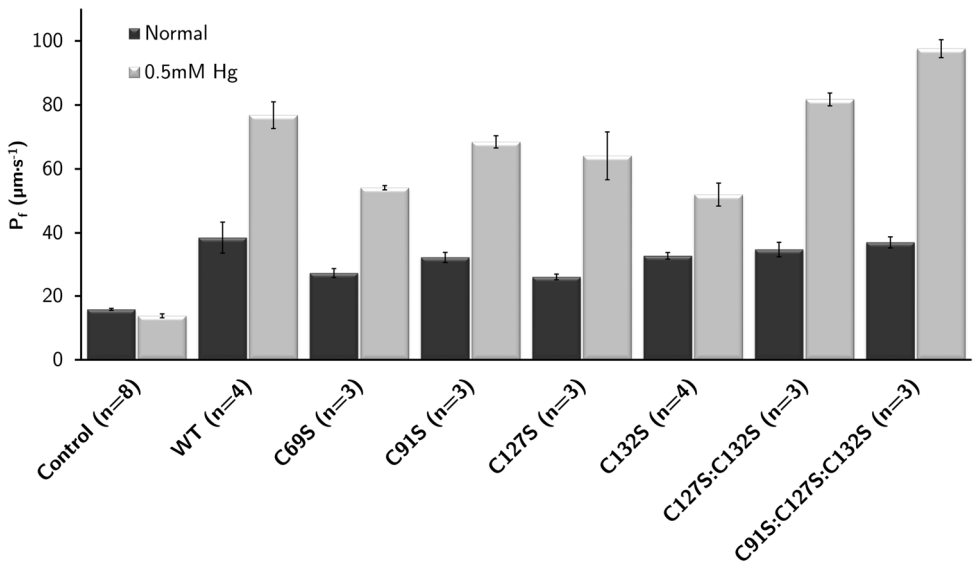

Figure 5.9 P_f with and without 0.5mM $HgCl_2$. Error bars are reported as standard error of the mean, with at least 3 independent measurements.

An alternative hypothesis

A functional study of eight PIP2 members in *Populus trichocarpa* revealed a varied response to mercury. Out of the seven variants that had the same cysteines as SoPIP2;1, six were inhibited and one was unchanged after treatment with mercury[248]. A curious example of possible mercury activation was seen in *Medicago truncatula* MtAqp1 even though that aquaporin has no cysteines at all[249]. The authors did not comment on this however.

If mercury does not act upon the cysteines to shift the equilibrium of SoPIP2;1, then what else is there? The lipid bilayer itself could provide an alternative. Mercury has been shown to decrease the fluidity of the membrane by binding to the amine head groups of phosphoethanolamine[250], the major constituent of the *E. coli* lipid extracts used for the liposomes in this study. Consistent with this, the empty control liposomes have been showing a small decrease in permeability upon mercury treatment (Figure 5.9) – something that has been noted in other studies[174]. Both AQP0[37] and AQP4[38] have altered functions based on bilayer composition, and Aqy1[56], VvTIP2;1[57] and corn root aquaporins[55] have been shown to be mechanosensitive. Given how few studies there are about correlation between aquaporin function and bilayer properties it is not unlikely that there are more instances of this behavior that are yet to be discovered. Taken together it is possible that the mercury effect seen is a result of the mercury ions changing the properties of the lipid bilayer. Therefore we propose that SoPIP2;1 can be regulated by membrane lipid composition.

In light of this hypothesis there are several implications that need to be taken into consideration and these issues need to be further investigated as it has strong implications for how aquaporin-mercury assays should be evaluated.

The *E. coli* polar lipid extracts that is commonly used in functional assays is different from native plant plasma membrane lipid composition. It could turn out that the mercury effect seen in the proteoliposomes is not present in the plant plasma membrane because of their different compositions. To my knowledge, all studies on plant plasma membranes report a significant inhibition upon treatment with mercury even though the aquaporin population mainly is PIPs in those membranes[251–254].

Mercury showed no effect at all on AtPIP2;1 in proteoliposomes even though it has the same cysteine sites as SoPIP2;1[137]. The explanation to this could lie in the way the

proteoliposomes were treated. The method used was a bit more elaborate than what was used in this thesis since the authors wanted to ensure the divalent cations tested were present on both sides of the lipid bilayer. The newly reconstituted liposomes were subjected to a hypoosmotic shock that opened transient pores so that the interior could equilibrate with the cation-supplemented exterior. This was followed by an extrusion that essentially re-equilibrates the lipid bilayers and could potentially nullify any effect mercury has on it. In addition, the authors did not measure vesicle size, but only estimated it to be equal to the extrusion filter pore size, which is far from certain, which gives an uncertainty in the P_f value calculated.

A recent study on OsNIPs inhibited by mercury found that cysteines were not responsible but instead histidines[255]. The authors conducted studies where they mutated all OsNIP3;3s histidines because mercury can in theory interact with the imidazole group. The results indicated that a histidine in the extracellular Loop C was responsible for the mercury sensitivity as all effect was lost upon mutation to phenylalanine or alanine. The question is whether this could be the case for SoPIP2;1s mercury activation as well? SoPIP2;1 has two extracellular accessible histidines: His210 in the selectivity filter on Helix 5, and His62 at the end of Helix 1. However, no unexplained electron density is found near any histidine residues in the mercury structure of SoPIP2;1. The case could also be that mercury indirectly affects histidines by binding elsewhere, so the question is still open for debate.

5.4 The central pore (Paper II)

In plant leaves CO_2 is absorbed from the air through rapid opening and closing of the stomata which in turn evaporates water. The cells are lined with different PIP aquaporins whose task is to either a) open and close the stomata or b) to regulate how much water is evaporated[256]. Having the same set of aquaporins tasked with simultaneous CO_2 uptake would simplify things for the plant and it turns out that reduction of PIPs drastically lowers the membrane CO_2 permeability in *Nicotiana tabacum*[257] as well as in *A. thaliana*[258].

The mercury crystal structure (**Paper II**) lacked the common four-fold symmetry aquaporins usually have in the asymmetrical unit. It gave us the possibility to examine the electron density of the central pore of the tetramer. This pore has been suggested to be responsible for conducting a variety of gases such as NO, CO_2 and NH_3[259]. In our model we could place a β-OG molecule lining the extracellular part of the central

pore (Figure 5.10). In the structure of AQP5 a lipid from the native membrane was seen occluding this pore[150]. For AQP5 this implicated that native lipids filled the central pore, making it impossible to transport CO_2 through it. In SoPIP2;1 the *in vitro* added detergent molecule instead implicates that something else occupies this space *in vivo*. Whether that is lipids or CO_2 or something else cannot be determined from these results.

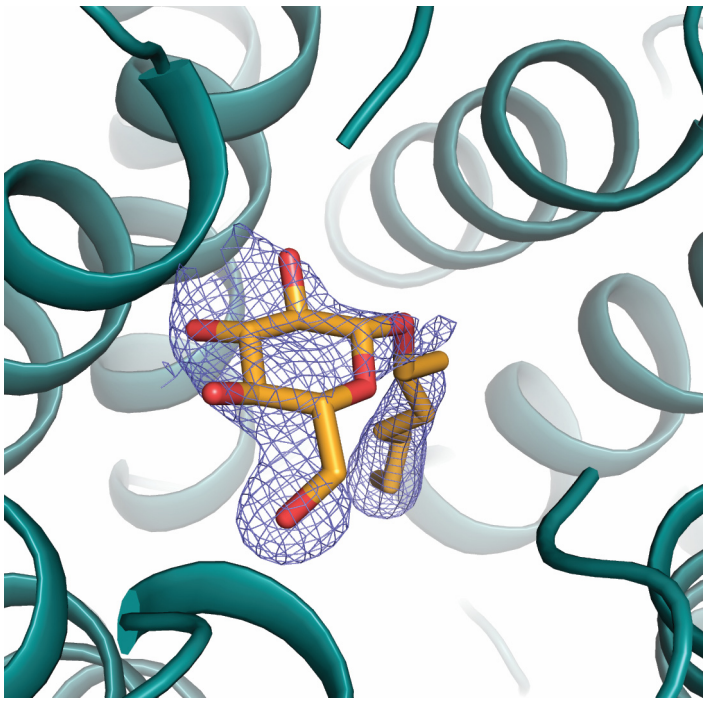

Figure 5.10 A β-OG molecule nicely fits the electron density in the central pore of the mercury-bound SoPIP2;1 structure.

6. Tools for structural and functional research

6.1 WAXS and caged calcium (Paper III)

In **Paper III**, we studied the effect of calcium on SoPIP2;1 in detergent micelles using wide-angle X-ray scattering. We wanted to see if we could visualize the closed conformation. By using caged calcium that is released upon UV illumination we could measure many ON/OFF scattering profiles in succession with a continuous flow.

The use of caged calcium

Caged calcium compounds have a very high affinity for Ca^{2+} that is drastically lowered upon illumination by UV light[260]. The caged compound we used was DM-Nitrophen (Figure 6.1). We wanted to ensure that the caged compound worked so we used a setup identical to the one at the beamline but with a micro spectrophotometer instead of an X-ray source. Arsenazo III (Figure 6.1) is a calcium sensitive dye that that has an absorption peak at 652 nm upon calcium binding. Our caged calcium and arsenazo III mixture was illuminated with UV at 365 nm while we monitored absorption at 652 nm. A sharp rise in absorption was observed and plateaued within one second, indicating a complete release of calcium ions from the caged compound (Figure 6.1). With the UV-LED still on we started the

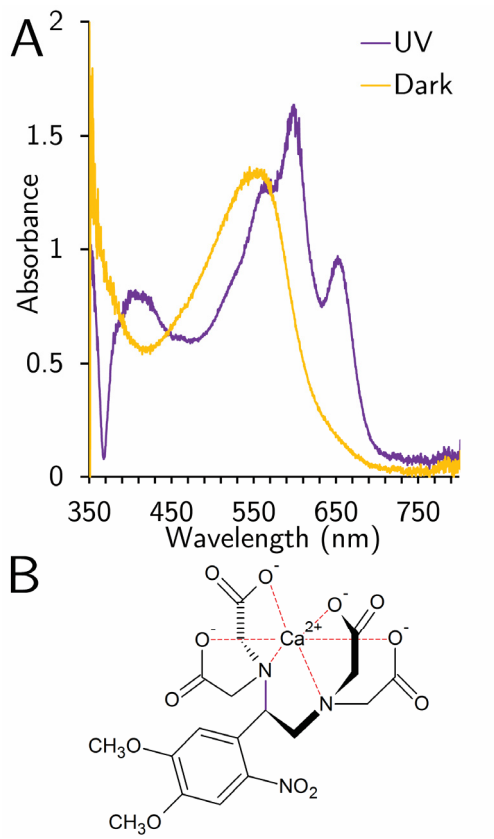

Figure 6.1 A) Absorption graph of caged calcium (orange) and caged calcium illuminated by UV-light (purple) B) Chemical structure of the caged calcium compound DM-Nitrophen and its photocleavable bond (purple)

sample pumps and continued to monitor the absorption at 652 nm, while we successively increased the flow rate. This way we could establish how fast we could flow our sample while maintaining full release of the caged calcium.

The heating effect

The temperature of the sample solution will increase as a side-effect of UV absorption and the photolysis of DM-Nitrophen. Even slight increases in temperature expand water, and change its scattering, which leads to a significant water signal even after buffer subtraction. To control for this, the heating effect is measured by irradiating the sample with IR to increase the temperature by an equal amount as the UV does.

Experimental setup and data acquisition

For the setup 200 mg of SoPIP2;1 was purified, frozen in N_2 and stored at -80°C. On the first day of the experiment the protein was thawed, incubated with 1mM of EGTA and SEC purified in freshly made buffer. This was to ensure elimination of all aggregation and residual calcium. A stock solution of DM-Nitrophen and calcium was made with the calcium concentration slightly lower than the DM-Nitrophen to ensure that all calcium is caged. The caged calcium was added to the protein solution to an excess of 0.5 mM. The concentration was chosen to ensure a 0.5 mM free concentration of calcium even when all available SoPIP2;1 had bound two calcium ions each.

The sample was pumped through PEEK-tubing into a thin glass quartz capillary that was mounted in the X-ray beam. The IR- and UV-sources were collected

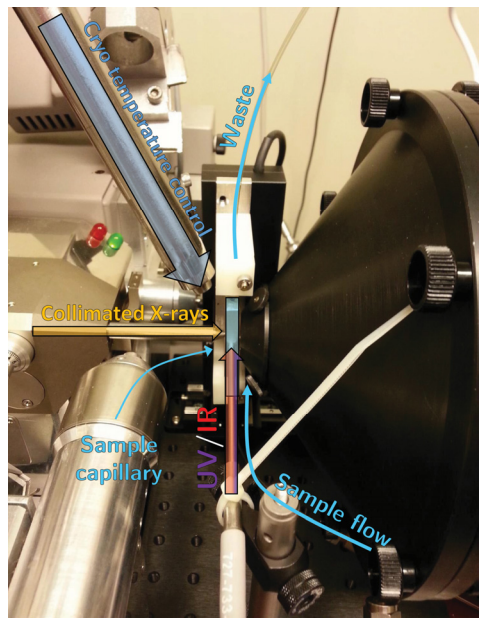

Figure 6.2 WAXS setup. A fiber is connected to the capillary which irradiates the sample with UV, or IR. The X-rays comes in perpendicular to the fiber and the scattering is collected with a CCD-detector (outside the right edge). A helium filled cone (black) minimizes background scattering from air.

with a Y-fiber which was mounted to the capillary holder perpendicular to the X-ray source (Figure 6.2), and a computer script automatically switched between light sources (Dark/UV/IR) during data collection.

Data sets of Dark, UV, and IR were collected in sequence while the pump was kept on a constant speed of 0.05 µL/s. The UV-LED was set to constant illumination during UV data collection. The IR laser showed fluctuations in intensity at the low amperes needed for our heating measurements. To eliminate those fluctuations we employed pulse width modulation of the IR-laser with a pulse generator that sent small bursts of IR every fraction of a second. The length of the pulses was adjusted to match the heating signature of the UV-LED, although inherent variations between data-sets forced us to do additional scaling in the data analysis at a later stage.

Data analysis and modelling

After radial averaging, the data processing was performed in three steps. First the dark datasets was subtracted from 1) UV-illuminated data sets (UV-Dark), and 2) IR-illuminated data sets (IR-Dark). The heating signature from the IR-Dark curves were matched to the UV-Dark curves and then subtracted from them to give the final 3) UV-IR curves (Figure 6.3) that represents the difference scattering caused by structural changes.

The previously solved structures of SoPIP2;1 in closed (PDB ID: 1Z98) and open (PDB ID: 2B5F) conformations was used as a starting point for MD-simulations. The aquaporin tetramer was put into a pre-equilibrated lipid bilayer and an equilibrium model was created by running the simulations for ~70 picoseconds. The model was then used to create the theoretical UV-IR curves.

A fully open or closed aquaporin might not be the most probable case so we tested five combinations of open and closed tetramer structures: 4 open, 3 open + 1 closed, 2 open + 2 closed (diagonally), 2 open + 2 closed (horizontally) and 1 open + 3 closed. These were compared to the expected fully closed system.

The best fit

The experimental difference curves, $\Delta S(q)$, show distinct features at the low q region ($0.1\ \text{Å}^{-1} \leq q \leq 0.6\ \text{Å}^{-1}$), similar to the light induced changes in WAXS spectra of proteins from the rhodopsin family[261,262].

Currently, the best fit to the experimental data comes from the difference between the fully closed and the fully open tetramer. As seen in figure 6.3a, the general features are there, but the fit is still not perfect. The model uses a lipid bilayer instead of a detergent micelle which could account for some of the discrepancies seen. In addition to this the flexible N- and C-termini was omitted from the model at this stage, but once included the fit is expected to improve. The biggest improvement to the model will likely come from using an equilibrium ensemble instead of a single equilibrated state. In solution SoPIP2;1 are not locked in a certain place but rather shift rapidly between the open and the closed conformation. An equilibrium ensemble would capture this and would provide a more accurate model to fit to the data.

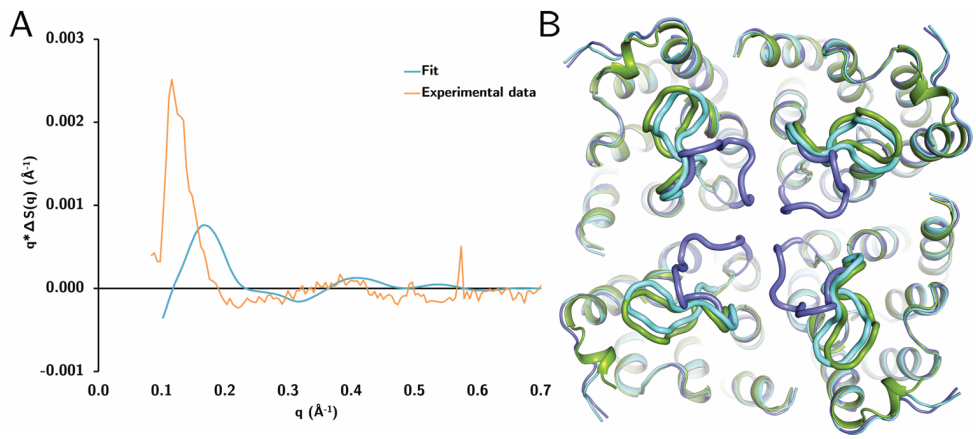

Figure 6.3 A) Experimental data and the best fit that comes from the difference between the fully closed and the fully open structure. B) Overlay of closed (green), open (blue) and best fit model (cyan).

Conclusion

There is, to my knowledge, only one other study using caged compounds together with SAS to study conformational changes in proteins[263]. This is the first step towards time-resolved WAXS (TR-WAXS) studies of non-photosensitive proteins. The caged compounds and UV-setups can be optimized to release tiny incremental amounts of calcium to give scattering snapshots of all intermediate conformations in protein gating.

6.2 Nanodiscs (Paper IV)

As described earlier, nanodiscs are discoidal lipid bilayers enclosed by two copies of MSP. Single copies of membrane proteins can be inserted into the discs and because of their defined size they are very monodisperse in solution. This serves as an excellent basis for SAXS studies of membrane proteins; something that has been very challenging due to the intrinsic properties of detergents[241]. Although the lipids are not handled well by standard modelling tools, new tools has been developed by Lise Arleth's group, as shown by their paper of bacteriorhodopsin modelled in nanodiscs[190].

In **Paper IV** we wanted to see how small backbone movements we could distinguish. Tetramers of SoPIP2;1 was successfully inserted into the lipid bilayer of the nanodisc system consisting of two copies of MSP1E3D1 and analyzed with SAXS in combination with SANS. The hydrocarbon chains from lipids scatter X-rays very weakly, which means the bilayer in nanodiscs is poorly resolved with SAXS. In SANS, however, the contrast between D_2O and the hydrogens in the hydrocarbon chains are very distinct. Combining the two methods yields the information needed for both the proteins and the lipids in the nanodisc[224].

Tetramer verification

To verify that SoPIP2;1 would not reconstitute as a mixed population of monomers and tetramers we made nanodiscs of different sizes. Monomer reconstitution was tried using the Cys69Ser mutant and the smaller nanodisc size with MSP1D1. Tetramer reconstitution was done as for the wild type with the larger MSP1E3D1 (Table 4.2). The smaller diameter of MSP1D1 was thought to force SoPIP2;1 to either reconstitute as a monomer or not at all. The Cys69Ser mutant would ensure that no cysteine bridge would hold together the dimer. SEC purifications of both MSP1D1 and MSP1E3D1 reconstitution mixtures showed that only in the latter case was correctly folded nanodiscs formed (Figure 6.4). With this information we felt confident that SoPIP2;1 only existed as tetramers in the larger nanodiscs, something that we later confirmed with the SAS modelling.

Data collection and modelling

SAXS data was collected first to evaluate the sample quality. Roughly 100 µL of sample was used for these measurements, which translates to about 0.065 mg, or 2

nanomole, of pure SoPIP2;1. In contrast, SANS collection required 400 µL of sample with a higher concentration, which translated to about 0.5 mg, or 16 nanomole, of pure SoPIP2;1. The almost ten-fold increase in sample amount is due to the significantly lag in neutron facility technology, compared to synchrotrons, but this is expected to change in the coming years, as detector quality and neutron flux continues to increase.

The initial models established that SoPIP2;1 did indeed reconstitute as a tetramer, and that it was located in the center of the nanodisc. Normally the empty nanodisc is oval, rather than circular, but the size of the tetramer forced the SoPIP2;1-nanodisc to adopt a more circular form. In fact, there is only room for 1-2 POPC molecules between SoPIP2;1 and the MSP1E3D1 protein. Even so, the lipids maintain an average area per headgroup of 71Å^2, compared to 67Å^2 in the empty disc, and 60Å^2 in bilayer structures[264].

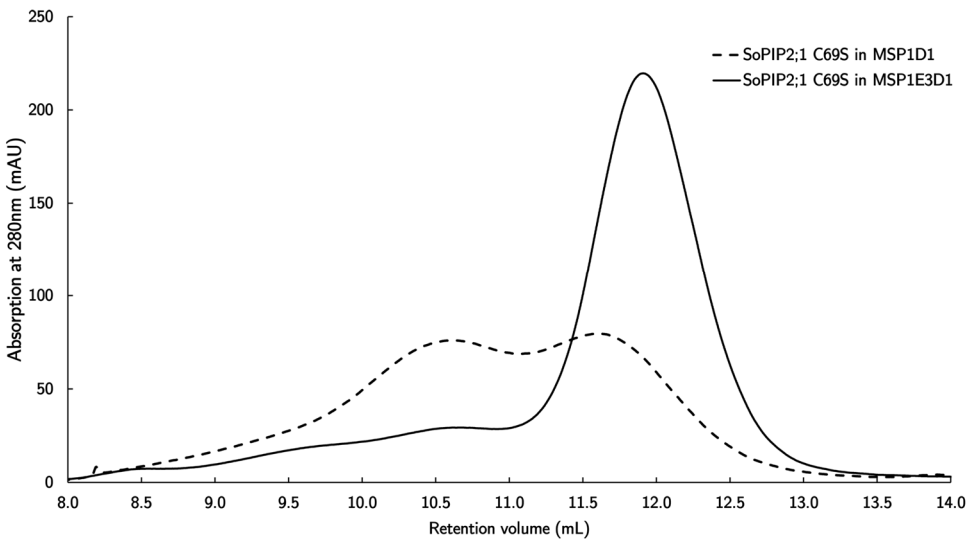

Figure 6.4 SEC profiles of SoPIP2;1 Cys69Ser reconstituted into either MSP1E3D1 or MSP1D1 nanodiscs. The smaller discs of MSP1D1 failed to form, since no peak is seen after the MSP1E3D1 peak.

Because of four-fold symmetry of SoPIP2;1 and the large volume it fills, the quality of the data exceeded the expectations based on the previous study on bacteriorhodpsin[190]. This allowed us to investigate more closely what can and can not be distinguished with this method. In the crystallographic structure of SoPIP2;1 there are 45/49 N-terminal and 7/18 C-terminal unmodelled residues in the closed and open structure respectively. Four different models were tested to evaluate how much of the flexible regions we could accurately model (Figure 6.5). We wanted to see whether or not the disordered N- and C-termini contributed significantly to the scattering, and if we could locate the lateral placement of these. Furthermore, we wanted to see if there were any significant differences in model quality when using the open structure compared to the closed structure.

In the first model we omitted the flexible regions at the N- and C-termini (Figure 6.5a), while in the second model the termini were modelled as one single flexible chain with their X-Y coordinates as extra free parameters (Figure 6.5b). The fit is visually better using the latter model. Specifically, the χ^2 decreases from 52 to 5.5, but the partial specific volume of the lipid belt, and the SoPIP2;1 tetramer, are unrealistic in both models (Table 6.1). It's concluded that these flexible regions are needed to accurately describe the scattering from the nanodisc-SoPIP2;1 complex, which leaves room for improvement.

In the third and fourth model we modelled the N- and C-termini as two separate flexible chains. This, in addition to Loop D, gave us the opportunity to distinguish between the closed and the closed structure. The biggest difference is the placement of the C-terminal which is located in the center of the tetramer in the closed structure (Figure 6.5c), but have moved away to the sides in the open structure (Figure 6.5d). Both fits provided more physically realistic parameters, with the closed model having a slightly lower χ^2 value (5) than the open model (15). The deviation of the open structure is also seen clearly near the first minimum at $q \sim 0.1$ Å^{-1}. These differences in fits are small though, and it cannot be said with certainty that the closed model is more likely than the open model.

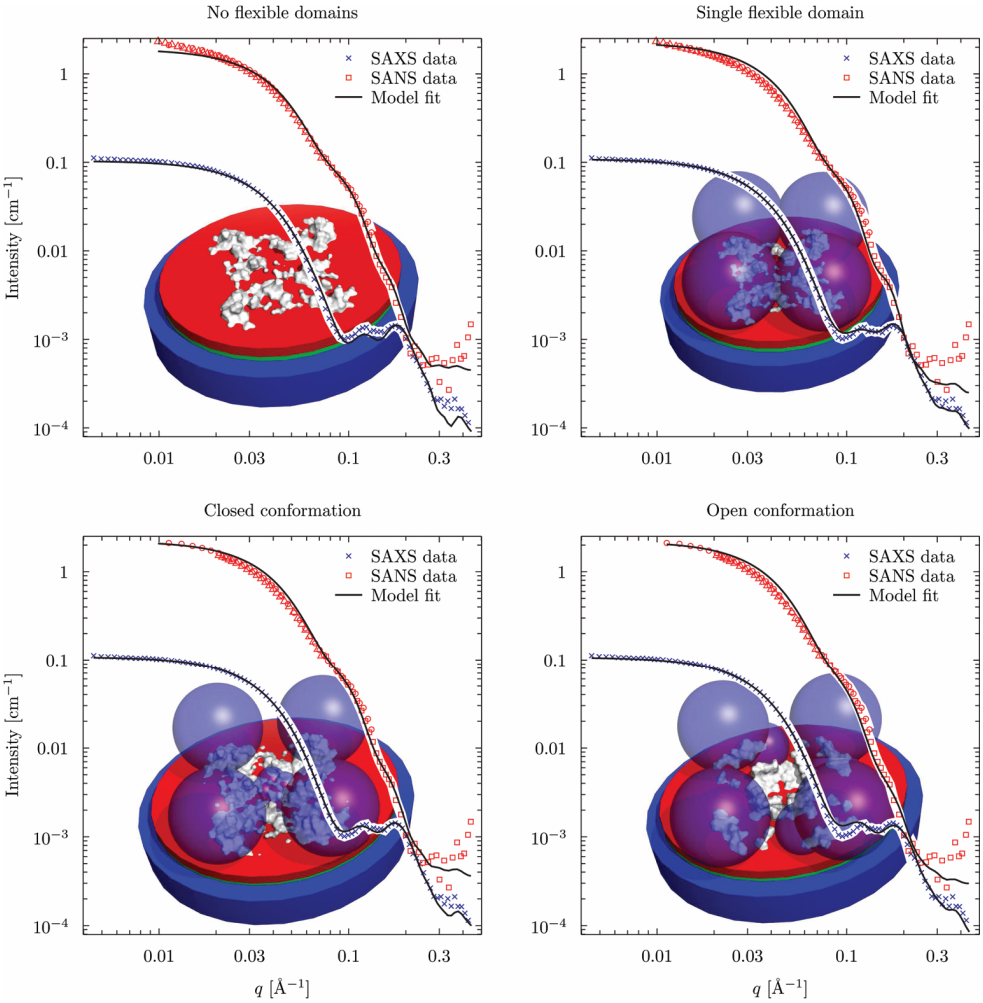

Figure 6.5 Four different models were tested. Each model was simultaneously fitted to the SAXS and the SANS data. Top left: No flexible domains on the cytoplasmic side gave the worst fit. Top right: A single flexible domain that included Loop D, and the C- & N-terminals gave a much better fit. Bottom left & right: Modelling the C- & N-terminals separate from Loop D gives us the ability to compare the open conformation with the closed conformation.

Summary

In our models of SoPIP2;1 reconstituted into nanodiscs we discovered that flexible regions, such as the N- and C-terminals of SoPIP2;1 contribute significantly to the total scattering of the protein, and must be included in the models. Since SoPIP2;1 is a gated protein we tried to distinguish between the open and the closed conformation

We got a slightly better fit with the closed model, but the difference compared to the open model was not significant enough to warrant a definite conclusion in that matter. The most likely scenario is that SoPIP2;1 exists in an equilibrium state between the open and the closed structure at the conditions the experiment took place in (non-phosphorylated, pH 7.5, no calcium). This is further discussed in **Paper III** where we studied SoPIP2;1 with WAXS to distinguish between the open and the closed conformation using UV-triggered calcium release. If one were to measure SAS on SoPIP2;1 in nanodiscs with calcium, to stabilize the closed conformation, the closed model would most likely fit better. That is, the reason why this study could not distinguish between the two forms is probably not because of limitations in the technology, but rather because SoPIP2;1 was neither fully open nor closed.

Table 6.1 Fitting parameters from the empty nanodiscs as well as the four different SoPIP2;1 models.

	Empty $\chi^2 = 457$	NoTag $\chi^2 = 52$	OneTag $\chi^2 = 5.5$	Closed $\chi^2 = 4.9$	Open $\chi^2 = 14.6$
Fitting parameters					
ϵ	**1.68** ± 0.026	**1.28** ± 0.07	**1.29** ± 0.18	**1.32** ± 9.98	**1.38** ± 0.09
$h_{bilayer,apolar}$	**20.6** ± 2.2	**25.57** ± 0.84	**30** ± 2.3	**27.63** ± 0.04	**28.7** ± 2.1
N_{lipids}	**209.41** ± 0.54	150*	150*	150*	150*
N_{water}	**4.34** ± 0.98	4.3*	4.3*	4.3*	4.3*
σ_X	**4.00** ± 0.23	**3.73** ± 0.45	**3.6** ± 1.2	**3.93** ± 0.57	**3.57** ± 0.60
σ_N	**2.00** ± 0.27	-	-	-	-
CV_{belt}	**1.033** ± 0.015	**0.900** ± 0.024	**1.07** ± 0.10	**0.97** ± 0.02	**0.98** ± 0.03
CV_{lipid}	**1.014** ± 0.004	**1.005** ± 0.014	**1.024** ± 0.045	**1.03** ± 0.02	**1.02** ± 0.02
CV_{Aq}	-	**1.046** ± 0.008	**1.038** ± 0.019	**1.028** ± 0.02	**1.029** ± 0.016
h_{endcap}	**6.6** ± 1.6	0*	0*	0*	0*
$l_{Kuhn,tag}$	-	-	**13** ± 10	**11.4** ± 3.5	**10.8** ± 4.9
X_{tag}	-	-	**15** ± 2164	-	-
Y_{tag}	-	-	**27.2** ± 1193	-	-
Deduced parameters					
R_{minor}	61.9	59.6	57.1	59.2	59.5
R_{minor}	36.8	46.5	44.3	44.9	43.1
$A_{head,lipid}$	66.8	76.1	69	70.5	73.8
D_{belt}	8.7	7.2	8.8	7.9	8
$V_{lipid,head}$	323.5	320.6	326.7	328.6	325.4
$V_{lipid,apolar}$	940	931.6	949.2	954.8	945.5
V_{belt}	$35.4 \cdot 10^3$	$30.9 \cdot 10^3$	$36.5 \cdot 10^3$	$33.2 \cdot 10^3$	$33.6 \cdot 10^3$

7. Future aspects and concluding remarks

7.1 SoPIP2;1 and plant aquaporins

Previous studies have shown that the closed conformation is destabilized by phosphorylation at Ser115 and Ser274 with a third phosphorylation site hypothesized at Ser188. We have demonstrated a mechanism for how SoPIP2;1 is closed by a decrease in pH, or by Ca^{2+} binding at two sites. The inhibition by calcium was proven in functional assays, and initial WAXS studies. In addition to this, we have suggested that membrane tension, or fluidity, can be employed by plants for regulation as well.

The mechanics behind SoPIP2;1 phosphorylation is an area where more insight is needed. It's difficult to artificially phosphorylate proteins. Most studies done on aquaporin phosphorylation are done in oocytes by, for example, adding kinase inhibitors and studying the effects[139]. Many aquaporins are also trafficked into, or out of, the plasma membrane in response to phosphorylation of their C-terminus[124]. The complexity *in vivo* is truly amazing.

It has also become evident to me that studies of water permeability as a function of lipid composition should be more commonplace. The study on AQP4 and AQP0 activity based on lipid composition shows a clear dependency on elasticity and thickness[37,38]. We need to investigate this issue further, and establish better protocols for measuring and reporting activity assays, but the biggest hurdle is that there is no means of measuring water transport through a single aquaporin, something that is possible for ions[84]. If that issue was overcome, much more accurate measurements would be possible.

The role of other heavy metals has not been evaluated here but heavy metal toxicity is problem in nature so it is important to understand the mechanisms behind this[265,266]. Aquaglyceroporins have less specificity and most likely transport more solutes than those that have been proven in assays to date. This also implies that they can transport solutes that have no evolutionary benefit to the organism, such as the arsenic transport in rice NIP aquaporins[267].

7.2 Commercialization of aquaporins

Many groups and organizations are already competing to build the first economically feasible aquaporin filter. It could be used to purify water from bacteria, salt and other unwanted things that make it undrinkable. However, the only commercially available product that has gained somewhat public knowledge because of aquaporins is a skin cream which is reported to increase the presence of aquaglyceroporins in skin cells[268]. The study is rudimentary at best and the article is recommended only as a teaching exercise.

On a more serious note, in medicine many diseases are connected to aquaporins and drugs that target these could be of great use. For example, diabetes insipidus, a disorder characterized by copious volumes of unconcentrated urine, is caused by improper trafficking of AQP2 to the kidney[269], and the malarial parasite *P. falciparum*, that infects hundreds of millions each year, has an aquaporin that is essential for its growth stage in human blood streams[270].

There are also many opportunities in the farm industry where there is always a need to increase harvest yields. In theory, modifying aquaporin regulation or expression in crops could make them grow faster by essentially blocking their safety mechanisms that otherwise protect them against drought, flooding, and other natural variables. The emerging use of factory like indoor farming facilities that employs specialized led-lights[271], provides the type of controlled environments where we could safely relieve the plant of its safety mechanisms in favor of growth.

7.3 Membrane proteins and lipids

The current main method of studying membrane proteins in detergent micelles is excluding a lot of the properties a lipid bilayer provides, and may give us the wrong idea of how these proteins work and behave. A continuous expansion of the biochemical toolkit is important for us to elucidate the finest details about the membrane proteins. In the future a lot more will be discovered about the protein-membrane relationship.

During this journey I have understood that the environment in which the membrane protein is situated is of much greater importance than previously considered. The tools which we use to study these proteins have to be carefully selected. Nanodiscs can be one of these tools. An overview of the field reveals a quickly growing interest in the

system (Figure 7.1) and been proven to be diverse, in variety of membrane proteins reconstituted, but also in techniques that benefit from its use.

Although this thesis has not elucidated any lipid-protein dynamics, it has shed more light on the relationship, both literally and figuratively. I have also glimpsed the future of membrane protein research by exploring the tools that can be used to substitute the lipid bilayer in a controlled lab environment, and I see that the future is as bright as our 4th generation synchrotrons.

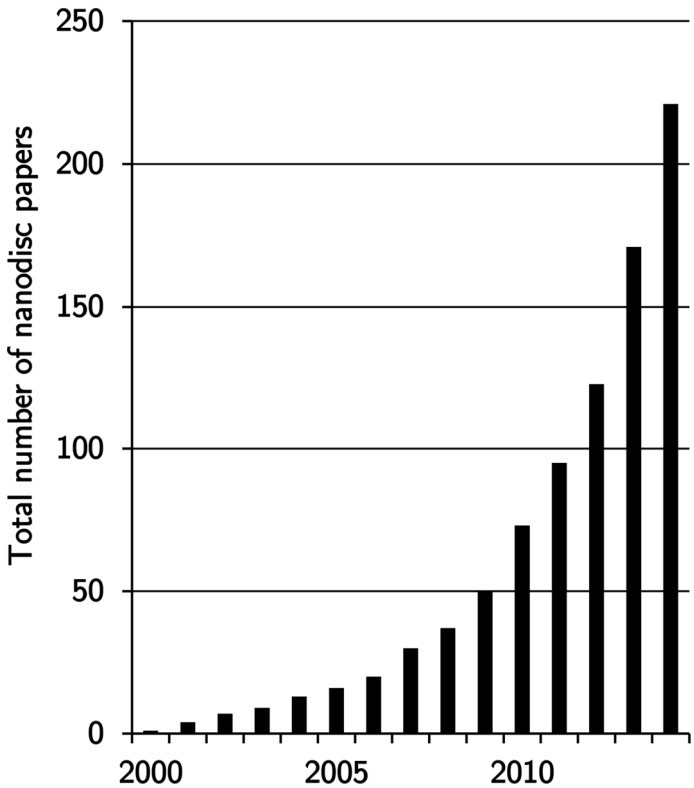

Figure 7.1 The cumulative number of nanodisc papers in the literature from 2000 to 2014 shows a clear growing interest in the system that is expected to continue to grow.

Acknowledgements

I want to thank my supervisor **Susanna** for taking me in and trusting me enough to let me do basically whatever I wanted for five years. The time here has been a tremendous learning journey and I truly appreciate my time working here on our projects.

This would not have happened without **Anna** who supervised my master project and lured Susanna in to hiring me afterwards. Anna's thorough lab techniques have always been a guiding star even though I myself will never succeed in reaching her level of neatness.

My co-supervisor **Kristina** turned out to be a much needed asset when I ended up being the last group member of my group here. Thank you specifically for barnacle and the group meetings. And thank you **Richard**, my examiner, for and putting me on this weird and out-of-my-comfort-zone project and creating Paper III out of thin air. It wouldn't have happened without **Jennie**, **Peter**, and **Amit** though. See you in Australia **Peter**.

I also want to shout out to the Copenhagen SAXS-team: **Lise**, **Pie**, **Sören** and **Sören**. Thank you for our collaboration. It was a pleasure, and an experience, and we even got a paper out of it, hurray!

Rosie, you are my mentor and I listen to every advice you give. Even when they are ridiculous and clearly wrong I still hear you out. I will continue to drink more wine with you as long as you STEP UP!

The party party people: **Rob Dods**, **David**, **Petra**, **Oskar**, **Emil**, **Petra**, **Ida**, **Rebecka, Ashley, Matthjis, Karin and Annette**. It's always a pleasure to drink cold beers and play games with you.

Elin, good luck with the structures, you know you deserve them, and **Rhawnie**, maybe now I have time to mediate ;) It's on my to-do-list.

To all the rest of the people in the lab I sadly don't have the time to write something special about right now, **Madde, Weixiao, Gisela, Cecilia, Majo**, **Maria**, **Parveen**, **Gergely**, **Sebastian**, **Rajiv, Linnéa, Stephan, Heikki, Alex and Alex**, keep up the

good work. It's great to have you all around. Each and every one of you has at some point contributed positively to this thesis.

A special acknowledgement goes to **Bruno** and especially **Lars** for keeping the lab up and running.

A special note goes to my only master student **Veronica**, who was of course as brilliant as she said when I first read her personal letter. I look forward to your first structure in a couple of years! You're in good company with my steph-groupmembers **Stefan** and **Jennifer.**

To all the people I've forgotten, please forgive me.

Tim! You're my best friend! Bring **Daisy**, suit up and come party with me! It will be LEGEN-

My family has always been important. I literally wouldn't be here without you. Your support is invaluable, and always always appreciated.

In the end, we have the beginning. The 13^{th} of September 2010 was a very special date. Not because this was the date I started my PhD, and not even because it was the day I met my partner in crime **Ida**, who taught me how to drink good beer, write python scripts, play clash of clans and how to surf in a bush.

No, the reason that date is special is because that is when I and **Jennie** started our weird journey together. And by journey I mean spend every waking and sleeping moment together for four and a half years. Who would have thought that we would manage to come through that alive? Even more surprising is that we now have a paper together!? You're my love, where I feel home. Thank you for everything

Lastly, as a bonus, here's a graph of my thesis progress over time just because I love graphs, and because I want you to love them too.

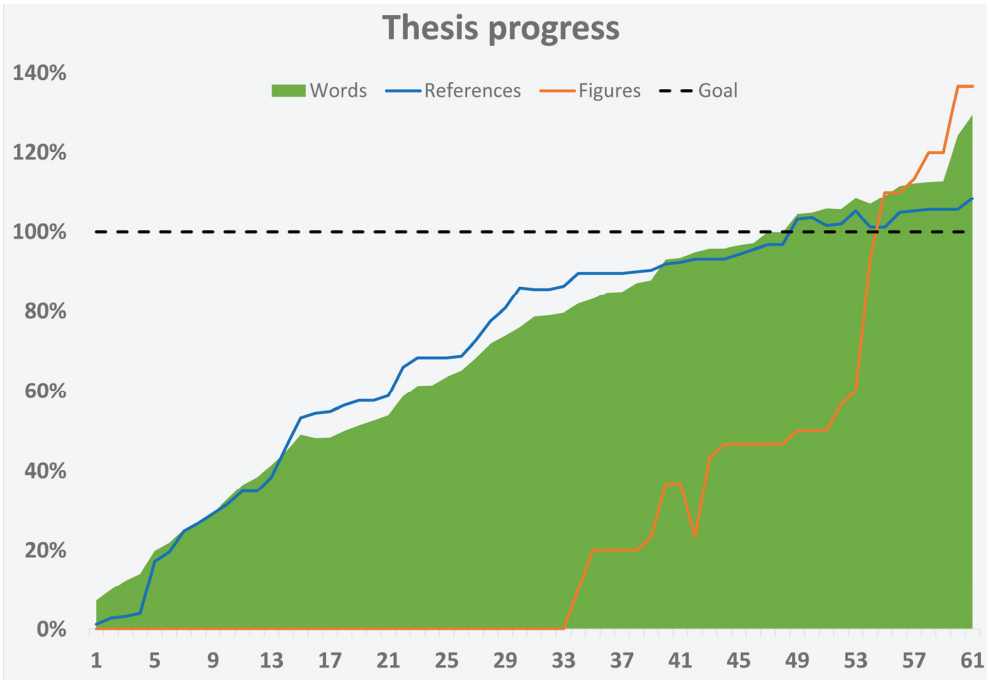

8. References

1. Ezkurdia, I. *et al.* The shrinking human protein coding complement: are there now fewer than 20,000 genes? *Arxiv* 34 (2013). doi:10.1101/001909
2. Osborne, T. *The vegetable proteins.* (Longmans, Green and Co, 1909).
3. Hartley, H. Origin of the Word 'Protein'. *Nature* **168,** 244–244 (1951).
4. McCoy, R., Meyer, C. & Rose, W. Nutrition classics from The Journal of Biological Chemistry 112:283-302, 1935-1936. Feeding experiments with mixtures of highly purified amino acids. 8. Isolation and identification of a new essential amino acid. *Nutr. Rev.* **32,** 16–18 (1974).
5. Sumner, J. The isolation crystallization of the enzyme Urease. *J. Biol. Chem.* **69,** 435–441 (1926).
6. Hünefeld, F. L. *Der Chemismus in der thierischen Organisation. Physiologisch-chemische Untersuchungen der materiellen Veränderungen, oder des Bildungslebens im thierischen Organismus; insbesondere des Blutbildungsprocesses, der Natur der Blut körperchen und ihrer Kernc.* (F.A. Brockhaus, 1840).
7. Kendrew, J. C. *et al.* A Three-Dimensional Model of the Myoglobin Molecule Obtained by X-Ray Analysis. *Nature* **181,** 662–666 (1958).
8. Berman, H. M. The Protein Data Bank. *Nucleic Acids Res.* **28,** 235–242 (2000).
9. White, S. H. The progress of membrane protein structure determination. *Protein Sci.* **13,** 1948–1949 (2004).
10. Almén, M. S., Nordström, K. J. V, Fredriksson, R. & Schiöth, H. B. Mapping the human membrane proteome: a majority of the human membrane proteins can be classified according to function and evolutionary origin. *BMC Biol.* **7,** 50 (2009).
11. Deisenhofer, J., Epp, O., Miki, K., Huber, R. & Michel, H. X-ray structure analysis of a membrane protein complex. *J. Mol. Biol.* **180,** 385–398 (1984).
12. Rask-Andersen, M., Almén, M. S. & Schiöth, H. B. Trends in the exploitation of novel drug targets. *Nat. Rev. Drug Discov.* **10,** 579–590 (2011).
13. Singer, S. & Nicolson, G. The fluid mosaic model of the structure of cell membranes. *Science (80-.).* **175,** 720–731 (1972).
14. Sud, M. *et al.* LMSD: LIPID MAPS structure database. *Nucleic Acids Res.* **35,** D527–32 (2007).
15. Yetukuri, L., Ekroos, K., Vida-Puig, A. & Orešič, M. Informatics and computational strategies for the study of lipids. *Molecular Biosystems* **4,** 121–127 (2008).
16. Daleke, D. L. Regulation of phospholipid asymmetry in the erythrocyte membrane. *Curr. Opin. Hematol.* **15,** 191–195 (2008).
17. Contreras, F. X., Sánchez-Magraner, L., Alonso, A. & Goñi, F. M. Transbilayer (flip-flop) lipid motion and lipid scrambling in membranes. *FEBS Letters* **584,** 1779–1786 (2010).
18. Seigneuret, M. & Devaux, P. F. ATP-dependent asymmetric distribution of spin-labeled phospholipids in the erythrocyte membrane: relation to shape changes. *Proc. Natl. Acad. Sci. U. S. A.* **81,** 3751–3755 (1984).
19. Simons, K. & Ikonen, E. Functional rafts in cell membranes. *Nature* **387,** 569–572 (1997).
20. Brown, D. a. & London, E. Structure and origin of ordered lipid domains in biological membranes. *J. Membr. Biol.* **164,** 103–114 (1998).
21. Cacas, J. L. *et al.* Lipids of plant membrane rafts. *Prog. Lipid Res.* **51,** 272–299 (2012).

22. Smaby, J. M., Momsen, M., Kulkarni, V. S. & Brown, R. E. Cholesterol-induced interfacial area condensations of galactosylceramides and sphingomyelins with identical acyl chains. *Biochemistry* **35,** 5696–5704 (1996).
23. Luckey, M. *Membrane structural biology with biochemical and biophysical functions*. (Cambridge University Press, 2008).
24. Sankaram, M. B. & Thompson, T. E. Interaction of cholesterol with various glycerophospholipids and sphingomyelin. *Biochemistry* **29,** 10670–10675 (1990).
25. Ohvo-Rekilä, H., Ramstedt, B., Leppimäki, P. & Peter Slotte, J. Cholesterol interactions with phospholipids in membranes. *Progress in Lipid Research* **41,** 66–97 (2002).
26. Itel, F. *et al.* CO2 permeability of cell membranes is regulated by membrane cholesterol and protein gas channels. *FASEB J.* **26,** 5182–5191 (2012).
27. Markham, J. E., Lynch, D. V., Napier, J. a., Dunn, T. M. & Cahoon, E. B. Plant sphingolipids: Function follows form. *Curr. Opin. Plant Biol.* **16,** 350–357 (2013).
28. Tjellström, H., Hellgren, L. I., Wieslander, A. & Sandelius, A. S. Lipid asymmetry in plant plasma membranes: phosphate deficiency-induced phospholipid replacement is restricted to the cytosolic leaflet. *FASEB J.* **24,** 1128–1138 (2010).
29. Tjellström, H., Andersson, M. X., Larsson, K. E. & Sandelius, A. S. Membrane phospholipids as a phosphate reserve: The dynamic nature of phospholipid-to-digalactosyl diacylglycerol exchange in higher plants. *Plant, Cell Environ.* **31,** 1388–1398 (2008).
30. Essigmann, B., Güler, S., Narang, R. ., Linke, D. & Benning, C. Phosphate availability affects the thylakoid lipid composition and the expression of SQD1, a gene required for sulfolipid biosynthesis in Arabidopsis thaliana. *Proc. Natl. Acad. Sci. U. S. A.* **95,** 1950–1955 (1998).
31. Halling, K. K. & Slotte, J. P. Membrane properties of plant sterols in phospholipid bilayers as determined by differential scanning calorimetry, resonance energy transfer and detergent-induced solubilization. *Biochim. Biophys. Acta* **1664,** 161–171 (2004).
32. Bao, H., Dalal, K., Wang, V., Rouiller, I. & Duong, F. The maltose ABC transporter: action of membrane lipids on the transporter stability, coupling and ATPase activity. *Biochim. Biophys. Acta* **1828,** 1723–1730 (2013).
33. Dumas, F., Tocanne, J.-F., Leblanc, G. & Lebrun, M.-C. Consequences of Hydrophobic Mismatch between Lipids and Melibiose Permease on Melibiose Transport. *Biochemistry* **39,** 4846–4854 (2000).
34. Pilot, J. D., East, J. M. & Lee, A. G. Effects of Bilayer Thickness on the Activity of Diacylglycerol Kinase of Escherichia coli. *Biochemistry* **40,** 8188–8195 (2001).
35. Lundbaek, J. A. *et al.* Capsaicin regulates voltage-dependent sodium channels by altering lipid bilayer elasticity. *Mol. Pharmacol.* **68,** 680–689 (2005).
36. Sangwan, V., Örvar, B. L., Beyerly, J., Hirt, H. & Dhindsa Rajinder, S. Opposite changes in membrane fluidity mimic cold and heat stress activation of distinct plant MAP kinase pathways. *Plant J.* **31,** 629–638 (2002).
37. Tong, J., Canty, J. T., Briggs, M. M. & McIntosh, T. J. The water permeability of lens aquaporin-0 depends on its lipid bilayer environment. *Exp. Eye Res.* **113,** 32–40 (2013).
38. Tong, J., Briggs, M. M. & McIntosh, T. J. Water permeability of aquaporin-4 channel depends on bilayer composition, thickness, and elasticity. *Biophys. J.* **103,** 1899–1908 (2012).
39. Alami, M., Dalal, K., Lelj-Garolla, B., Sligar, S. G. & Duong, F. Nanodiscs unravel the interaction between the SecYEG channel and its cytosolic partner SecA. *EMBO J.* **26,** 1995–2004 (2007).

40. Lill, R., Dowhan, W. & Wickner, W. The ATPase activity of secA is regulated by acidic phospholipids, secY, and the leader and mature domains of precursor proteins. *Cell* **60,** 271–280 (1990).
41. Frauenfeld, J. *et al.* Cryo-EM structure of the ribosome-SecYE complex in the membrane environment. *Nat. Struct. Mol. Biol.* **18,** 614–621 (2011).
42. Inagaki, S. *et al.* Modulation of the interaction between neurotensin receptor NTS1 and Gq protein by lipid. *J. Mol. Biol.* **417,** 95–111 (2012).
43. Baenziger, J. E., Morris, M.-L., Darsaut, T. E. & Ryan, S. E. Effect of Membrane Lipid Composition on the Conformational Equilibria of the Nicotinic Acetylcholine Receptor. *J. Biol. Chem.* **275,** 777–784 (2000).
44. Amin, D. N. & Hazelbauer, G. L. Influence of membrane lipid composition on a transmembrane bacterial chemoreceptor. *J. Biol. Chem.* **287,** 41697–41705 (2012).
45. Romanenko, V. G., Rothblat, G. H. & Levitan, I. Modulation of endothelial inward-rectifier K+ current by optical isomers of cholesterol. *Biophys. J.* **83,** 3211–3222 (2002).
46. Fürst, O., Nichols, C. G., Lamoureux, G. & D'Avanzo, N. Identification of a cholesterol-binding pocket in inward rectifier k(+) (kir) channels. *Biophys. J.* **107,** 2786–2796 (2014).
47. Chang, H. M., Reitstetter, R., Mason, R. P. & Gruener, R. Attenuation of channel kinetics and conductance by cholesterol: an interpretation using structural stress as a unifying concept. *J. Membr. Biol.* **143,** 51–63 (1995).
48. Lambeth, J. D. Cytochrome P-450scc. Cardiolipin as an effector of activity of a mitochondrial cytochrome P-450. *J. Biol. Chem.* **256,** 4757–4762 (1981).
49. Goormaghtigh, E., Brasseur, R. & Ruysschaert, J. M. Adriamycin inactivates cytochrome c oxidase by exclusion of the enzyme from its cardiolipin essential environment. *Biochem. Biophys. Res. Commun.* **104,** 314–320 (1982).
50. Claypool, S. M., Oktay, Y., Boontheung, P., Loo, J. A. & Koehler, C. M. Cardiolipin defines the interactome of the major ADP/ATP carrier protein of the mitochondrial inner membrane. *J. Cell Biol.* **182,** 937–950 (2008).
51. Klingenberg, M. Cardiolipin and mitochondrial carriers. *Biochim. Biophys. Acta* **1788,** 2048–2058 (2009).
52. Beyer, K. & Klingenberg, M. ADP/ATP carrier protein from beef heart mitochondria has high amounts of tightly bound cardiolipin, as revealed by 31P nuclear magnetic resonance. *Biochemistry* **24,** 3821–3826 (1985).
53. Guharay, F. & Sachs, F. Stretch-activated single ion channel currents in tissue-cultured embryonic chick skeletal muscle. *J. Physiol.* **352,** 685–701 (1984).
54. Sukharev, S. I., Blount, P., Martinac, B., Blattner, F. R. & Kung, C. A large-conductance mechanosensitive channel in E. coli encoded by mscL alone. *Nature* **368,** 265–268 (1994).
55. Wan, X., Steudle, E. & Hartung, W. Gating of water channels (aquaporins) in cortical cells of young corn roots by mechanical stimuli (pressure pulses): effects of ABA and of HgCl2. *J. Exp. Bot.* **55,** 411–22 (2004).
56. Fischer, G. *et al.* Crystal structure of a yeast aquaporin at 1.15 Å reveals a novel gating mechanism. *PLoS Biol.* **7,** 1–13 (2009).
57. Leitão, L., Prista, C., Loureiro-Dias, M. C., Moura, T. F. & Soveral, G. The grapevine tonoplast aquaporin TIP2;1 is a pressure gated water channel. *Biochem. Biophys. Res. Commun.* **450,** 289–294 (2014).

58. Sargiacomo, M., Sudol, M., Tang, Z. & Lisanti, M. P. Signal transducing molecules and glycosyl-phosphatidylinositol-linked proteins form a caveolin-rich insoluble complex in MDCK cells. *J. Cell Biol.* **122,** 789–807 (1993).
59. Brown, D. a. & Rose, J. K. Sorting of GPI-anchored proteins to glycolipid-enriched membrane subdomains during transport to the apical cell surface. *Cell* **68,** 533–544 (1992).
60. Danielsen, E. M. & Van Deurs, B. A transferrin-like GPI-linked iron-binding protein in detergent-insoluble noncaveolar microdomains at the apical surface of fetal intestinal epithelial cells. *J. Cell Biol.* **131,** 939–950 (1995).
61. Surma, M. a., Klose, C. & Simons, K. Lipid-dependent protein sorting at the trans-Golgi network. *Biochimica et Biophysica Acta - Molecular and Cell Biology of Lipids* **1821,** 1059–1067 (2012).
62. Guo, Y., Sirkis, D. W. & Schekman, R. Protein Sorting at the trans-Golgi Network. *Annu. Rev. Cell Dev. Biol.* **30,** 169–206 (2014).
63. Paganelli, C. V & Solomon, A. K. The rate of exchange of tritiated water across the human red cell membrane. *J. Gen. Physiol.* **41,** 259–277 (1957).
64. Heckmann, K. *Passive permeability of cell membranes, biomembranes. Passive permeability of cell membranes, biomembranes* **3,** (Plenum Press, New York, 1972).
65. Macey, R. I. Transport of water and urea in red blood cells. *Am. J. Physiol.* **246,** 195–203 (1984).
66. Denker, B. M., Smith, B. L., Kuhajda, F. P. & Agre, P. Identification, purification, and partial characterization of a novel Mr 28,000 integral membrane protein from erythrocytes and renal tubules. *J. Biol. Chem.* **263,** 15634–15642 (1988).
67. Preston, G. M. & Agre, P. Isolation of the cDNA for erythrocyte integral membrane protein of 28 kilodaltons: member of an ancient channel family. *Proc. Natl. Acad. Sci. U. S. A.* **88,** 11110–11114 (1991).
68. Preston, G. M., Carroll, T. P., Guggino, W. B. & Agre, P. Appearance of Water Channels in Xenopus Oocytes Expressing Red Cell CHIP28 Protein. *Science (80-.).* **256,** 385–387 (1992).
69. Agre, P. & Kozono, D. Aquaporin water channels: Molecular mechanisms for human diseases. in *FEBS Letters* **555,** 72–78 (2003).
70. King, L. S., Kozono, D. & Agre, P. From structure to disease: the evolving tale of aquaporin biology. *Nat. Rev. Mol. Cell Biol.* **5,** 687–698 (2004).
71. Morishita, Y., Sakube, Y., Sasaki, S. & Ishibashi, K. Molecular mechanisms and drug development in aquaporin water channel diseases: aquaporin superfamily (superaquaporins): expansion of aquaporins restricted to multicellular organisms. *J. Pharmacol. Sci.* **96,** 276–279 (2004).
72. Nielsen, S. *et al.* Vasopressin increases water permeability of kidney collecting duct by inducing translocation of aquaporin-CD water channels to plasma membrane. *Proc. Natl. Acad. Sci. U. S. A.* **92,** 1013–1017 (1995).
73. Hara-Chikuma, M. & Verkman, a S. Aquaporin-3 functions as a glycerol transporter in mammalian skin. *Biol. cell* **97,** 479–486 (2005).
74. Chen, Y.-C., Cadnapaphornchai, M. a & Schrier, R. W. Clinical update on renal aquaporins. *Biol. Cell* **97,** 357–371 (2005).
75. Amiry-Moghaddam, M. & Ottersen, O. P. The molecular basis of water transport in the brain. *Nat. Rev. Neurosci.* **4,** 991–1001 (2003).
76. Hara-Chikuma, M. & Verkman, A. . Prevention of skin tumorigenesis and impairment of epidermal cell proliferation by targeted aquaporin-3 gene disruption. *Mol. Cell. Biol.* **28,** 326–332 (2008).
77. Ishibashi, K., Hara, S. & Kondo, S. Aquaporin water channels in mammals. *Clinical and Experimental Nephrology* **13,** 107–117 (2009).

78. Ishibashi, K. *et al.* Cloning and functional expression of a new water channel abundantly expressed in the testis permeable to water, glycerol, and urea. *J. Biol. Chem.* **272,** 20782–20786 (1997).
79. Echevarría, M., Windhager, E. E. & Frindt, G. Selectivity of the renal collecting duct water channel aquaporin-3. *J. Biol. Chem.* **271,** 25079–25082 (1996).
80. Tsukaguchi, H. *et al.* Molecular characterization of a broad selectivity neutral solute channel. *J. Biol. Chem.* **273,** 24737–24743 (1998).
81. Ishibashi, K., Morinaga, T., Kuwahara, M., Sasaki, S. & Imai, M. Cloning and identification of a new member of water channel (AQP10) as an aquaglyceroporin. *Biochim. Biophys. Acta* **1576,** 335–340 (2002).
82. Madeira, A. *et al.* Human aquaporin-11 is a water and glycerol channel and localizes in the vicinity of lipid droplets in human adipocytes. *Obesity (Silver Spring).* **00,** 1–8 (2014).
83. Ishibashi, K. *et al.* Cloning and functional expression of a new aquaporin (AQP9) abundantly expressed in the peripheral leukocytes permeable to water and urea, but not to glycerol. *Biochem. Biophys. Res. Commun.* **244,** 268–274 (1998).
84. Hazama, A., Kozono, D., Guggino, W. B., Agre, P. & Yasui, M. Ion permeation of AQP6 water channel protein. Single channel recordings after Hg2+ activation. *J. Biol. Chem.* **277,** 29224–29230 (2002).
85. Ikeda, M. *et al.* Characterization of aquaporin-6 as a nitrate channel in mammalian cells. Requirement of pore-lining residue threonine 63. *J. Biol. Chem.* **277,** 39873–39879 (2002).
86. Yasui, M. *et al.* Rapid gating and anion permeability of an intracellular aquaporin. *Nature* **402,** 184–7 (1999).
87. Geyer, R. R., Musa-Aziz, R., Qin, X. & Boron, W. F. Relative CO(2)/NH(3) selectivities of mammalian aquaporins 0-9. *Am. J. Physiol. Cell Physiol.* **304,** 985–994 (2013).
88. Harper, E. M., Palmer, T. J. & Alphey, J. R. Effect of expressing the water channel aquaporin-1 on the CO2 permeability of Xenopus oocytes. *Geological Magazine* **134,** 403–407 (1997).
89. Holm, L. M. *et al.* NH3 and NH4 + permeability in aquaporin-expressing Xenopus oocytes. *Pflugers Arch. Eur. J. Physiol.* **450,** 415–428 (2005).
90. Bienert, G. P. *et al.* Specific aquaporins facilitate the diffusion of hydrogen peroxide across membranes. *J. Biol. Chem.* **282,** 1183–1192 (2007).
91. Liu, Z. *et al.* Arsenite transport by mammalian aquaglyceroporins AQP7 and AQP9. *Proc. Natl. Acad. Sci. U. S. A.* **99,** 6053–6058 (2002).
92. Steudle, E. The cohesion-tension mechanism and the acquisition of water by plant roots. *Annu. Rev. Plant Physiol. Plant Mol. Biol.* **52,** 847–875 (2001).
93. Volkov, V. *et al.* Water permeability differs between growing and non-growing barley leaf tissues. *J. Exp. Bot.* **58,** 377–390 (2007).
94. Maurel, C., Verdoucq, L., Luu, D.-T. & Santoni, V. Plant aquaporins: membrane channels with multiple integrated functions. *Annu. Rev. Plant Biol.* **59,** 595–624 (2008).
95. Azad, A. K., Katsuhara, M., Sawa, Y., Ishikawa, T. & Shibata, H. Characterization of four plasma membrane aquaporins in tulip petals: A putative homolog is regulated by phosphorylation. *Plant Cell Physiol.* **49,** 1196–1208 (2008).
96. Johanson, U. The Complete Set of Genes Encoding Major Intrinsic Proteins in Arabidopsis Provides a Framework for a New Nomenclature for Major Intrinsic Proteins in Plants. *PLANT Physiol.* **126,** 1358–1369 (2001).
97. Chaumont, F., Barrieu, F. & Wojcik, E. Aquaporins constitute a large and highly divergent protein family in maize. *PLANT Physiol.* **125,** 1206–1215 (2001).

98. Sade, N. *et al.* Improving plant stress tolerance and yield production: Is the tonoplast aquaporin SlTIP2;2 a key to isohydric to anisohydric conversion? *New Phytol.* **181,** 651–661 (2009).
99. Sakurai, J., Ishikawa, F., Yamaguchi, T., Uemura, M. & Maeshima, M. Identification of 33 rice aquaporin genes and analysis of their expression and function. *Plant Cell Physiol.* **46,** 1568–77 (2005).
100. Fouquet, R., Léon, C., Ollat, N. & Barrieu, F. Identification of grapevine aquaporins and expression analysis in developing berries. *Plant Cell Rep.* **27,** 1541–1550 (2008).
101. Zhang, D. Y. *et al.* Genome-Wide Sequence Characterization and Expression Analysis of Major Intrinsic Proteins in Soybean (Glycine max L.). *PLoS One* **8,** 1–13 (2013).
102. Johanson, U. & Gustavsson, S. A new subfamily of major intrinsic proteins in plants. *Mol. Biol. Evol.* **19,** 456–61 (2002).
103. Danielson, J. a H. & Johanson, U. Unexpected complexity of the aquaporin gene family in the moss Physcomitrella patens. *BMC Plant Biol.* **8,** 45 (2008).
104. Lopez, D. *et al.* Insights into Populus XIP aquaporins: evolutionary expansion, protein functionality, and environmental regulation. *J. Exp. Bot.* **63,** 2217–30 (2012).
105. Gustavsson, S., Lebrun, A.-S., Nordén, K., Chaumont, F. & Johanson, U. A novel plant major intrinsic protein in Physcomitrella patens most similar to bacterial glycerol channels. *Plant Physiol.* **139,** 287–95 (2005).
106. Quigley, F., Rosenberg, J. M., Shachar-Hill, Y. & Bohnert, H. J. From genome to function: the Arabidopsis aquaporins. *Genome Biol.* **3,** RESEARCH0001 (2002).
107. Ma, J. F. *et al.* A silicon transporter in rice. *Nature* **440,** 688–691 (2006).
108. Takano, J. *et al.* The Arabidopsis major intrinsic protein NIP5;1 is essential for efficient boron uptake and plant development under boron limitation. *Plant Cell* **18,** 1498–1509 (2006).
109. Mizutani, M., Watanabe, S., Nakagawa, T. & Maeshima, M. Aquaporin NIP2;1 is mainly localized to the ER membrane and shows root-specific accumulation in Arabidopsis thaliana. *Plant Cell Physiol.* **47,** 1420–1426 (2006).
110. Noronha, H. *et al.* The grape aquaporin VvSIP1 transports water across the ER membrane. *J. Exp. Bot.* **65,** 981–993 (2014).
111. Ishikawa, F., Suga, S., Uemura, T., Sato, M. H. & Maeshima, M. Novel type aquaporin SIPs are mainly localized to the ER membrane and show cell-specific expression in Arabidopsis thaliana. *FEBS Lett.* **579,** 5814–5820 (2005).
112. Gerbeau, P., Güçlü, J., Ripoche, P. & Maurel, C. Aquaporin Nt-TIPa can account for the high permeability of tobacco cell vacuolar membrane to small neutral solutes. *Plant J.* **18,** 577–587 (1999).
113. Bienert, G. P., Bienert, M. D., Jahn, T. P., Boutry, M. & Chaumont, F. Solanaceae XIPs are plasma membrane aquaporins that facilitate the transport of many uncharged substrates. *Plant J.* **66,** 306–317 (2011).
114. Biela, A. *et al.* The Nicotiana tabacum plasma membrane aquaporin NtAQP1 is mercury-insensitive and permeable for glycerol. *Plant J.* **18,** 565–570 (1999).
115. Rivers, R. L. *et al.* Functional analysis of nodulin 26, an aquaporin in soybean root nodule symbiosomes. *J. Biol. Chem.* **272,** 16256–16261 (1997).
116. Choi, W. G. & Roberts, D. M. Arabidopsis NIP2;1, a major intrinsic protein transporter of lactic acid induced by anoxic stress. *J. Biol. Chem.* **282,** 24209–24218 (2007).
117. Uehlein, N., Lovisolo, C., Siefritz, F. & Kaldenhoff, R. The tobacco aquaporin NtAQP1 is a membrane CO2 pore with physiological functions. *Nature* **425,** 734–737 (2003).

118. Mori, I. C. *et al.* CO2 transport by PIP2 aquaporins of barley. *Plant Cell Physiol.* **55,** 251–257 (2014).
119. Nielsen, S. *et al.* Aquaporins in the kidney: from molecules to medicine. *Physiol. Rev.* **82,** 205–244 (2002).
120. Luu, D. T., Martiniãre, A., Sorieul, M., Runions, J. & Maurel, C. Fluorescence recovery after photobleaching reveals high cycling dynamics of plasma membrane aquaporins in Arabidopsis roots under salt stress. *Plant J.* **69,** 894–905 (2012).
121. Vera-Estrella, R., Barkla, B. J., Bohnert, H. J. & Pantoja, O. Novel regulation of aquaporins during osmotic stress. *Plant Physiol.* **135,** 2318–2329 (2004).
122. Boursiac, Y. *et al.* Early Effects of Salinity on Water Transport in Arabidopsis Roots. Molecular and Cellular Features of Aquaporin Expression. *Plant Physiol.* **139,** 790–805 (2005).
123. Boursiac, Y. *et al.* Stimulus-induced downregulation of root water transport involves reactive oxygen species-activated cell signalling and plasma membrane intrinsic protein internalization. *Plant J.* **56,** 207–218 (2008).
124. Chaumont, F. & Tyerman, S. D. Aquaporins: highly regulated channels controlling plant water relations. *Plant Physiol.* **164,** 1600–18 (2014).
125. Chaumont, F., Barrieu, F., Jung, R. & Chrispeels, M. J. Plasma membrane intrinsic proteins from maize cluster in two sequence subgroups with differential aquaporin activity. *Plant Physiol.* **122,** 1025–1034 (2000).
126. Zelazny, E. *et al.* FRET imaging in living maize cells reveals that plasma membrane aquaporins interact to regulate their subcellular localization. *Proc. Natl. Acad. Sci. U. S. A.* **104,** 12359–12364 (2007).
127. Sorieul, M., Santoni, V., Maurel, C. & Luu, D. T. Mechanisms and Effects of Retention of Over-Expressed Aquaporin AtPIP2;1 in the Endoplasmic Reticulum. *Traffic* **12,** 473–482 (2011).
128. Zelazny, E., Miecielica, U., Borst, J. W., Hemminga, M. a. & Chaumont, F. An N-terminal diacidic motif is required for the trafficking of maize aquaporins ZmPIP2;4 and ZmPIP2;5 to the plasma membrane. *Plant J.* **57,** 346–355 (2009).
129. Takano, J. *et al.* Polar localization and degradation of Arabidopsis boron transporters through distinct trafficking pathways. *Proc. Natl. Acad. Sci. U. S. A.* **107,** 5220–5225 (2010).
130. Ma, J. F. *et al.* An efflux transporter of silicon in rice. *Nature* **448,** 209–212 (2007).
131. Li, X. *et al.* Single-Molecule Analysis of PIP2;1 Dynamics and Partitioning Reveals Multiple Modes of Arabidopsis Plasma Membrane Aquaporin Regulation. *Plant Cell* **23,** 3780–3797 (2011).
132. Törnroth-Horsefield, S. *et al.* Structural mechanism of plant aquaporin gating. *Nature* **439,** 688–94 (2006).
133. Gout, E., Boisson, A., Aubert, S., Douce, R. & Bligny, R. Origin of the cytoplasmic pH changes during anaerobic stress in higher plant cells. Carbon-13 and phosphorous-31 nuclear magnetic resonance studies. *Plant Physiol.* **125,** 912–925 (2001).
134. Alleva, K. *et al.* Plasma membrane of Beta vulgaris storage root shows high water channel activity regulated by cytoplasmic pH and a dual range of calcium concentrations. *J. Exp. Bot.* **57,** 609–621 (2006).
135. Gerbeau, P. *et al.* The water permeability of Arabidopsis plasma membrane is regulated by divalent cations and pH. *Plant J.* **30,** 71–81 (2002).
136. Tournaire-Roux, C. *et al.* Cytosolic pH regulates root water transport during anoxic stress through gating of aquaporins. *Nature* **425,** 393–397 (2003).
137. Verdoucq, L., Grondin, A. & Maurel, C. Structure-function analysis of plant aquaporin AtPIP2;1 gating by divalent cations and protons. *Biochem. J.* **415,** 409–16 (2008).

138. Fischer, M. & Kaldenhoff, R. On the pH regulation of plant aquaporins. *J. Biol. Chem.* **283,** 33889–33892 (2008).
139. Johansson, I., Larsson, C., Ek, B. & Kjellbom, P. The major integral proteins of spinach leaf plasma membranes are putative aquaporins and are phosphorylated in response to Ca2+ and apoplastic water potential. *Plant Cell* **8,** 1181–1191 (1996).
140. Weaver, C. D., Crombie, B., Stacey, G. & Roberts, D. M. Calcium-dependent phosphorylation of symbiosome membrane proteins from nitrogen-fixing soybean nodules : evidence for phosphorylation of nodulin-26. *Plant Physiol.* **95,** 222–227 (1991).
141. Johansson, I. Water Transport Activity of the Plasma Membrane Aquaporin PM28A Is Regulated by Phosphorylation. *plant cell online* **10,** 451–460 (1998).
142. Johnson, K. D. & Chrispeels, M. J. Tonoplast-bound protein kinase phosphorylates tonoplast intrinsic protein. *Plant Physiol.* **100,** 1787–1795 (1992).
143. Inoue, K., Takeuchi, Y., Nishimura, M. & Hara-Nishimura, I. Characterization of two integral membrane proteins located in the protein bodies of pumpkin seeds. *Plant Mol. Biol.* **28,** 1089–1101 (1995).
144. Leitão, L., Prista, C., Moura, T. F., Loureiro-Dias, M. C. & Soveral, G. Grapevine aquaporins: Gating of a tonoplast intrinsic protein (TIP2;1) by cytosolic pH. *PLoS One* **7,** (2012).
145. Soto, G. *et al.* TIP5;1 is an aquaporin specifically targeted to pollen mitochondria and is probably involved in nitrogen remobilization in Arabidopsis thaliana. *Plant J.* **64,** 1038–1047 (2010).
146. Harries, W. E. C., Akhavan, D., Miercke, L. J. W., Khademi, S. & Stroud, R. M. The channel architecture of aquaporin 0 at a 2.2-A resolution. *Proc. Natl. Acad. Sci. U. S. A.* **101,** 14045–14050 (2004).
147. Sui, H., Han, B. G., Lee, J. K., Walian, P. & Jap, B. K. Structural basis of water-specific transport through the AQP1 water channel. *Nature* **414,** 872–878 (2001).
148. Frick, A. *et al.* X-ray structure of human aquaporin 2 and its implications for nephrogenic diabetes insipidus and trafficking. *Proc. Natl. Acad. Sci. U. S. A.* **111,** 1–6 (2014).
149. Ho, J. D. *et al.* Crystal structure of human aquaporin 4 at 1.8 A and its mechanism of conductance. *Proc. Natl. Acad. Sci. U. S. A.* **106,** 7437–7442 (2009).
150. Horsefield, R. *et al.* High-resolution x-ray structure of human aquaporin 5. *Proc. Natl. Acad. Sci. U. S. A.* **105,** 13327–32 (2008).
151. Savage, D. F., Egea, P. F., Robles-colmenares, Y., Iii, J. D. O. C. & Stroud, R. M. Architecture and Selectivity ° X-Ray Structure in Aquaporins 2 . 5 : A of Aquaporin Z. *Structure* **1,** (2003).
152. Fu, D. *et al.* Structure of a glycerol-conducting channel and the basis for its selectivity. *Science* **290,** 481–486 (2000).
153. Lee, J. K. *et al.* Structural basis for conductance by the archaeal aquaporin AqpM at 1.68 A. *Proc. Natl. Acad. Sci. U. S. A.* **102,** 18932–18937 (2005).
154. Newby, Z. E. R. *et al.* Crystal structure of the aquaglyceroporin PfAQP from the malarial parasite Plasmodium falciparum. *Nat. Struct. Mol. Biol.* **15,** 619–625 (2008).
155. Murata, K. *et al.* Structural determinants of water permeation through aquaporin-1. *Nature* **407,** 599–605 (2000).
156. Zeidel, M. L., Ambudkar, S. V, Smith, B. L. & Agre, P. Reconstitution of functional water channels in liposomes containing purified red cell CHIP28 protein. *Biochemistry* **31,** 7436–7440 (1992).
157. Choi, J.-H., Lee, H.-J. & Moon, S.-H. Effects of Electrolytes on the Transport Phenomena in a Cation-Exchange Membrane. *J. Colloid Interface Sci.* **238,** 188–195 (2001).

158. De Grotthuss, C. J. D. Sur la decomposition de l'eau et des corps qu'elle tient en dissolution a l'aide de l'electricite galvanique. *Ann. Chim. LVIII* **58,** 54–73 (1806).
159. Markovitch, O. *et al.* Special pair dance and partner selection: Elementary steps in proton transport in liquid water. *J. Phys. Chem. B* **112,** 9456–9466 (2008).
160. Lapid, H., Agmon, N., Petersen, M. K. & Voth, G. A. A bond-order analysis of the mechanism for hydrated proton mobility in liquid water. *J. Chem. Phys.* **122,** (2005).
161. Shevchuk, R., Agmon, N. & Rao, F. Network analysis of proton transfer in liquid water. *J. Chem. Phys.* **140,** 244502 (2014).
162. Tielrooij, K. J., Timmer, R. L. A., Bakker, H. J. & Bonn, M. Structure dynamics of the proton in liquid water probed with terahertz time-domain spectroscopy. *Phys. Rev. Lett.* **102,** (2009).
163. Tajkhorshid, E. *et al.* Control of the selectivity of the aquaporin water channel family by global orientational tuning. *Science* **296,** 525–530 (2002).
164. De Groot, B. L. & Grubmüller, H. Water permeation across biological membranes: mechanism and dynamics of aquaporin-1 and GlpF. *Science* **294,** 2353–2357 (2001).
165. Kosinska-Eriksson, U. *et al.* Subangstrom resolution X-ray structure details aquaporin-water interactions. *Science* **340,** 1346–9 (2013).
166. De Groot, B. L. & Grubmüller, H. The dynamics and energetics of water permeation and proton exclusion in aquaporins. *Current Opinion in Structural Biology* **15,** 176–183 (2005).
167. Wu, B., Steinbronn, C., Alsterfjord, M., Zeuthen, T. & Beitz, E. Concerted action of two cation filters in the aquaporin water channel. *EMBO J.* **28,** 2188–2194 (2009).
168. Li, H. *et al.* Enhancement of proton conductance by mutations of the selectivity filter of aquaporin-1. *J. Mol. Biol.* **407,** 607–620 (2011).
169. Macey, R. I. & Farmer, R. E. Inhibition of water and solute permeability in human red cells. *Biochim. Biophys. Acta* **211,** 104–6 (1970).
170. Savage, D. F. & Stroud, R. M. Structural basis of aquaporin inhibition by mercury. *J. Mol. Biol.* **368,** 607–17 (2007).
171. Preston, G. M., Jung, J. S., Guggino, W. B. & Agre, P. The mercury-sensitive residue at cysteine 189 in the CHIP28 water channel. *J. Biol. Chem.* **268,** 17–20 (1993).
172. Hirano, Y. *et al.* Molecular mechanisms of how mercury inhibits water permeation through aquaporin-1: understanding by molecular dynamics simulation. *Biophys. J.* **98,** 1512–9 (2010).
173. Yukutake, Y. *et al.* Mercury chloride decreases the water permeability of aquaporin-4-reconstituted proteoliposomes. *Biol. Cell* **100,** 355–363 (2008).
174. Yakata, K., Tani, K. & Fujiyoshi, Y. Water permeability and characterization of aquaporin-11. *J. Struct. Biol.* **174,** 315–320 (2011).
175. Ma, T., Yang, B., Kuo, W. L. & Verkman, a S. cDNA cloning and gene structure of a novel water channel expressed exclusively in human kidney: evidence for a gene cluster of aquaporins at chromosome locus 12q13. *Genomics* **35,** 543–550 (1996).
176. Chandy, G., Zampighi, G. a., Kreman, M. & Hall, J. E. Comparison of the water transporting properties of MIP and AQP1. *J. Membr. Biol.* **159,** 29–39 (1997).
177. Costello, M. J., McIntosh, T. J. & Robertson, J. D. Distribution of gap junctions and square array junctions in the mammalian lens. *Investig. Ophthalmol. Vis. Sci.* **30,** 975–989 (1989).
178. Gonen, T., Sliz, P., Kistler, J., Cheng, Y. & Walz, T. Aquaporin-0 membrane junctions reveal the structure of a closed water pore. *Nature* **429,** 193–197 (2004).
179. Reichow, S. L. *et al.* Allosteric mechanism of water-channel gating by Ca2+-calmodulin. *Nat. Struct. Mol. Biol.* **20,** 1085–92 (2013).

180. Nemeth-Cahalan, K. L. & Hall, J. E. pH and Calcium Regulate the Water Permeability of Aquaporin 0. *J. Biol. Chem.* **275,** 6777–6782 (2000).
181. Sachdeva, R. & Singh, B. Insights into structural mechanisms of gating induced regulation of aquaporins. *Prog. Biophys. Mol. Biol.* **114,** 69–79 (2014).
182. Jiang, J., Daniels, B. V. & Fu, D. Crystal structure of AqpZ tetramer reveals two distinct Arg-189 conformations associated with water permeation through the narrowest constriction of the water-conducting channel. *J. Biol. Chem.* **281,** 454–460 (2006).
183. Maa, Y. F. & Prestrelski, S. J. Biopharmaceutical powders: particle formation and formulation considerations. *Curr. Pharm. Biotechnol.* **1,** 283–302 (2000).
184. Bayburt, T. H., Grinkova, Y. V. & Sligar, S. G. Self-Assembly of Discoidal Phospholipid Bilayer Nanoparticles with Membrane Scaffold Proteins. *Nano Lett.* **2,** 853–856 (2002).
185. Denisov, I. G., Grinkova, Y. V, Lazarides, a a & Sligar, S. G. Directed self-assembly of monodisperse phospholipid bilayer Nanodiscs with controlled size. *J. Am. Chem. Soc.* **126,** 3477–87 (2004).
186. Denisov, I. G., McLean, M. A., Shaw, A. W., Grinkova, Y. V & Sligar, S. G. Thermotropic phase transition in soluble nanoscale lipid bilayers. *J. Phys. Chem. B* **109,** 15580–8 (2005).
187. Bayburt, T. H. & Sligar, S. G. Membrane protein assembly into Nanodiscs. *FEBS Lett.* **584,** 1721–1727 (2010).
188. Bao, H., Duong, F. & Chan, C. S. A step-by-step method for the reconstitution of an ABC transporter into nanodisc lipid particles. *J. Vis. Exp.* e3910 (2012). doi:10.3791/3910
189. Bayburt, T. H. *et al.* Monomeric rhodopsin is sufficient for normal rhodopsin kinase (GRK1) phosphorylation and arrestin-1 binding. *J. Biol. Chem.* **286,** 1420–1428 (2011).
190. Kynde, S. a. R. *et al.* Small-angle scattering gives direct structural information about a membrane protein inside a lipid environment. *Acta Crystallogr. D. Biol. Crystallogr.* **70,** 371–83 (2014).
191. Adamson, R. J. & Watts, A. Kinetics of the early events of GPCR signalling. *FEBS Lett.* **588,** 4701–4707 (2014).
192. Brewer, K. D., Li, W., Horne, B. E. & Rizo, J. Reluctance to membrane binding enables accessibility of the synaptobrevin SNARE motif for SNARE complex formation. *Proc. Natl. Acad. Sci. U. S. A.* **108,** 12723–8 (2011).
193. Shin, J., Lou, X., Kweon, D.-H. & Shin, Y.-K. Multiple conformations of a single SNAREpin between two nanodisc membranes reveal diverse pre-fusion states. *Biochem. J.* **459,** 95–102 (2014).
194. Krishnakumar, S. S. *et al.* Conformational dynamics of calcium-triggered activation of fusion by synaptotagmin. *Biophys. J.* **105,** 2507–16 (2013).
195. Bibow, S. *et al.* Measuring membrane protein bond orientations in nanodiscs via residual dipolar couplings. *Protein Sci.* **23,** 851–856 (2014).
196. Denisov, I. G. & Sligar, S. G. Cytochromes P450 in nanodiscs. *Biochim. Biophys. Acta* **1814,** 223–9 (2011).
197. Bayburt, T. H. & Sligar, S. G. Single-molecule height measurements on microsomal cytochrome P450 in nanometer-scale phospholipid bilayer disks. *Proc. Natl. Acad. Sci. U. S. A.* **99,** 6725–6730 (2002).
198. Sušac, L., Horst, R. & Wüthrich, K. Solution-NMR characterization of outer-membrane protein A from E. coli in lipid bilayer nanodiscs and detergent micelles. *Chembiochem* **15,** 995–1000 (2014).
199. Grisshammer, R. Understanding recombinant expression of membrane proteins. *Current Opinion in Biotechnology* **17,** 337–340 (2006).

200. He, Y., Wang, K. & Yan, N. The recombinant expression systems for structure determination of eukaryotic membrane proteins. *Protein & Cell* **5,** 658–672 (2014).
201. Guilliermond, A. *Zygosaccharomyces Pastori, nouvelle espèce de levures à copulation hété rogamique*. (Société mycologique de France, 1920).
202. Ogata, K., Nishikawa, H. & Ohsugi, M. A Yeast Capable of Utilizing Methanol. *Agricultural and Biological Chemistry* **33,** 1519–1520 (1969).
203. Cereghino, J. L. & Cregg, J. M. Heterologous protein expression in the methylotrophic yeast Pichia pastoris. *FEMS Microbiology Reviews* **24,** 45–66 (2000).
204. Edebo, L. A new press for the disruption of micro-organisms and other cells. *J. Biochem. Microbiol. Technol. Eng.* **2,** 453–479 (1960).
205. Drew, D., Lerch, M., Kunji, E., Slotboom, D.-J. & de Gier, J.-W. Optimization of membrane protein overexpression and purification using GFP fusions. *Nat. Methods* **3,** 303–313 (2006).
206. Sonoda, Y. *et al.* Benchmarking membrane protein detergent stability for improving throughput of high-resolution X-ray structures. *Structure* **19,** 17–25 (2011).
207. Newstead, S., Kim, H., von Heijne, G., Iwata, S. & Drew, D. High-throughput fluorescent-based optimization of eukaryotic membrane protein overexpression and purification in Saccharomyces cerevisiae. *Proc. Natl. Acad. Sci. U. S. A.* **104,** 13936–41 (2007).
208. Bamber, L. *et al.* Yeast mitochondrial ADP/ATP carriers are monomeric in detergents. *Proc. Natl. Acad. Sci. U. S. A.* **103,** 16224–16229 (2006).
209. Oliver, R. C. *et al.* Dependence of micelle size and shape on detergent alkyl chain length and head group. *PLoS One* **8,** e62488 (2013).
210. Klammt, C. *et al.* Evaluation of detergents for the soluble expression of α-helical and β-barrel-type integral membrane proteins by a preparative scale individual cell-free expression system. *FEBS J.* **272,** 6024–6038 (2005).
211. Chae, P. S. *et al.* Maltose-neopentyl glycol (MNG) amphiphiles for solubilization, stabilization and crystallization of membrane proteins. *Nat. Methods* **7,** 1003–1008 (2010).
212. Herrmann, K. W. Non-ionic-cationic micellar properties of dimethyldodecylamineoxide. *J. Phys. Chem.* **66,** 295–300 (1962).
213. Herrmann, K. . Micellar properties of some zwitterionic surfactants. *J. Colloid Interface Sci.* **22,** 352–359 (1966).
214. De Vendittis, E., Palumbo, G., Parlato, G. & Bocchini, V. A fluorimetric method for the estimation of the critical micelle concentration of surfactants. *Analytical Biochemistry* **115,** 278–286 (1981).
215. Le Maire, M., Champeil, P. & Møller, J. V. Interaction of membrane proteins and lipids with solubilizing detergents. *Biochimica et Biophysica Acta - Biomembranes* **1508,** 86–111 (2000).
216. Johnson, S. M., Bangham, a D., Hill, M. W. & Korn, E. D. Single bilayer liposomes. *Biochim. Biophys. Acta* **233,** 820–826 (1971).
217. Olson, F., Hunt, C. a, Szoka, F. C., Vail, W. J. & Papahadjopoulos, D. Preparation of liposomes of defined size distribution by extrusion through polycarbonate membranes. *Biochim. Biophys. Acta* **557,** 9–23 (1979).
218. Rigaud, J. L. *et al.* Bio-Beads: an efficient strategy for two-dimensional crystallization of membrane proteins. *J. Struct. Biol.* **118,** 226–235 (1997).
219. Ritchie, T. K. *et al.* Chapter 11 - Reconstitution of Membrane Proteins in Phospholipid Bilayer Nanodiscs. *Methods in Enzymology* **464,** 211–231 (2009).
220. Silvius, J. R. Thermotropic phase transitions of pure lipids in model membranes and their modifications by membrane proteins. *Lipid-protein Interact.* **2,** 239–281 (1982).

221. Latimer, P. & Pyle, B. E. Light scattering at various angles. Theoretical predictions of the effects of particle volume changes. *Biophys. J.* **12,** 764–773 (1972).
222. Van Heeswijk, M. P. E. & van Os, C. H. Osmotic water permeabilities of brush border and basolateral membrane vesicles from rat renal cortex and small intestine. *J. Membr. Biol.* **92,** 183–193 (1986).
223. Grzelakowski, M., Cherenet, M. F., Shen, Y. & Kumar, M. A framework for accurate evaluation of the promise of aquaporin based biomimetic membranes. *J. Memb. Sci.* (2015). doi:10.1016/j.memsci.2015.01.023
224. Chao, W., Kim, J., Rekawa, S., Fischer, P. & Anderson, E. H. Demonstration of 12 nm resolution Fresnel zone plate lens based soft x-ray microscopy. *Opt. Express* **17,** 17669–17677 (2009).
225. Sonoda, Y. *et al.* Tricks of the trade used to accelerate high-resolution structure determination of membrane proteins. *FEBS Letters* **584,** 2539–2547 (2010).
226. Guan, L. *et al.* Manipulating phospholipids for crystallization of a membrane transport protein. *Proc. Natl. Acad. Sci. U. S. A.* **103,** 1723–6 (2006).
227. Caffrey, M. A comprehensive review of the lipid cubic phase or in meso method for crystallizing membrane and soluble proteins and complexes. *Acta Crystallogr. Sect. F Struct. Biol. Commun.* **71,** 3–18 (2015).
228. Cherezov, V., Clogston, J., Papiz, M. Z. & Caffrey, M. Room to move: Crystallizing membrane proteins in swollen lipidic mesophases. *J. Mol. Biol.* **357,** 1605–1618 (2006).
229. DiMaio, F. *et al.* Improved molecular replacement by density- and energy-guided protein structure optimization. *Nature* **473,** 540–543 (2011).
230. Tidow, H. *et al.* A bimodular mechanism of calcium control in eukaryotes. *Nature* **491,** 468–472 (2012).
231. Guinier, A. La diffraction des rayons X aux tres petits angles: applications a l'etude de phenomenes ultramicroscopiques. (1939).
232. Svergun, D. I. & Koch, M. H. J. Small-angle scattering studies of biological macromolecules in solution. *Reports on Progress in Physics* **66,** 1735–1782 (2003).
233. Mylonas, E. & Svergun, D. I. Accuracy of molecular mass determination of proteins in solution by small-angle X-ray scattering. in *Journal of Applied Crystallography* **40,** s245–s249 (2007).
234. Jacques, D. a. & Trewhella, J. Small-angle scattering for structural biology - Expanding the frontier while avoiding the pitfalls. *Protein Science* **19,** 642–657 (2010).
235. Sokolova, A. V., Volkov, V. V. & Svergun, D. I. Database for rapid protein classification based on small-angle X-ray scattering data. *Crystallogr. Reports* **48,** 959–965 (2003).
236. Svergun, D., Barberato, C. & Koch, M. H. CRYSOL - A program to evaluate X-ray solution scattering of biological macromolecules from atomic coordinates. *J. Appl. Crystallogr.* **28,** 768–773 (1995).
237. Svergun, D. I. Restoring low resolution structure of biological macromolecules from solution scattering using simulated annealing. *Biophys. J.* **76,** 2879–2886 (1999).
238. Franke, D. & Svergun, D. I. DAMMIF, a program for rapid ab-initio shape determination in small-angle scattering. *J. Appl. Crystallogr.* **42,** 342–346 (2009).
239. O'Neill, H., Heller, W. T., Helton, K. E., Urban, V. S. & Greenbaum, E. Small-angle X-ray scattering study of photosystem i - detergent complexes: Implications for membrane protein crystallization. *J. Phys. Chem. B* **111,** 4211–4219 (2007).
240. Mo, Y., Lee, B. K., Ankner, J. F., Becker, J. M. & Heller, W. T. Detergent-associated solution conformations of helical and beta-barrel membrane proteins. *J. Phys. Chem. B* **112,** 13349–13354 (2008).

241. Berthaud, A., Manzi, J., Pérez, J. & Mangenot, S. Modeling detergent organization around aquaporin-0 using small-angle X-ray scattering. *J. Am. Chem. Soc.* **134,** 10080–10088 (2012).
242. Pernot, P. *et al.* Upgraded ESRF BM29 beamline for SAXS on macromolecules in solution. *J. Synchrotron Radiat.* **20,** 660–664 (2013).
243. Koutsioubas, A., Berthaud, A., Mangenot, S. & Pérez, J. Ab initio and all-atom modeling of detergent organization around Aquaporin-0 based on SAXS data. *J. Phys. Chem. B* **117,** 13588–94 (2013).
244. Engelman, D. M. & Moore, P. B. Determination of quaternary structure by small angle neutron scattering. *Annu. Rev. Biophys. Bioeng.* **4,** 219–241 (1975).
245. Jacrot, B. The study of biological structures by neutron scattering from solution. *Reports on Progress in Physics* **39,** 911–953 (2001).
246. Nyblom, M. *et al.* Structural and functional analysis of SoPIP2;1 mutants adds insight into plant aquaporin gating. *J. Mol. Biol.* **387,** 653–68 (2009).
247. Beitz, E. T(E)Xtopo: shaded membrane protein topology plots in LAT(E)X2epsilon. *Bioinformatics* **16,** 1050–1051 (2000).
248. Secchi, F., MacIver, B., Zeidel, M. L. & Zwieniecki, M. a. Functional analysis of putative genes encoding the PIP2 water channel subfamily in Populus trichocarpa. *Tree Physiol.* **29,** 1467–1477 (2009).
249. Krajinski, F. *et al.* Arbuscular mycorrhiza development regulates the mRNA abundance of Mtaqp1 encoding a mercury-insensitive aquaporin of Medicago truncatula. *Planta* **211,** 85–90 (2000).
250. Delnomdedieu, M., Boudou, A., Desmazès, J.-P. & Georgescauld, D. Interaction of mercury chloride with the primary amine group of model membranes containing phosphatidylserine and phosphatidylethanolamine. *Biochim. Biophys. Acta - Biomembr.* **986,** 191–199 (1989).
251. Lu, Z. & Neumann, P. Water Stress Inhibits Hydraulic Conductance and Leaf Growth in Rice Seedlings but Not the Transport of Water via Mercury-Sensitive Water Channels in the Root. *Plant physiology* **120,** 143–152 (1999).
252. Maggio, a. & Joly, R. J. Effects of Mercuric Chloride on the Hydraulic Conductivity of Tomato Root Systems (Evidence for a Channel-Mediated Water Pathway). *Plant Physiol.* **109,** 331–335 (1995).
253. Lovisolo, C., Tramontini, S., Flexas, J. & Schubert, A. Mercurial inhibition of root hydraulic conductance in Vitis spp. rootstocks under water stress. *Environ. Exp. Bot.* **63,** 178–182 (2008).
254. Pou, A., Medrano, H., Flexas, J. & Tyerman, S. D. A putative role for TIP and PIP aquaporins in dynamics of leaf hydraulic and stomatal conductances in grapevine under water stress and re-watering. *Plant, Cell Environ.* **36,** 828–843 (2013).
255. Katsuhara, M. *et al.* Functional and molecular characteristics of rice and barley NIP aquaporins transporting water, hydrogen peroxide and arsenite. *Plant Biotechnol.* **219,** 213–219 (2014).
256. Heinen, R. B., Ye, Q. & Chaumont, F. Role of aquaporins in leaf physiology. *J. Exp. Bot.* **60,** 2971–2985 (2009).
257. Uehlein, N. *et al.* Function of Nicotiana tabacum aquaporins as chloroplast gas pores challenges the concept of membrane CO2 permeability. *Plant Cell* **20,** 648–657 (2008).
258. Sade, N. *et al.* The Role of Plasma Membrane Aquaporins in Regulating the Bundle Sheath-Mesophyll Continuum and Leaf Hydraulics. *Plant Physiol.* **166,** 1609–1620 (2014).
259. Herrera, M. & Garvin, J. L. Aquaporins as gas channels. *Pflugers Archiv European Journal of Physiology* **462,** 623–630 (2011).
260. Ellis-Davies, G. C., Kaplan, J. H. & Barsotti, R. J. Laser photolysis of caged calcium: rates of calcium release by nitrophenyl-EGTA and DM-nitrophen. *Biophys. J.* **70,** 1006–1016 (1996).

261. Andersson, M. *et al.* Structural Dynamics of Light-Driven Proton Pumps. *Structure* **17,** 1265–1275 (2009).
262. Malmerberg, E. *et al.* Time-resolved WAXS reveals accelerated conformational changes in iodoretinal-substituted proteorhodopsin. *Biophys. J.* **101,** 1345–1353 (2011).
263. Yamada, Y., Matsuo, T., Iwamoto, H. & Yagi, N. A compact intermediate state of calmodulin in the process of target binding. *Biochemistry* **51,** 3963–3970 (2012).
264. Kučerka, N., Tristram-Nagle, S. & Nagle, J. F. Structure of fully hydrated fluid phase lipid bilayers with monounsaturated chains. *J. Membr. Biol.* **208,** 193–202 (2006).
265. Tamás, L. *et al.* Role of reactive oxygen species-generating enzymes and hydrogen peroxide during cadmium, mercury and osmotic stresses in barley root tip. *Planta* **231,** 221–231 (2010).
266. Azevedo, R. & Rodriguez, E. Phytotoxicity of Mercury in Plants: A Review. *Journal of Botany* **2012,** 1–6 (2012).
267. Li, R.-Y. *et al.* The rice aquaporin Lsi1 mediates uptake of methylated arsenic species. *Plant Physiol.* **150,** 2071–2080 (2009).
268. Schrader, a. *et al.* Effects of glyceryl glucoside on AQP3 expression, barrier function and hydration of human skin. *Skin Pharmacol. Physiol.* **25,** 192–199 (2012).
269. Tamarappoo, B. K. & Verkman, a. S. Defective aquaporin-2 trafficking in nephrogenic diabetes insipidus and correction by chemical chaperones. *J. Clin. Invest.* **101,** 2257–2267 (1998).
270. Promeneur, D. *et al.* Aquaglyceroporin PbAQP during intraerythrocytic development of the malaria parasite Plasmodium berghei. *Proc. Natl. Acad. Sci. U. S. A.* **104,** 2211–2216 (2007).
271. Kozai, T. Resource use efficiency of closed plant production system with artificial light: concept, estimation and application to plant factory. *Proc. Jpn. Acad. Ser. B. Phys. Biol. Sci.* **89,** 447–61 (2013).